NASA
Technical Memorandum 83246

AVRADCOM
Technical Report 82-B-7

NASA-TM-83246

1983 0010747

Preliminary Rotor Wake Measurements With a Laser Velocimeter

Danny R. Hoad, David B. Rhodes, and James F. Meyers

MARCH 1983

NASA

U.S. ARMY
AVRADCOM

Preliminary Rotor Wake Measurements With a Laser Velocimeter

Danny R. Hoad
Structures Laboratory
AVRADCOM Research and Technology Laboratories
Langley Research Center
Hampton, Virginia

David B. Rhodes and James F. Meyers
Langley Research Center
Hampton, Virginia

INTRODUCTION

The helicopter rotor wake is extremely complex because of the presence of multiple blade root and tip vortices. The interaction of these vortices causes a highly distorted wake structure, particularly at moderate helicopter advance ratios ($\mu = 0$ to 0.2) and high rates of descent of the helicopter. Predictions of time-dependent and spatial velocity variations in this highly distorted flow field are, at best, only qualitative. Even a basic understanding of the flow field environment is lacking, and only a limited amount of experimental data is available. Advances in disciplines that require knowledge of these rotor wake effects will be limited until the details of the rotor wake environment are understood. These details can only be obtained through precise measurement of the rotor wake structure.

The available data on rotor wake structure include measurements made with total-pressure probes, hot-wire and hot-film anemometers, photographic techniques, local-surface-pressure taps (from which local in-flow velocities can be inferred), and advanced techniques like laser velocimetry. Each of the data sets obtained with these systems has been valuable to the helicopter research community in developing a new appreciation of the complexity of the rotor wake structure. Each, however, has its limitations as well as its benefits. No single method can be considered the best for all measurement requirements. For instance, the laser velocimeter (LV) eliminates the influence of probe presence on the velocity being measured and makes it possible to obtain measurements between rotor blades; however, it is expensive and can be difficult to put into operation.

The LV is capable of measuring velocity time histories or velocity variation with rotor azimuth. However, this is a difficult undertaking because the velocity measurements obtained are not made at regular intervals of time, but occur only when a scattering particle happens to pass through the LV sample volume. The arrival of these particles in time can be approximated by a Poisson distribution function (ref. 1). Successful experiments have been conducted (refs. 2 to 4) using a "data window" technique that gathers LV data only when the rotor blade is at a prescribed azimuth. Another successful technique (refs. 5 and 6) involves associating a rotor blade azimuth position measurement with each sample velocity measurement rather than restricting measurements to a data window. The latter technique, which is used in the Langley 4- by 7-Meter Tunnel to acquire LV data, is considered more time-efficient. This report presents preliminary results of an experiment designed to use LV measurements to determine the effects of rotor-fuselage spacing and fuselage width on rotor wake velocity. Detailed wake measurements were obtained to evaluate the effects of these parameters on variations in local time-dependent velocity near the rotor blades.

SYMBOLS

The axis system used for the velocity measurements and measurement locations presented in this report is presented in figure 1(a). The values for physical quantities defined herein are expressed in the International System of Units (SI); how-

ever, some measurements were made in U.S. Customary Units and were converted by factors given in reference 7.

C_T thrust coefficient, $\text{Thrust}/\rho\pi R^2(2\pi\Omega R)^2$

f   LV burst signal frequency, Hz

f_{BR} Bragg shift frequency, Hz

L_{fr} fringe spacing, m

N_i number of velocity measurements in ith histogram interval as percent of total number of measurements

N_o order number; harmonic of one rotor revolution

R   rotor radius (0.5 m)

S   rotor-fuselage spacing, m

u   local velocity sample vector aligned with x-axis, m/sec (see fig. 1)

$\bar{u}$ ensemble mean of u measurement component, m/sec

u'   velocity fluctuation in u measurement component, m/sec

v   local velocity sample vector aligned with z-axis, m/sec (see fig. 1)

$\bar{v}$ ensemble mean of v measurement component, m/sec

v'   velocity fluctuation in v measurement component, m/sec

V_∞ free-stream velocity, m/sec

W   fuselage width, m

x,y,z   coordinate system relative to rotor hub, m

Γ_k autocovariance function, m^2/sec^2

$\Delta\psi$ time between arrivals of sample measurements, described in azimuth intervals, deg

θ cross-beam angle, deg

λ beam wavelength, m

μ helicopter advance ratio, $V_\infty/2\pi\Omega R$

ρ free-stream density, kg/m^3

Ω rotor rotational speed, Hz

Superscript:

''   peak value

TEST APPARATUS

Laser Velocimeter

The optical system used for this investigation was a dual-color four-beam fringe-type laser velocimeter (LV) operating in the backscatter mode. A schematic of this system is shown in figure 2. Viewed along the optical axis, the diamond-shaped beam pattern was composed of two vertically spaced blue beams at 488.0×10^{-9} m wavelength and two horizontally spaced green beams at 514.5×10^{-9} m wavelength. These two wavelengths were selected by a color separator from the multiwavelength output of an argon ion laser operating at a total output power of 3 W. The two beams were routed into a standard two-component LV transmission package. There, each beam was split into two beams of equal intensity, and one beam from each pair was passed through an acousto-optic modulator (Bragg cell). The beam spacings were then stepped down from 50 mm to 22 mm, which was the distance required for the four-hole mirror and initial lens of the unique afocal zoom-lens system. This zoom-lens system was designed to maintain a constant cross-beam angle at the sample volume throughout the zoom range (ref. 8). The system has three lenses: two positive lenses separated by a distance that is the sum of their focal lengths, and a negative scan lens. The final objective lens is 250 mm in diameter, and the negative scan lens is 32 mm in diameter.

A summary of the optical characteristics of the LV system is presented in table I. The lens system maintained a constant collecting solid angle in this coaxial configuration to provide a constant signal amplitude. The final folding mirror was the prime translation device of the sample volume for this investigation and was capable of two degrees of freedom about a horizontal and a vertical axis.

At the crossover point of the four-beam intersection in the flow, an ellipsoidal sample volume was formed which contained a distinctive fringe pattern, as described in reference 9. The internal fringe spacing L_{fr} was a function of wavelength λ and angle θ between the crossing beams at the sample volume:

$$L_{fr} = \frac{\lambda}{2 \sin(\theta/2)} \tag{1}$$

As a particle passed through the sample volume, light was scattered with an intensity proportional to the incident intensity in the fringe pattern. Part of the scattered light was collected by the transmitting optics. The collected scattered light was deflected to the receiver package at the four-hole mirror between the negative lens of the zoom system and the transmitting optics package. In the receiver package, the two combined wavelengths were separated and directed by a dichroic mirror to two separate photomultiplier tubes (PMT's), where each optical signal was converted to an electronic signal, and a classical signal burst was generated. (See ref. 9.)

The Bragg cell provided directional information for the velocity measurement. In this particular test, the effective Bragg shift was electronically reduced from 40 MHz to 1 MHz for improved resolution, since the velocities expected from this

3

rotor were below 8 m/sec. The velocity calculated from the LV measurements is a direct function of the fringe spacing described earlier, the effective Bragg shift frequency f_{BR}, and the frequency f within the LV burst, as measured by the electronic counters:

$$u \quad \text{or} \quad v = (f - f_{BR})L_{fr} \tag{2}$$

This LV system was installed just outside the tunnel flow in the test chamber of the Langley 4- by 7-Meter Tunnel, which was configured as an open-throat tunnel with the floor in place. The beam-crossing optics had a focal range from 2.45 to 4.9 m and a collecting solid angle of 0.00132 sr. The sample volume was 0.63 cm long and 0.18 mm in diameter, and was positioned at desired locations within the rotor plane using the pan-tilt folding mirror and the zoom-lens system. The photograph of the LV optics platform in figure 3 shows the laser beam paths and the rotor model in the background.

The LV electronics system was essentially identical to that described in reference 10, with the exception of the LV buffer interface. The buffer interface used in these tests was capable of storing two channels of velocity data; however, instead of storing the elapsed time between data arrivals, the new buffer captured rotor azimuth simultaneously with the two-component velocity measurements. The buffer interface required that the two velocity components be coincident in time in order for the buffer to accept the measurement as valid and to sample the azimuth position. Operation of the LV buffer interface was similar to that described in reference 10, but in this experiment 30 separate buffer cycles were initiated at each desired measurement position instead of just 1. Each computer-controlled cycle was halted either when the interface memory was full (4096 data points) or after 1 minute of elapsed time.

Particles were provided by the smoke generator system described in reference 10. The particle size distribution is given in figure 4 (fig. 8(a) of ref. 10). It is important to note, however, that the optics system for this experiment was totally different from that described in reference 10, and therefore the overall measurement probability distributions shown in figures 8(b) and 8(c) of reference 10 do not apply in this case.

Rotor Model

The model used in this investigation was an externally powered 1-m-diameter four-blade rotor with three fuselages of various widths. The rotor was driven by an external electric motor mounted on the model support system by a six-component balance. (See fig. 1(b).) A fairing was provided over the motor and balance to minimize flow interference caused by mounting hardware. (See fig. 3.) Three fuselages were provided (fig. 5), all 1.0 m long, with maximum fuselage widths of 6.25 cm (0.125R), 12.5 cm (0.250R), and 18.75 cm (0.375R) (fig. 6). In this configuration, the rotor-fuselage spacing and fuselage width could be varied to investigate the effects of these parameters on the rotor downwash flow field. The separation distances and fuselage widths used for this investigation are shown in figure 6.

The rotor system was operated at a thrust coefficient C_T of 0.006, a rotor rotational speed Ω of 25 revolutions per second, and an advance ratio μ of 0.053, with the rotor tip path plane parallel to the tunnel horizontal reference. LV measurements were obtained in a plane that was parallel to the tip path plane and inter-

sected the hub and flapping hinges. Since the model was mounted upside down, the rotor blades coned downward due to thrust. Therefore, measurements between rotor blades had to be obtained by moving the LV sample volume downward from the rotor hub plane. Rotor azimuth was provided by enhancing a 72-per-revolution (1 + 71) pulse train to obtain digital levels varying from 0 to 720. These levels were then associated with 0.5° rotor azimuth increments from 0° to 360°. Rotor performance was monitored continually and was maintained as closely as possible to test conditions throughout each data point. Selected rotor and tunnel parameters were passed from the existing tunnel data acquisition computer to the LV data acquisition computer prior to each LV buffer cycle.

DATA ACQUISITION AND REDUCTION

Statistical Quantities

The LV samples a velocity field in time with the variability of a Poisson distribution. (See ref. 1.) The velocity measurement from a particle is only one sample of velocity within the probability density function of the flow field. If the standard deviation of the velocity measured is large, the probability of this single measurement being a good representation of the expected value of the true flow velocity is statistically rather low. Therefore, it is necessary to acquire an adequate number of samples in order to completely define the statistical probability density function of the velocity measurements. During the data reduction process, two assumptions are made: (1) the particles embedded in the flow are not only randomly dispersed in space but are also randomly dispersed in the velocity field; and (2) the measurement sample ensemble obtained over a finite period of time is a good statistical representation of the stationary-flow condition at the measurement location. In this investigation, it will be shown that flow phenomena affecting this stationarity can have serious effects on the velocity measurements obtained.

This investigation was conducted to determine the periodic variation and standard deviation of local velocity with rotor azimuth. These azimuth-dependent quantities could be obtained by sorting the velocity information into ensembles of equal azimuth (0.5° resolution) and performing the statistical calculations described in reference 10 on each azimuth ensemble. Time-averaged mean velocity calculations were made based on the simple arithmetic mean,

$$\bar{v} = \frac{\Sigma v_i}{\text{Number of velocity measurements}} \tag{3}$$

It was not necessary to make corrections for velocity bias or Bragg cell bias, as noted in reference 10.

Error Analysis

The overall measurement precision was obtained by determining the accuracy of each variable in the system that could affect the accuracy of the velocity measurements. Reference 11 provides a complete description of the sources of errors involved in laser velocimetry, as well as of the error analysis method. These error sources, presented in table II, yield an overall effective total bias error in the mean from -1.0 to +0.74 percent. These values were calculated from an algebraic sum

5

of the partial bias errors. The total effect of random error on the mean was ±0.58 percent uncertainty. This value was obtained by taking the square root of the sum of the squares of the partial random errors.

Instrument-related measurement uncertainties were caused by cross-beam-angle uncertainty, nonparallelism of fringes, clock synchronization, and quantizing error. The cross-beam-angle uncertainty, which resulted from inaccuracies in the measurement of the cross-beam angle, produced a constant but unknown bias error in the measurement of particle velocity. However, these inaccuracies did not produce any random uncertainties in the mean velocity measurements. The uncertainty due to nonparallelism of fringes yielded a bias and a random uncertainty in the mean velocity measurement. The synchronization between the signal burst and the clock in the high-speed burst counter caused a bias error and a negligible random error in the mean velocity measurement. For this test, the effects of the quantizing error caused by the digitization of time in the high-speed burst counter were negligible for the measurement of mean velocity.

In a large velocity gradient, velocity measurement errors can occur due to the length of the sample volume, which allows contributions from the high-velocity flow at one end and the low-velocity flow at the other end to be included in the measurement. If the gradient is linear over the length of the sample volume, as is assumed in the present study, the mean velocity measurement is not affected. Further, the results of this test show that the flow was below 10 m/sec with a turbulence intensity of less than 10 percent, indicating that the velocity gradients were very small. Thus, in general, the error caused by velocity gradients can be neglected.

Since the LV measures particle velocities and not the gas velocity, the final measurement accuracy is dependent on the ability of the particle to follow the flow faithfully. In the present study, kerosene droplets were used as the seed material. The particle size distribution is shown in figure 4. Based on the results reported in reference 11, these particles will follow a velocity gradient of 1500 (m/sec)/sec within approximately 5 percent. Thus, it is concluded that these particles will faithfully follow the flow field studied in this test.

TEST PROCEDURES

This investigation was conducted in the Langley 4- by 7-Meter Tunnel. Rotor wake velocity measurements were obtained in at least 8 locations in the plane of the hub for 10 different rotor-fuselage configurations: rotor only, and 3 rotor-fuselage spacings (S/R = 0.224, 0.275, and 0.324) each for 3 different fuselage widths (W/R = 0.125, 0.250, and 0.375). (See table AI for a listing of measurement locations.) Most of these measurements were obtained along the x-axis upstream of the rotor hub. Some data were acquired very near and in the surface of the cone inscribed by the rotor blades; this required making velocity measurements between rotor blades.

The LV data were acquired as particles passed through the sample volume. Particles were injected into the flow at sufficient density and size to produce a high arrival rate. As the counter-processor validated each measurement, it was accepted and stored in the high-speed buffer along with the appropriate rotor azimuth. A coincidence time restriction of 1.0×10^{-6} sec was placed on the u- and v-component measurements. This computer-controlled process continued until the buffer was filled or the time limit was exceeded. The entire measurement sequence was repeated 30 times for each measurement location.

RESULTS AND DISCUSSION

Examples of velocity measurements obtained for each sample volume location are presented in the appendix. Only selected samples of these data will be discussed in the text, along with simulated samples of predicted time-dependent velocity profiles. Power spectral density and autocorrelation function estimates of the experimental and simulated data sets are presented and discussed. Time-averaged calculations of the experimental data acquired are presented in figures 7 and 8.

Effects of Rotor-Fuselage Configuration on Time-Averaged Velocity Measurements

Data presented in figures 7 and 8 are time-averaged samples of data obtained along the x-axis in the plane of the rotor hub (i.e., the measurements were made between the rotor blades and the fuselage). (See fig. 1.) These data are presented as horizontal (u) and vertical (v) velocity components as a function of distance from the hub normalized by rotor radius R. The effect of body width at a fixed rotor-fuselage spacing is presented in figure 7. The primary effect of body width occurs at the inner radius of the rotor, which is the area most affected by the fuselage presence. As expected, the vertical velocity component decreased and the horizontal velocity component increased with increasing fuselage width. This had a channeling effect on the flow.

The effects of rotor-fuselage separation for each fuselage width are presented in figure 8. The presence of the 0.125R body at different distances from the rotor is barely evident in the velocity measurements obtained (fig. 8(a)), but the effects of separation distance for the other two bodies are larger (figs. 8(b) and (c)). In general, the rotor wake is being channeled between the fuselage and the rotor in the close-coupled configuration (S/R = 0.224), as evidenced by the higher horizontal and lower vertical velocity components at x/R = 0.1. (See fig. 8(b).) Slightly increased vertical and decreased horizontal velocity components for the close-coupled rotor-fuselage configuration at x/R = 0.3 indicate acceleration of the rotor wake conditions around the nose of the fuselage. These effects can be observed in the data for the 0.250R and 0.375R bodies; the wider body obviously shows larger magnitude effects.

Analysis of Time-Dependent Data

It appears from the LV data presented in the appendix that no real periodic velocity variation with rotor blade passage (azimuth) can be defined. Since the prime objective of this program was to identify this time-dependent variation, it would seem that the project was not successful. However, to fully understand the LV process and its application to rotor wake measurements, it is imperative to identify the cause of the apparent lack of time-dependent variation in the data. Three possibilities can explain this result: (1) the azimuth indicator was not operating correctly and provided erroneous azimuth measurements; (2) the velocity truly did not vary with time; or (3) some flow phenomenon caused variability in the velocity time history during the measurement period, thus washing out the time-dependent velocity measurements (i.e., there was a lack of stationarity in the flow field).

To address the first possibility, a sample velocity measurement was selected for analysis. Figure 9 shows a sample (one buffer load) of the velocity measurements obtained when the sample volume was located in the path of the rotor blades. Veloc-

ity components as a function of azimuth are presented in figure 9(a), and figure 9(b) presents the velocity histogram (or probability density function) of these components. Each dot in figure 9(a) represents a single velocity measurement. Note the apparent voids in the velocity data at azimuth angles from 30° to 60°, 120° to 140°, 210° to 230°, and 300° to 320°. The voids are caused by the passage of each blade through the sample volume. If the azimuth measurement had been malfunctioning, these voids would not exist here or in the other data acquired during the time the beams were being clipped by the rotor blades. Note also that although velocity measurements were made between the blades, there are still no apparent time-dependent velocity characteristics. It is evident that the azimuth measurement was functioning properly and is not a probable cause of the lack of time-dependent velocity variations at the selected measurement locations.

The second possibility, that the velocity did not vary with time, was examined by calculating the wake velocities using an analytical prediction method frequently employed in rotor-wake analyses. This method, developed by Landgrebe (ref. 12), was used to estimate the time-dependent velocity characteristics for this rotor wake without fuselage. The classical wake calculations (undistorted helix) used for this particular program did not allow distortion of the wake shape due to wake interaction. Precise correlation of the velocity magnitude with the LV measurement was not attempted in this case, since only an example of the time-dependent nature of the rotor wake at the desired location was required. Thus, the velocity magnitudes did not have to be very accurate for this prediction.

Three velocity predictions are presented in figure 10. The solid line in figure 10(a) represents the estimated velocity time history. For this example, the simulation calculation assumed a normal density function distribution for the velocity ensemble at each azimuth, with a standard deviation of 1 percent in both the vertical and the horizontal component. The dots in this figure were simulated using a Poisson time distribution (ref. 1) and represent samples of the assumed velocity distribution. The waveform character of the velocity time histories is preserved, probably because the turbulence levels were random fluctuations. Random turbulence, however, can be a serious matter if the intensities are large, as seen in the simulated calculations obtained with an assumed turbulence of 10 percent (fig. 10(b)). In this case, no velocity waveform characteristic would be apparent unless it were already known. It should be noted that actual turbulence intensity level in the closed test section of the 4- by 7-m tunnel is 0.3 percent for the horizontal component and 1.0 percent for the vertical component, which is well within the limits for retaining the velocity waveform characteristics.

For this particular investigation, the tunnel was operated with the test section open. After the investigation, measurements of tunnel turbulence values indicated that a pulsation, or discrete-frequency velocity fluctuation, was present at about 1.5 Hz. The magnitude of this discrete-frequency pulsation at the lowest speed tested was on the order of 8 percent in the vertical component and 5 percent in the horizontal component with reference to the free-stream velocity. (See fig. 11.) Unfortunately, turbulence measurements were not obtained at velocities as low as those used in this investigation.

To consider a worst-case possibility, the 10-percent turbulence intensity was chosen for the open-tunnel simulation calculations. Such large vertical and horizontal discrete-frequency fluctuations could result in a large variation (as much as 4°) in the angle of the flow presented to the rotor system, assuming that the velocity components were shifted in phase 180° relative to the pulsation. The Landgrebe prediction technique (ref. 12) was used to estimate the periodic variation in the

azimuth-dependent velocity at one point in the rotor wake. Based on these predictions, simulated LV measurements were generated for a model in the open test section. These simulated measurements were obtained using the same calculations described previously, but with the addition of periodic (1.5 Hz) free-stream velocity fluctuations. As can be seen from figure 10(c), no time-dependent velocity characteristic is evident.

These results indicate that the periodic free-stream velocity fluctuations caused a nonstationary flow condition at the measurement location. The LV (or, for that matter, any instrument physically located at a point in this environment) would have measured the velocity characteristics of this nonstationary oscillating rotor wake in addition to those of the stationary wake desired. Measurements obtained experimentally at the same locations used in calculating the simulated results shown in figure 10 (i.e., $x/R = 0.3$, $y/R = 0$, and $z/R = 0$) also show this lack of time-dependent velocity characteristic. (See fig. 12.) The remarkable similarity of the data scatter in these figures leads to the postulation that the high turbulence level and its periodic nature obscured the time-dependent characteristics of the velocity measurements. However, it is important to note that this is only a definite possibility and has not yet been proven.

Spectral Characteristics

To further analyze the effects of this periodic turbulence, the data (both experimental and simulated) were transformed into the frequency domain using autocovariance and fast Fourier transform (FFT) techniques. It is well known that an autocovariance of a random-noise data set that has a periodic component buried within it will provide a measure (frequency and amplitude) of the periodic component expressed by the autocovariance function. An FFT of this autocovariance function will then give an estimate of the power spectral density of the data set. It has been demonstrated (ref. 13) that direct calculation of the autocovariance function is necessary for LV data transformation.

The autocovariance function reveals any coherent relationship of the data under investigation as a function of time. In this test, the autocovariance function was determined as a function of azimuth, so that minor discrepancies due to small variations in rotor speed would not affect the calculations. In laser velocimetry, the individual measurements of velocity occur at random times; this requires a knowledge of the time (in this case, azimuth angle $\Delta\psi$) between successive measurements. All possible velocity pairings were made for a total differential azimuth angle of less than one revolution. The cross products were then summed, as was the number of times each differential azimuth angle occurred. Normalization of the cross-product summations by the number of occurrences of each angle yielded the final autocovariance function. This process may be expressed as

$$\Gamma_k = \frac{\sum_{j=0}^{N-k} u(j)\ u(j+k)\ I(j)\ I(j+k)}{\sum_{j=0}^{N-k} I(j)\ I(j+k)} \tag{4}$$

9

where

N   number of measurements (i.e., particles)

$u(j)$ jth velocity measurement (with mean removed)

$u(j+k)$ velocity measurement $k\Delta\psi$ from j (with mean removed)

$I(j)$ binary indicator ($I(j) = 1$)

$I(j+k)$ binary indicator ($I(j+k) = 1$ if there is a velocity measurement at j + k, and $I(j+k) = 0$ otherwise)

$\Delta\psi$ autocovariance delay angle

Once the autocovariance function was calculated, it was multiplied by a Bartlett window function to reduce the effect of the side lobes in the spectral window. FFT techniques were applied to the results to yield the power spectral density (PSD) of the flow field under observation.

The simulated data set presented in figure 10(a), which represented a sample condition in the closed tunnel, was transformed in this manner. The results are presented in figure 13. These simulated data can be seen to have a very strong periodic content in the time domain (fig. 10(a)) - 4 per revolution in the u component and 8 per revolution in the v component. The autocovariance function in figure 13(a) shows the classical sinusoidal variation of the discrete frequency in the u and v components. The estimates of power spectral density that were produced by fast Fourier transforms of the autocovariance function are presented in figure 13(b). These results are presented as a function of order number (or multiples of rotor revolutions). The PSD shows the discrete-frequency velocity characteristics at those values observed in the velocity time histories. (See fig. 10(a).)

By performing this same transformation on the data in figure 10(c), any discrete-frequency velocity components that exist will be seen in the autocovariance function and the PSD. This data set simulated data acquisition in the tunnel with the test section open at a point where periodic turbulence washed out any apparent time-dependent velocity characteristics. The results of spectral transformation are presented in figure 14. No apparent periodic content is evident in the autocovariance function, but a very weak 8-per-revolution frequency content may be present, as shown in the v component in figure 14(b).

The results of these calculations on the simulated LV data suggest two important conclusions. First, if a discrete-frequency content exists in the random LV data, the spectral transformation process described should identify it. Second, if the apparent lack of time-dependent velocity characteristics in the experimental data is in fact a result of the periodic turbulence in the open test section, then spectral transformation of the experimental data will show no periodic content. This transformation was performed on the experimental LV data, and the results are presented in figure 15. No periodic content is observable in either the autocovariance function or the power spectral density. Data for many other rotor configurations and LV measurement positions were transformed into the frequency domain with similar results.

CONCLUDING REMARKS

An experimental investigation was conducted using a laser velocimeter (LV) to determine the effects of various fuselage widths and rotor-fuselage separations on time-averaged and detailed time-dependent rotor wake velocity characteristics. The results of the investigation were ambiguous in that no apparent time-dependent velocity characteristics were observed in the experimental data. Simulated LV sampling of a theoretically determined velocity time history demonstrated the probable cause of these results. Using a recognized analytical prediction method, it appeared that velocity variations should have existed at the measurement locations chosen. Time-dependent variations in velocity should have been preserved for turbulence characteristics typical of the closed test section. However, these time-dependent velocity characteristics were totally washed out in the open-throat tunnel configuration. Autocovariance calculations and power spectral density estimates were used to verify that the time-dependent velocity characteristics were not merely buried within the observed random-velocity time history.

Based on these results, it is most probable that the discrete-frequency pulsation existing in the facility in the open-throat configuration at the speeds tested set up a nonstationary flow field, thus presenting different test conditions to the LV instrument over the time period of an ensemble measurement. When this program was planned, flow stationarity in the test facility was assumed, and flow fluctuations at frequencies below the rotor rotational frequency were ignored. The data acquisition technique was not designed to record elapsed time between measurements larger than the time for one revolution. This limitation made it impossible to isolate velocity fluctuations at frequencies less than the rotor rotational frequency. Since these velocity fluctuations could not be separated from those at frequencies of interest, they could not be prevented from contributing to the scatter and the amplitude uncertainty in the rotor-related periodic content. However, it is important to point out that operation at higher rotor disk loadings or different tunnel velocities, where these periodic turbulence levels are lower, might have produced better results. It is recommended that any future programs for which large time-dependent velocity gradients exist as a stationary process should be conducted in the closed test section of the facility. Programs using the open test section should be examined closely to insure that this discrete-frequency turbulence will not create a nonstationary flow field that may render the measurements useless.

Langley Research Center
National Aeronautics and Space Administration
Hampton, VA 23665
November 29, 1982

TABLE I.- OPTICAL CHARACTERISTICS OF LV SYSTEM

Input beam diameter, mm 1.8
Input beam separation, mm 22
Output beam diameter, mm .... 8.1 to 17.3
Output beam separation, cm .... 9.7 to 20.3
Included angle, θ, deg 2.36
Scan range, m .... 2.45 to 4.9
Diameter of objective lens, mm 250
Approximate number of fringes in sample volume 15

Fringe spacing, m:
  $\lambda = 488.0 \times 10^{-9}$ m .... 11.85×10^{-6}
  $\lambda = 514.5 \times 10^{-9}$ m .... 12.5×10^{-6}

Sample volume:
  Length, mm 6.3
  Diameter, mm 0.18

Collection solid angle, sr 0.00132

TABLE II.- MEAN VELOCITY ERROR SOURCES

Error source	Bias, percent	Random, percent
Velocity bias	Corrected	NA
Bragg bias	Corrected	NA
Cross-beam-angle uncertainty	±0.87	NA
Nonparallelism of fringes	-0.28	±0.42
Time jitter	0	0
Clock synchronization	.15	NA
Quantizing error	(a)	±.0001
Velocity gradient	(a)	(a)
Measurement location uncertainty	(b)	(b)
Particle lag	(a)	(a)
Statistical uncertainty (typical)	NA	±0.40
Total error	+0.74 to -1.0	±0.58

[a]Negligible.
[b]Not measured.
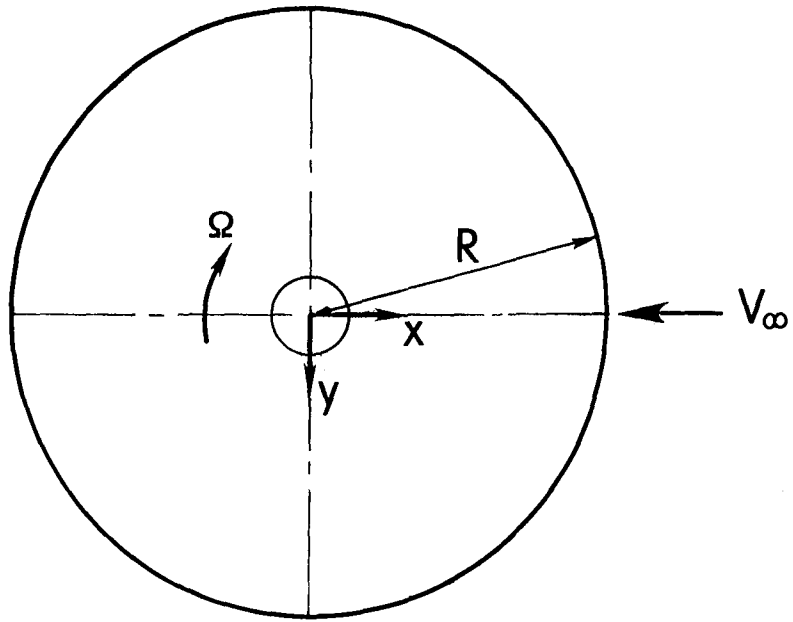
(a) Top view.
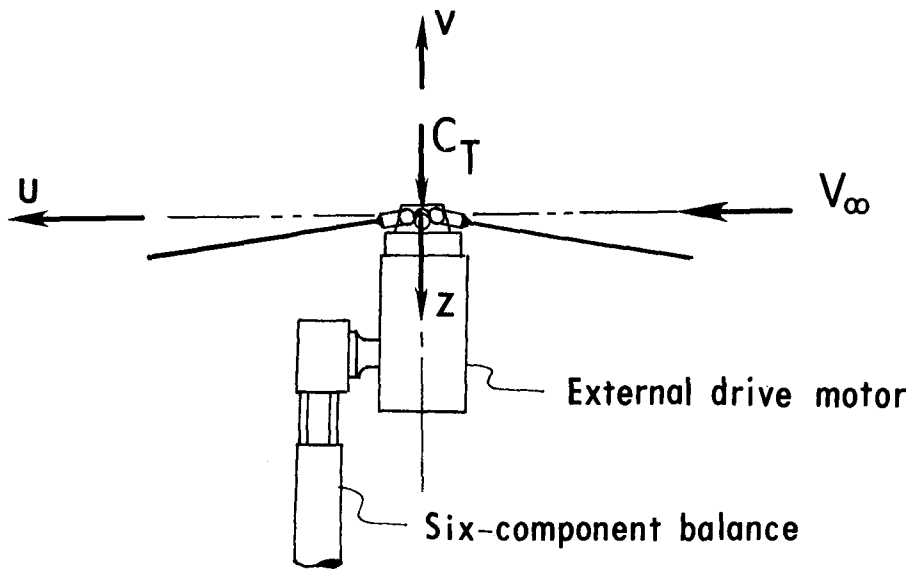
(b) Side view.

Figure 1.- Schematic of rotor system tested, including axis system.
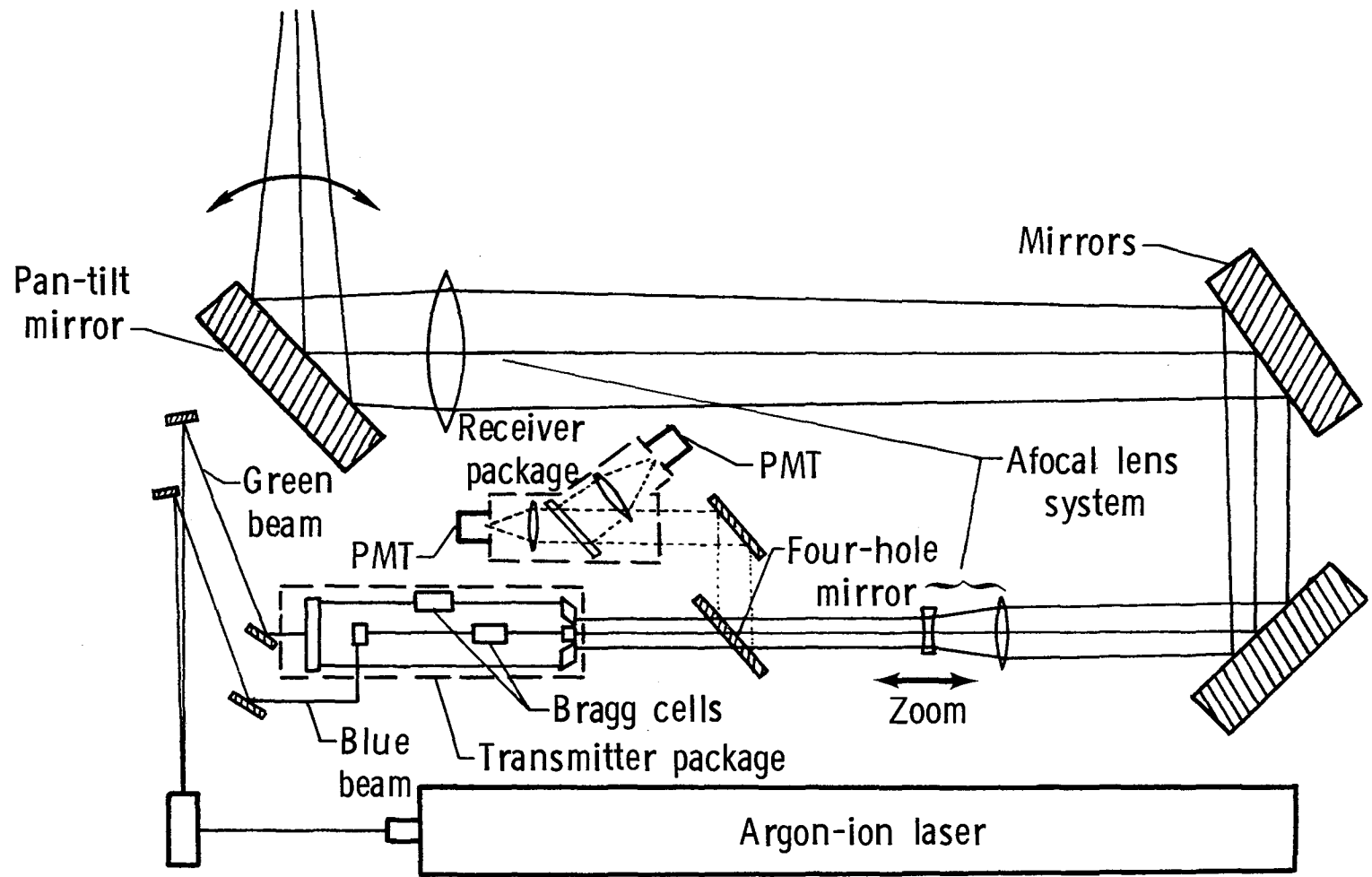
Figure 2.- Schematic of laser velocimeter optics package.
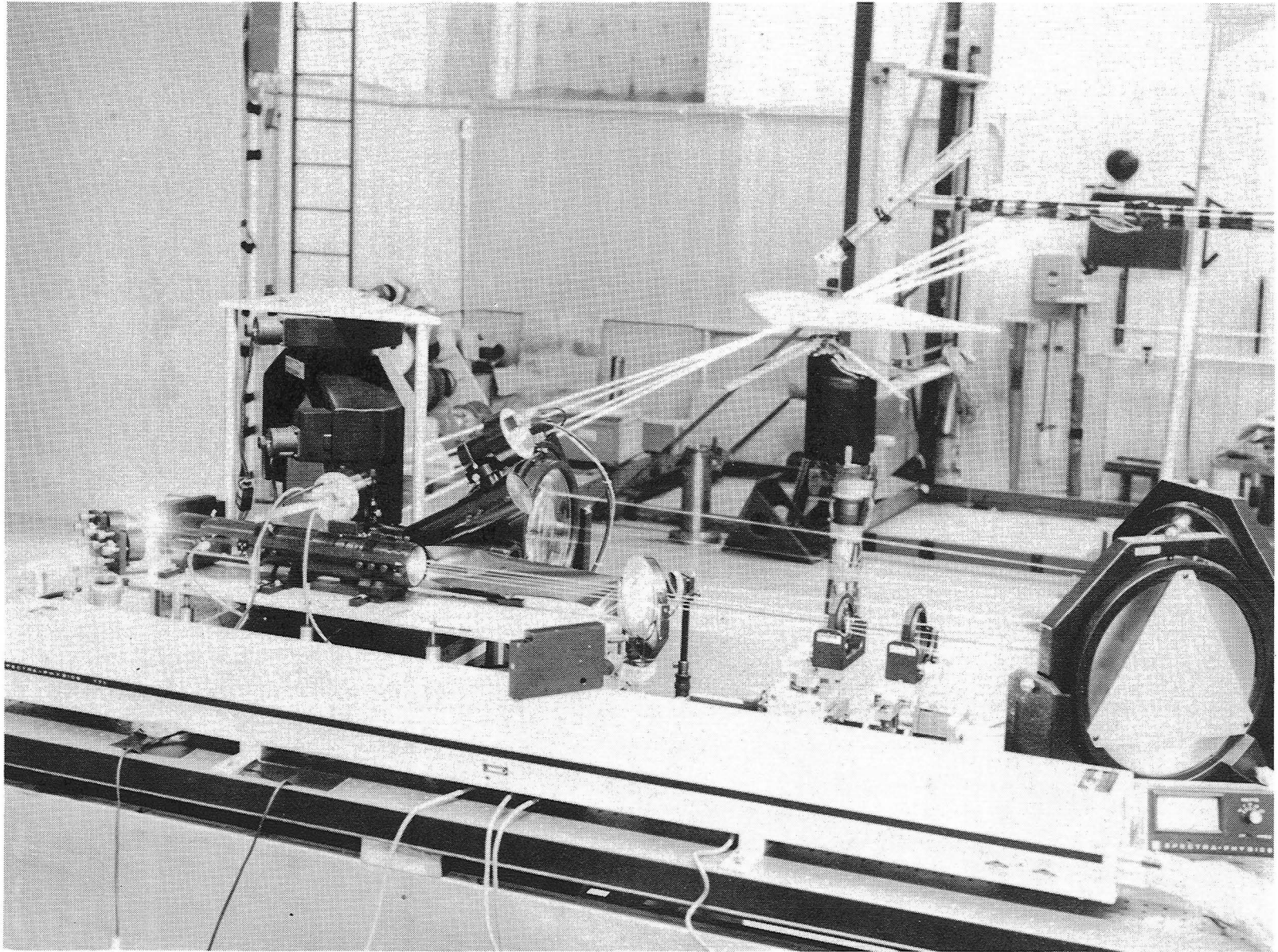
L-80-8575

Figure 3.- Laser velocimeter optics platform and rotor model installed in
Langley 4- by 7-Meter Tunnel.
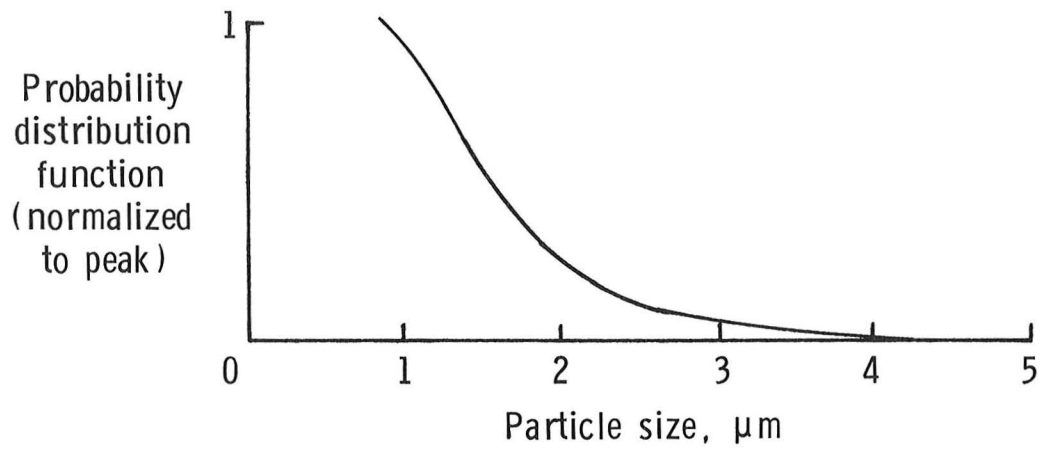
Figure 4.- Particle size distribution. (From ref. 10.)
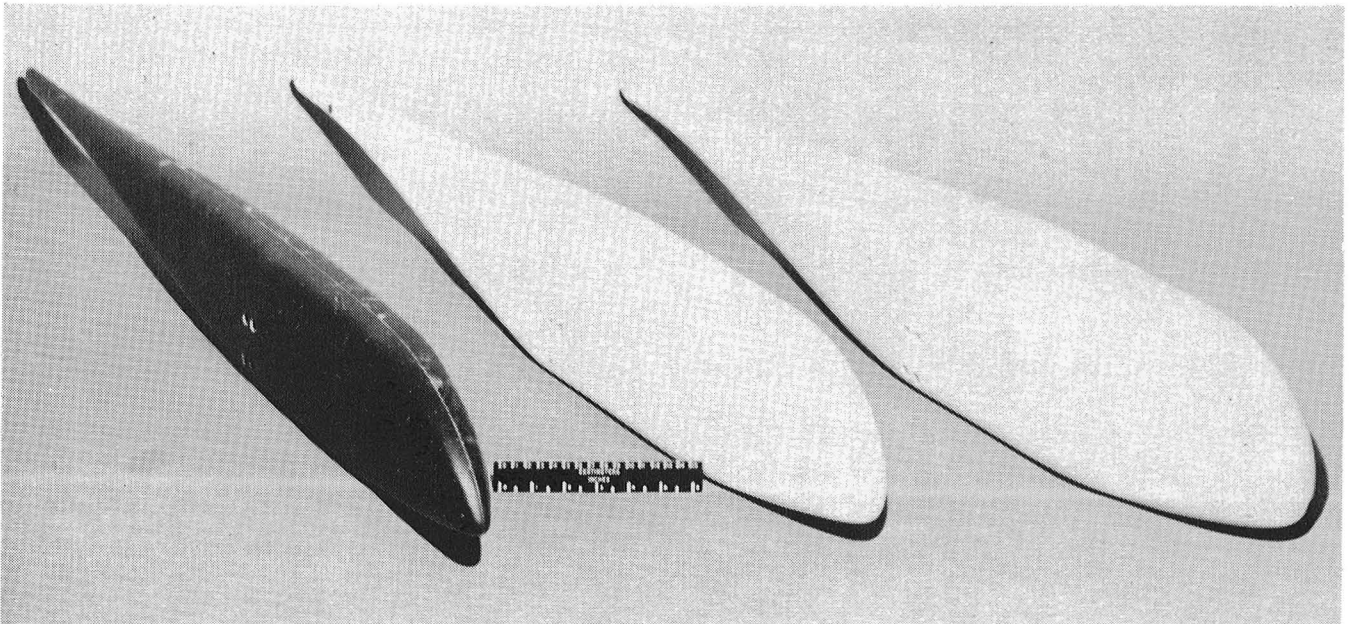
L-79-4220

Figure 5.- Three fuselage sizes used.
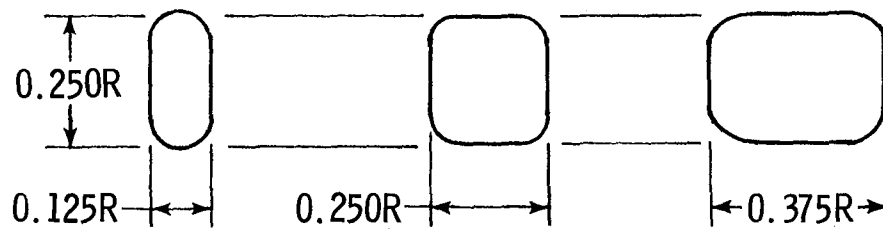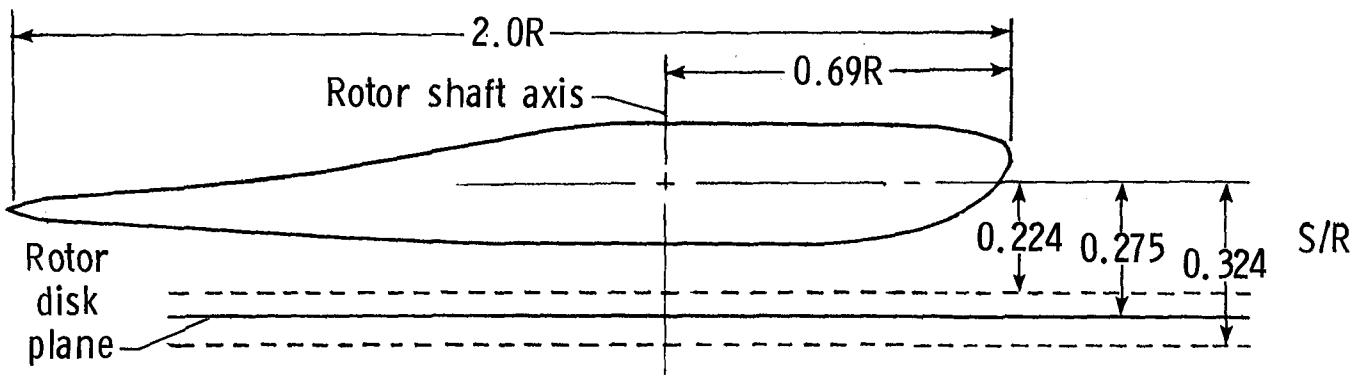
Figure 6.- Parametric options available for rotor system.
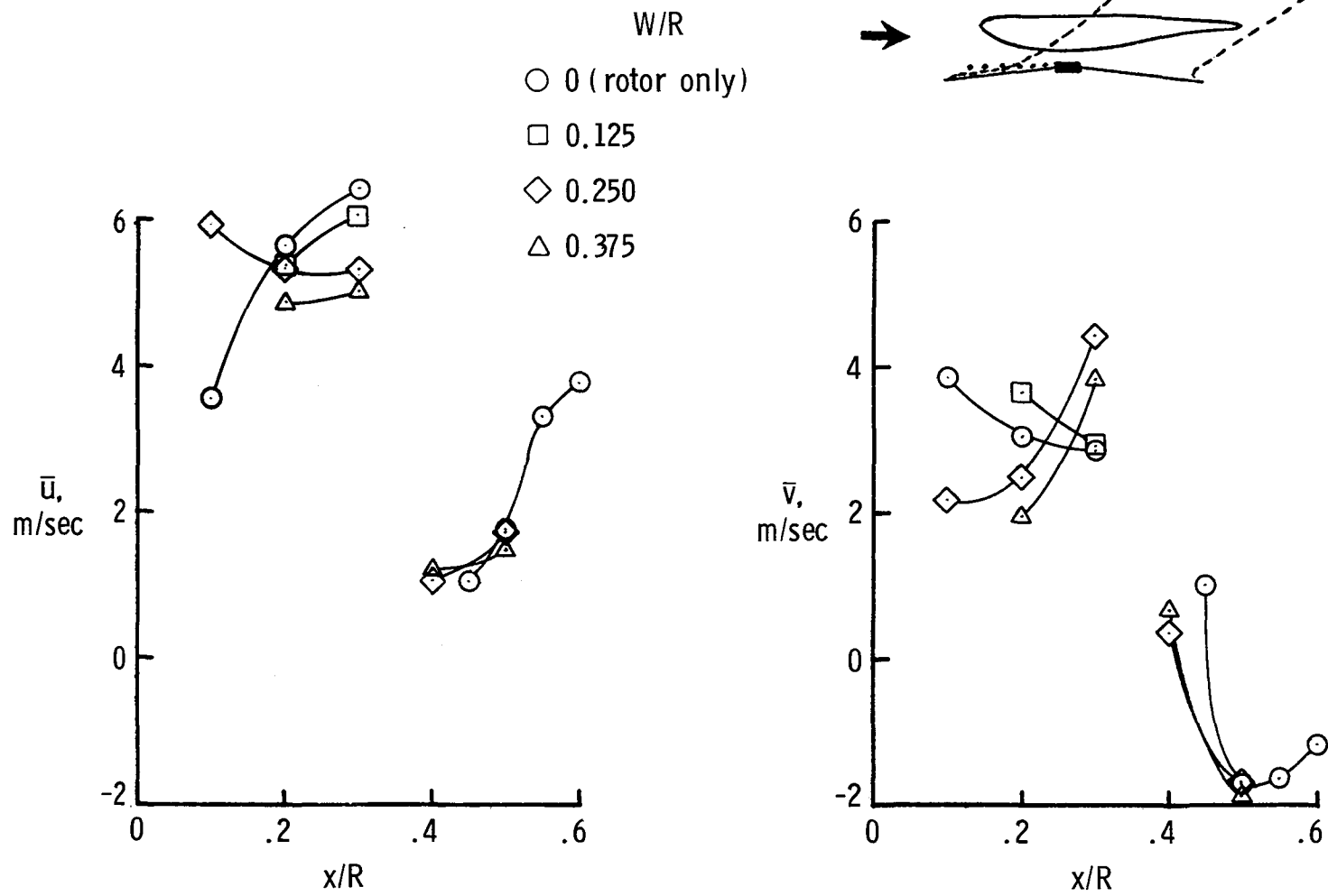
Figure 7.- Effect of body width on velocities measured. y/R = 0; z/R = 0; S/R = 0.224.

S/R

○ ∞ (rotor only)

□ 0.324

◇ 0.275

△ 0.224

(a) W/R = 0.125.
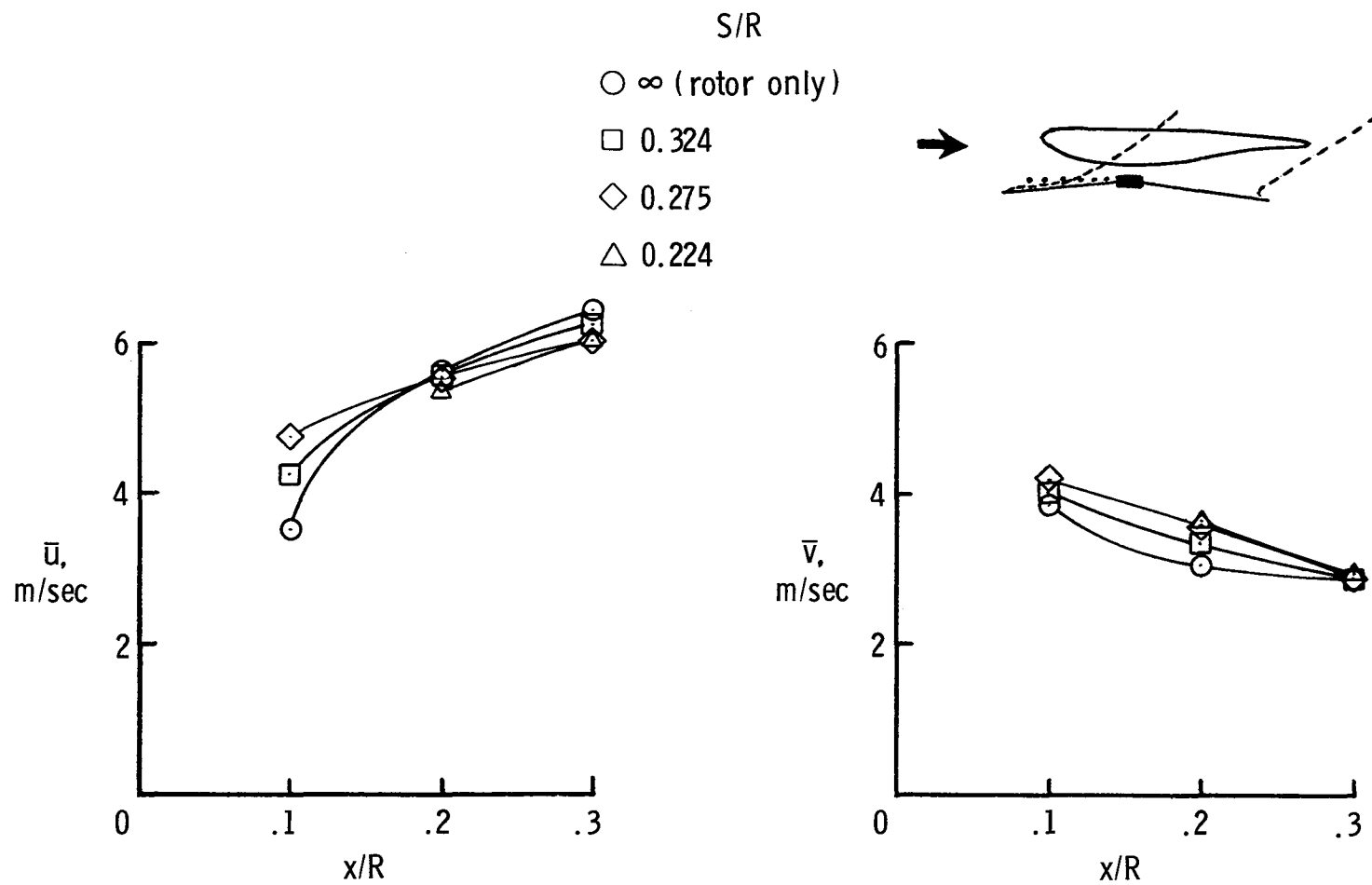
Figure 8.- Effect of rotor-body spacing on velocities measured. y/R = 0; z/R = 0.
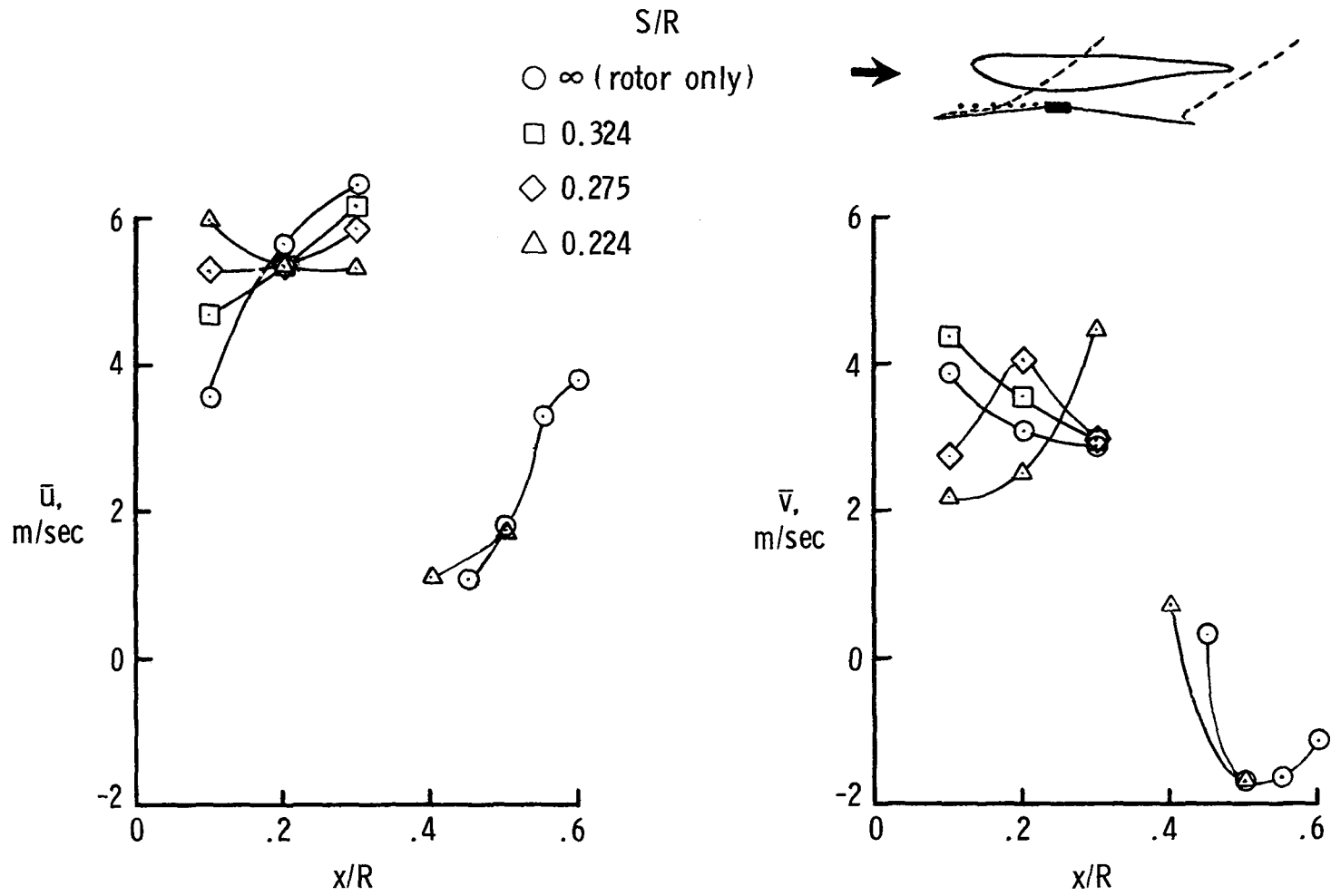
(b) W/R = 0.250.

Figure 8.- Continued.

S/R

○ ∞ (rotor only)

□ 0.324

◇ 0.275

△ 0.224
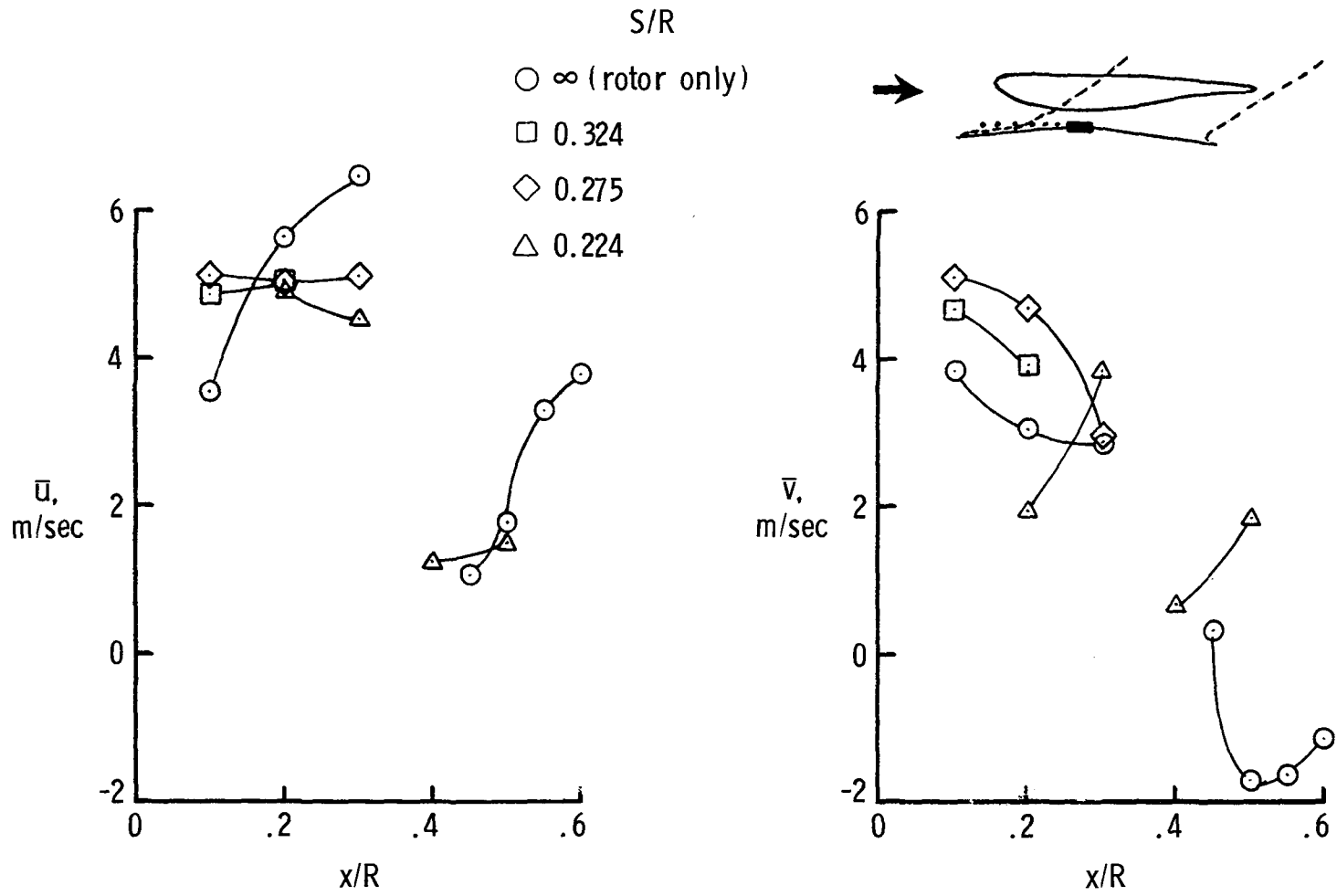
(c)   W/R = 0.375.

Figure 8.- Concluded.
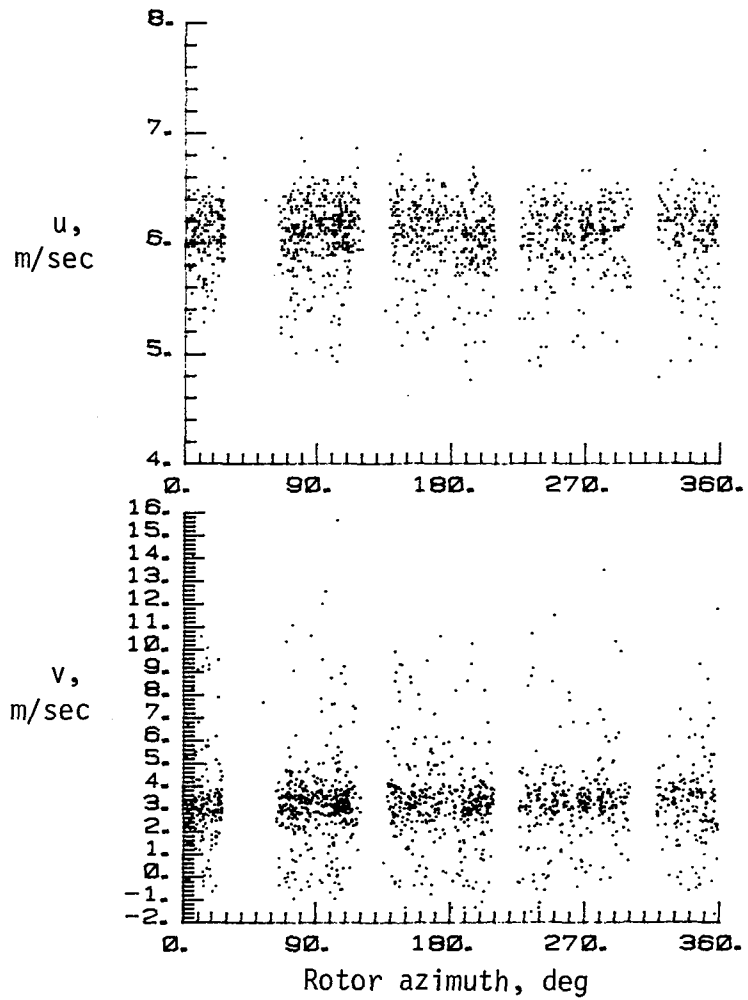
(a) Velocity components as a
    function of azimuth.
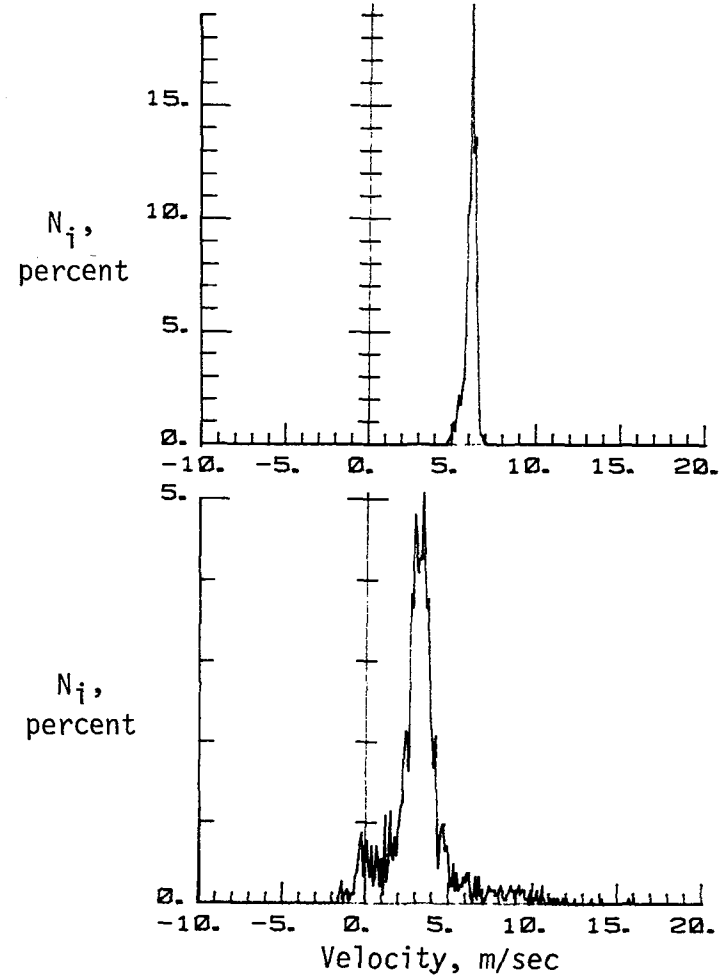
(b) Histograms of velocity components.

Figure 9.- Laser velocimeter measurements in rotor-only wake. x/R = 0.3;
y/R = 0;   z/R = 0.043.
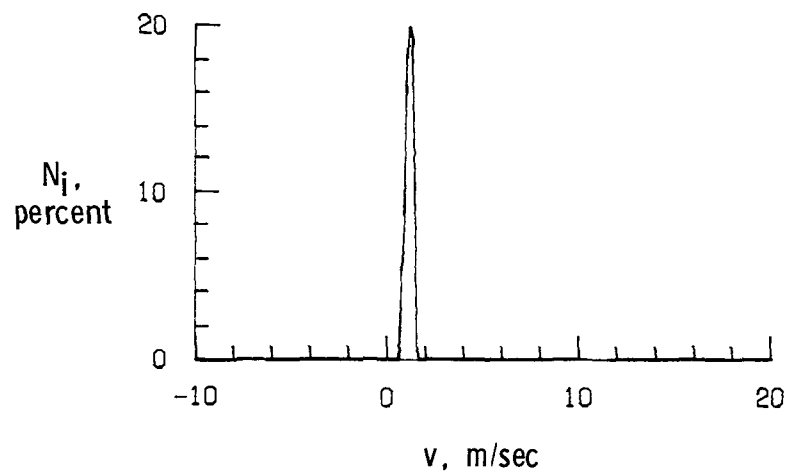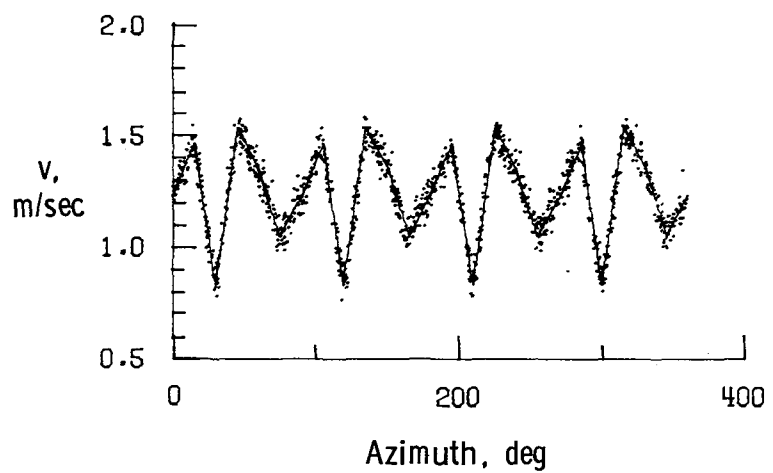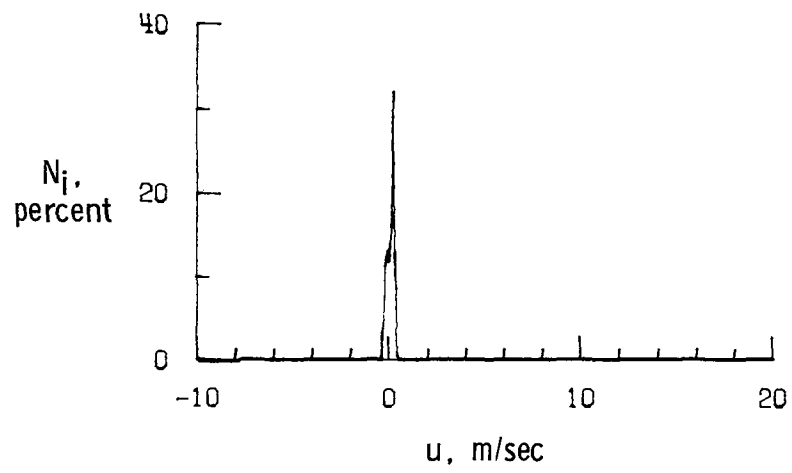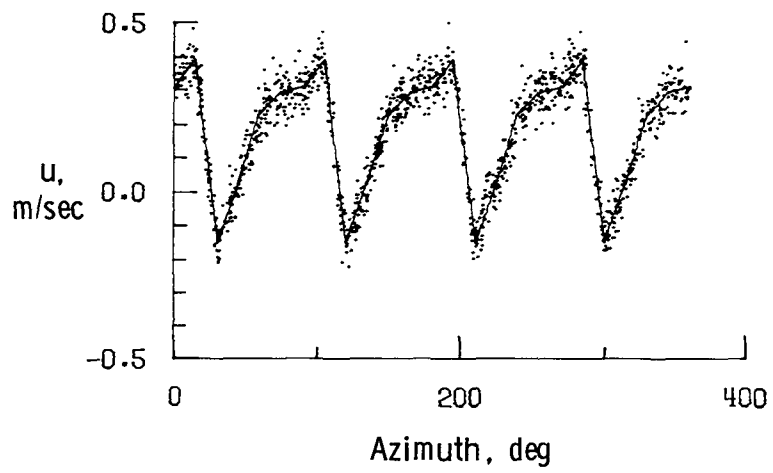
(a) Closed tunnel, 1 percent random tunnel turbulence.

Figure 10.- Simulated laser velocimeter values obtained using theoretically determined velocity time history.
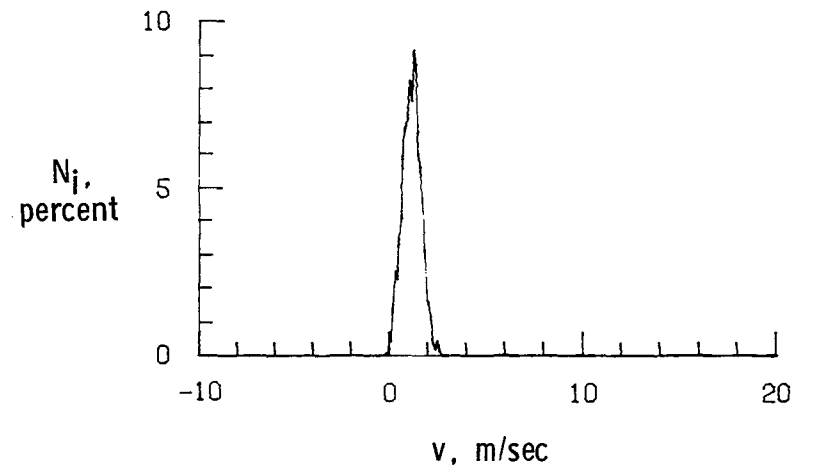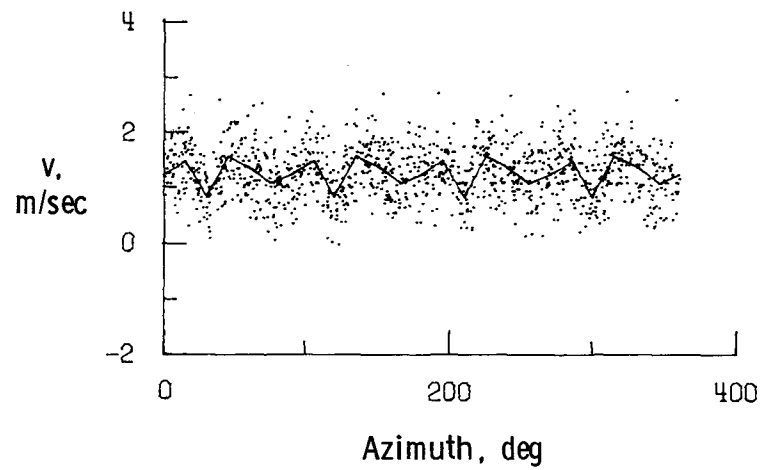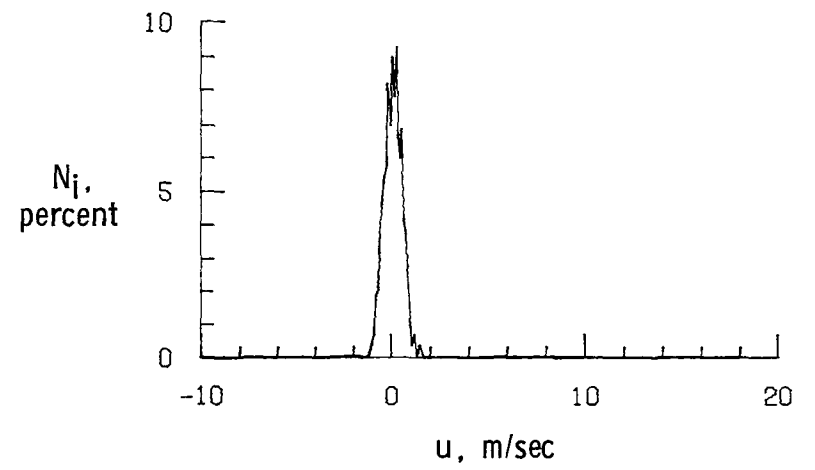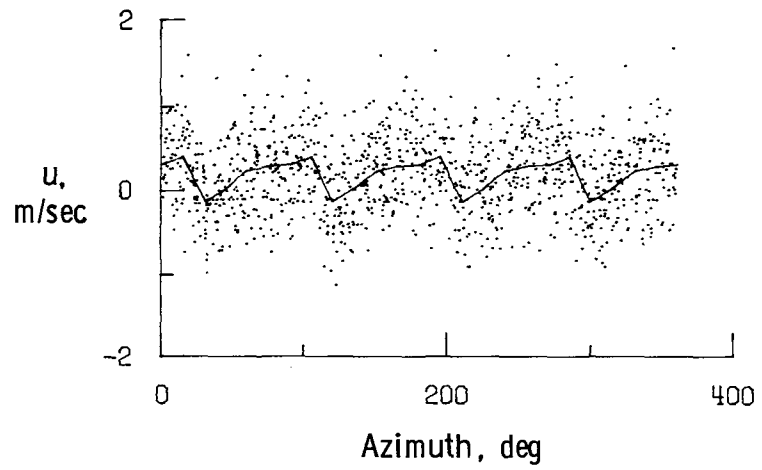
(b) Closed tunnel, 10 percent random tunnel turbulence.

Figure 10.- Continued.
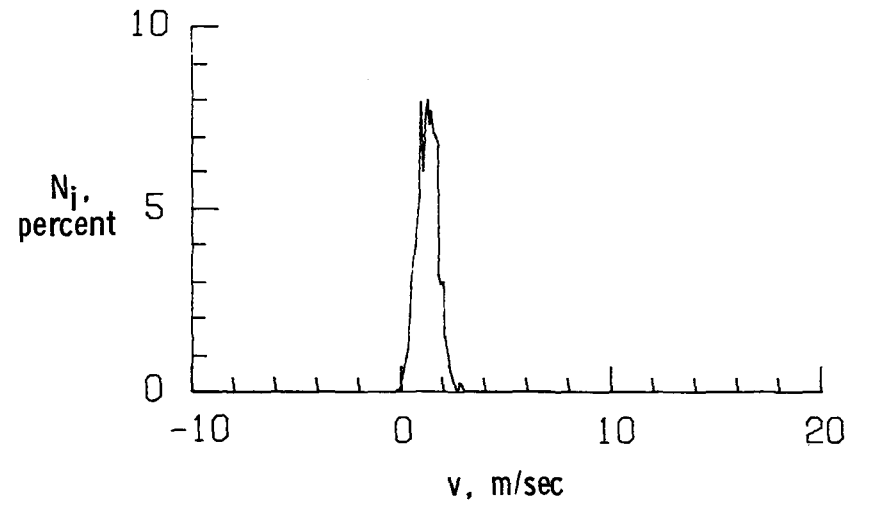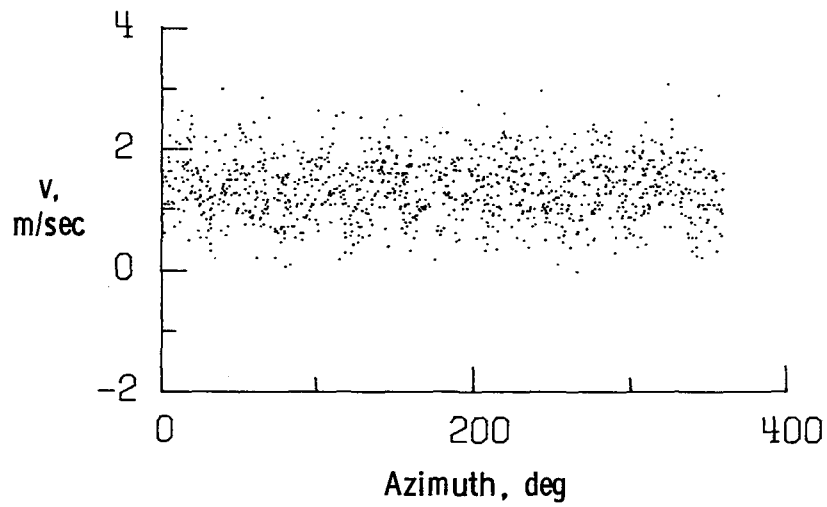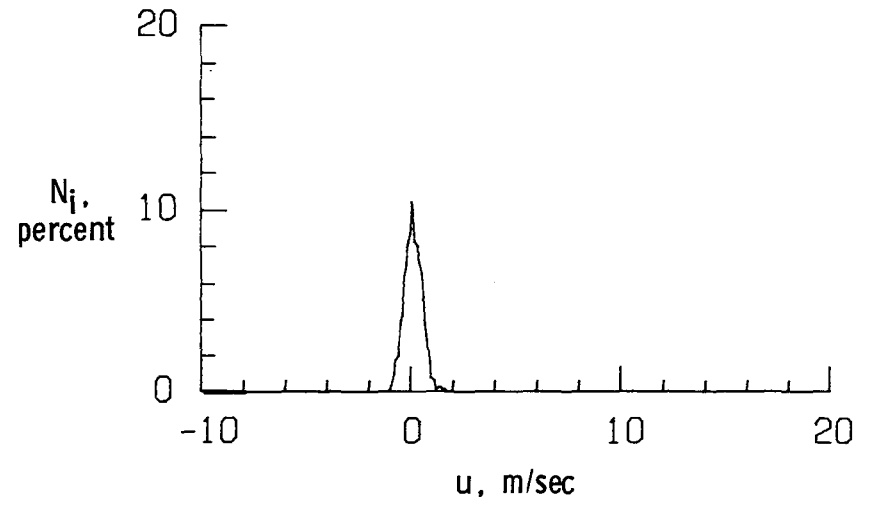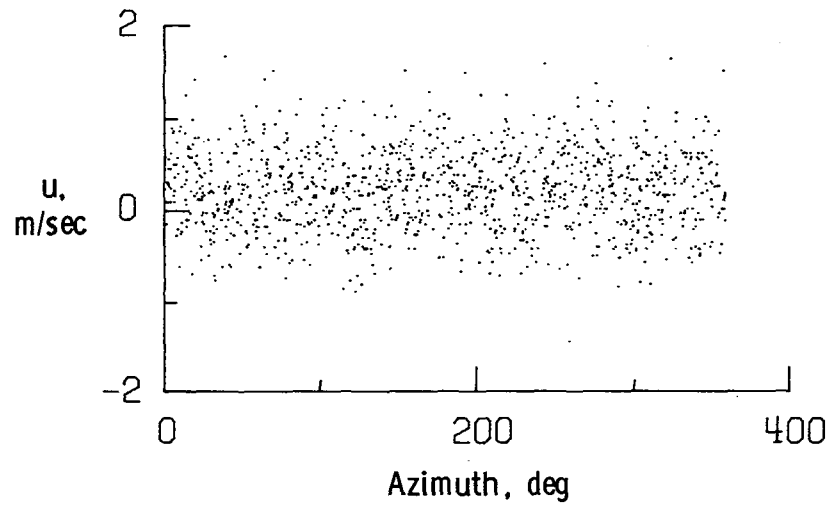
(c) Open tunnel, 10 percent periodic tunnel turbulence.

Figure 10.- Concluded.
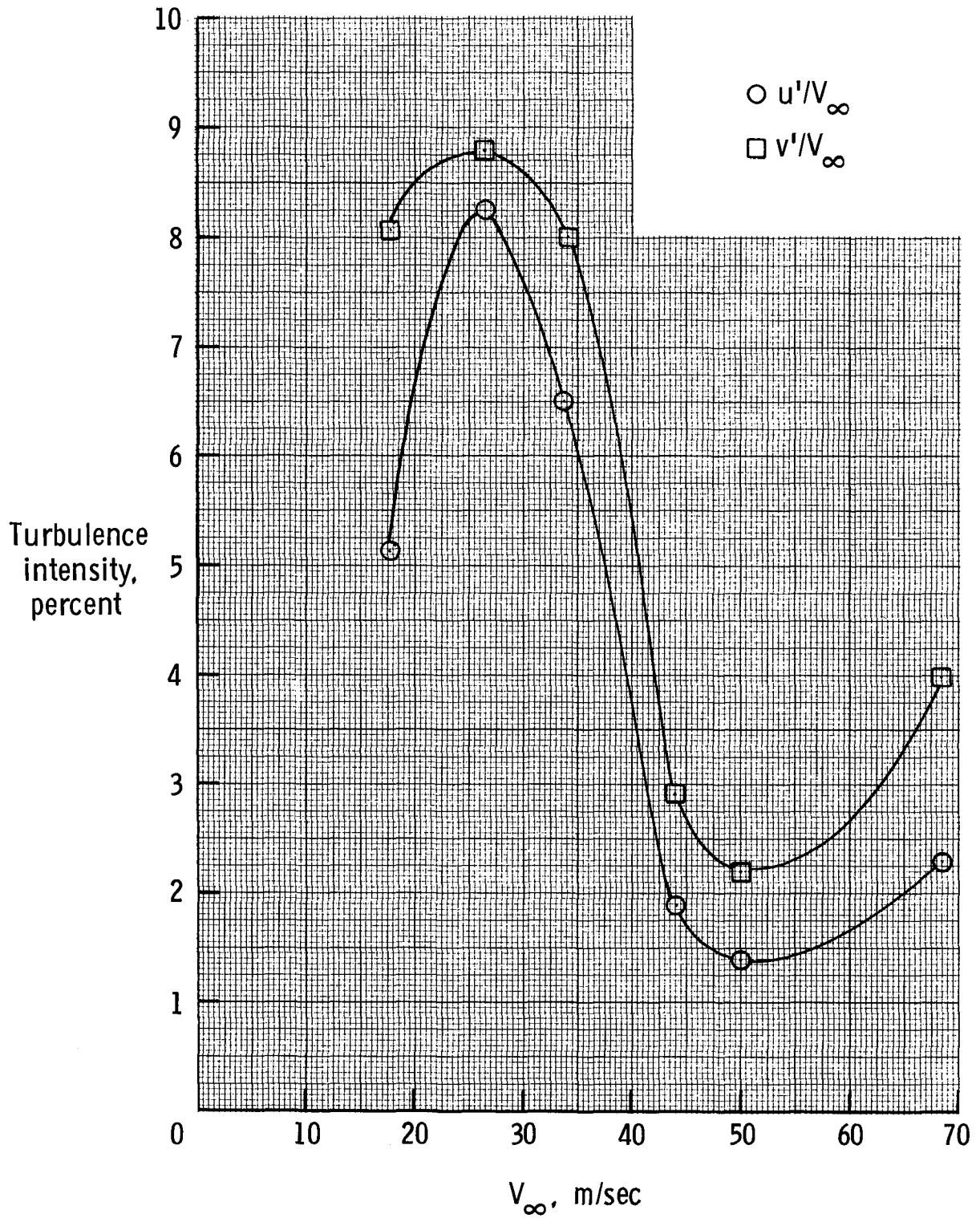
Figure 11.- Turbulence intensity characteristics of open test section of Langley 4- by 7-Meter Tunnel.
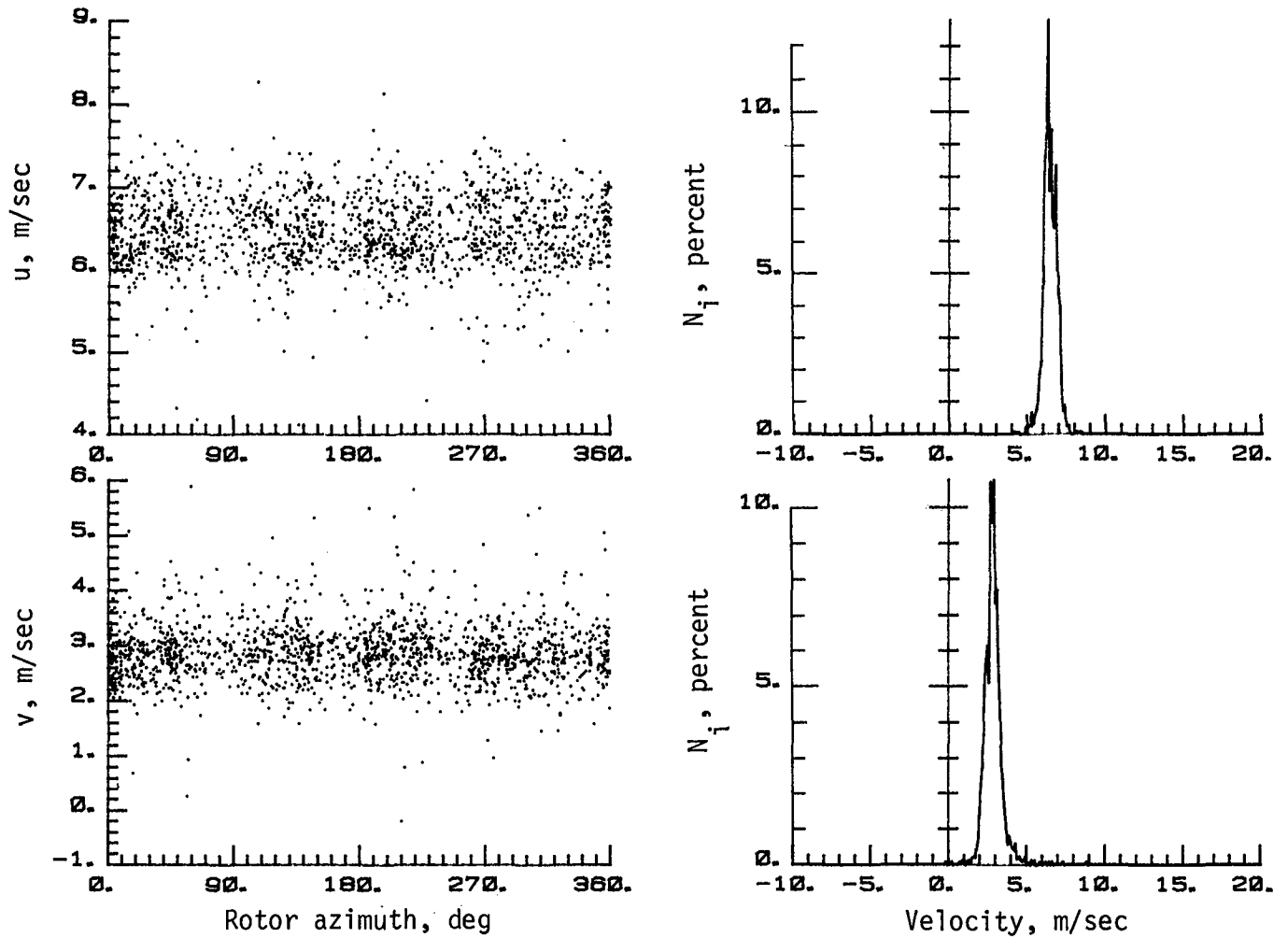
(a) Velocity components as a function of azimuth.

(b) Histograms of velocity components.

Figure 12.- Laser velocimeter measurements in rotor-only wake. $x/R = 0.3$; $y/R = 0$; $z/R = 0$.

28
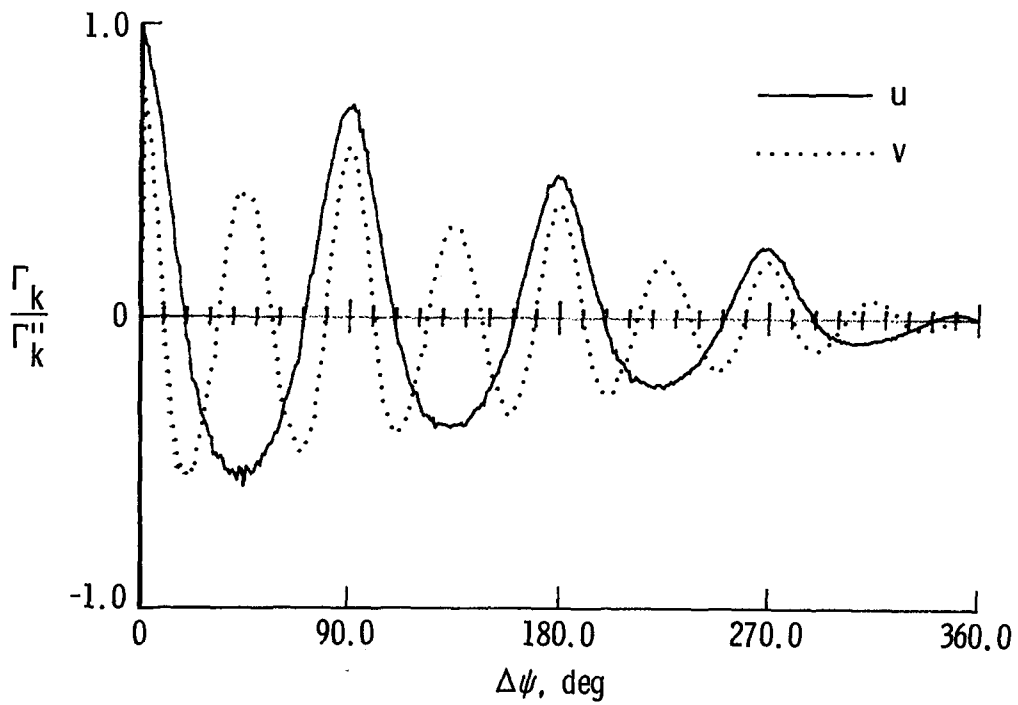
(a) Autocovariance function.
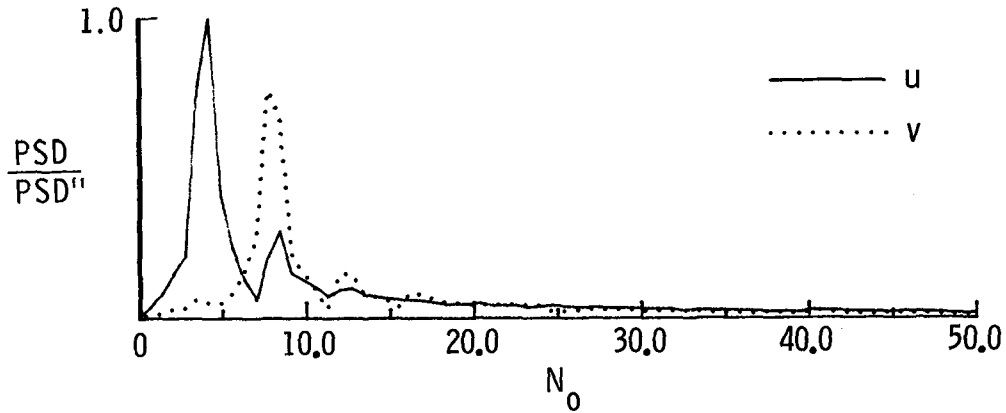
(b) Power spectral density.

Figure 13.- Spectral transformation of simulated laser velocimeter values obtained using theoretically determined velocity time history. Closed tunnel; random tunnel turbulence.
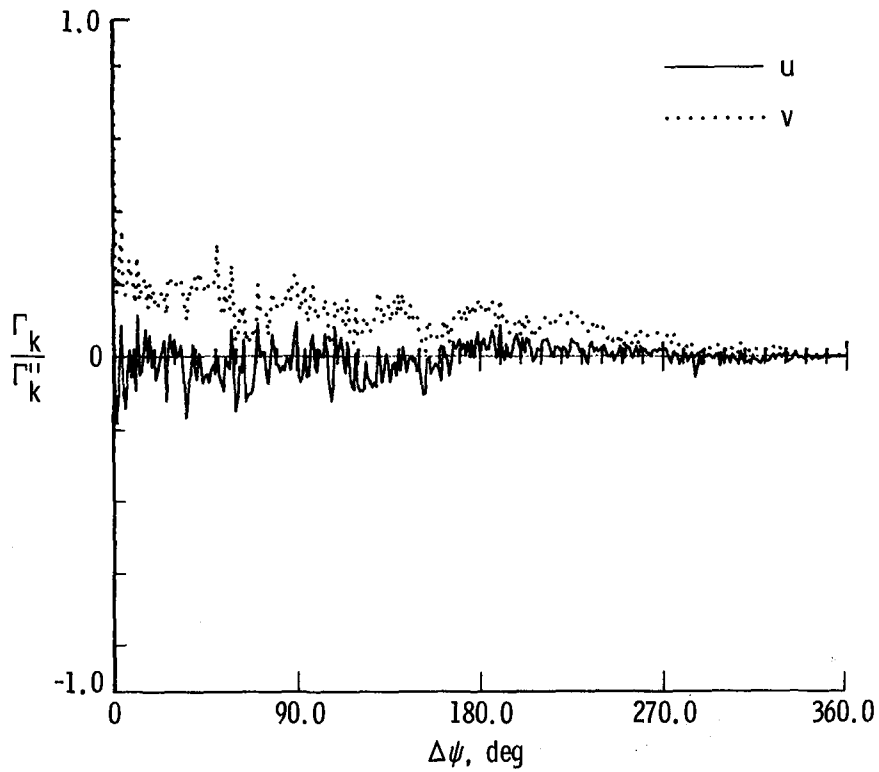
(a) Autocovariance function.
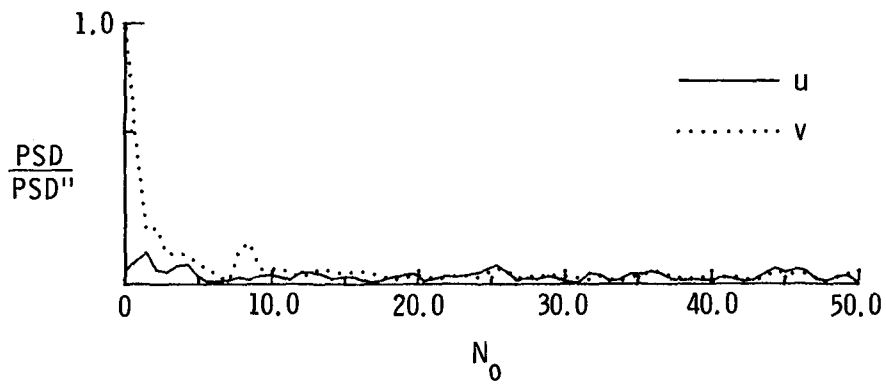
(b) Power spectral density.

Figure 14.- Spectral transformation of simulated laser velocimeter values obtained using theoretically determined velocity time history. Open tunnel; periodic tunnel turbulence.
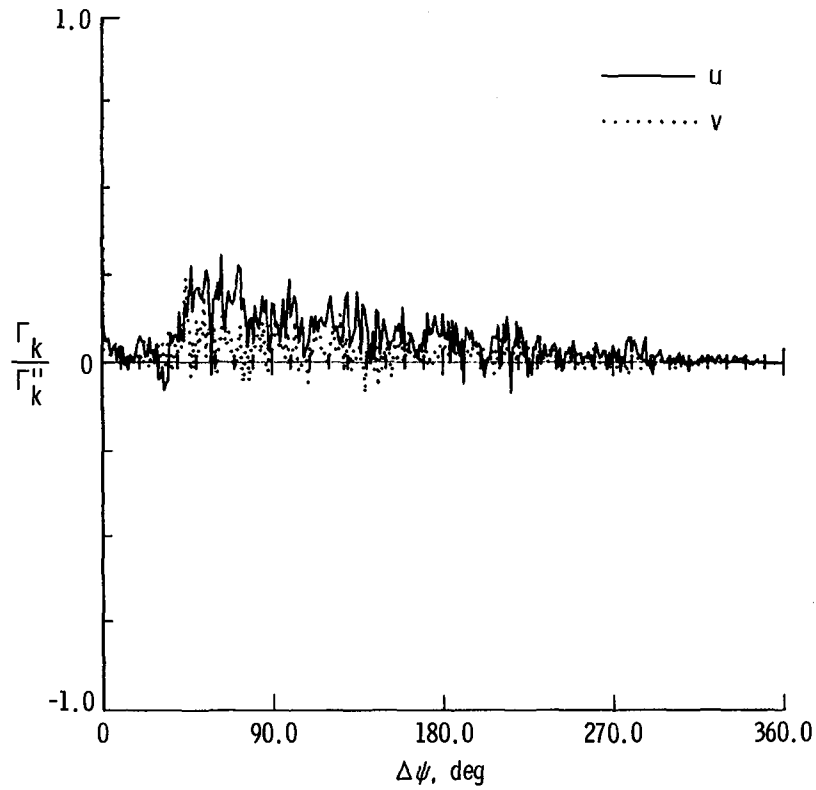
(a) Autocovariance function.
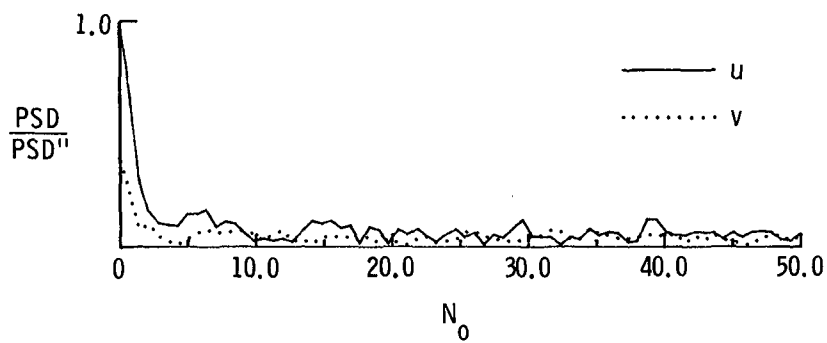
(b) Power spectral density.

Figure 15.- Spectral transformation of laser velocimeter measurements in rotor-only wake. $x/R = 0.3$; $y/R = 0$; $z/R = 0$.

APPENDIX

SAMPLE VELOCITY MEASUREMENTS

      Samples of each velocity measurement obtained in this investigation are given in
this appendix. Each figure represents one buffer load (out of 30) for each rotor
configuration and position tested. Each dot in the plots represents a single mea-
surement, and since the data system was restricted to coincidence (data accepted only
when obtained by both u and v counters simultaneously), each v component dot
has a corresponding u component dot. Histograms, or probability density functions,
are presented for each set of u- and v-component measurements. A sample interpreta-
tion of these histograms can be found in appendix B of reference 10.

      The presentation of the figures for the data acquired in this investigation is
given in table AI.

APPENDIX

TABLE AI.- MEASUREMENT LOCATIONS

Rotor-fuselage configuration	x/R	y/R	z/R	Figure
Rotor only				
	0.1	0	0	A1(a)
	.2	.1	0	A1(b)
	.2	-.1	0	A1(c)
	.2	0	0	A1(d)
	.3	0	0	A1(e)
	.45	0	0	A1(f)
	.5	0	0	A1(g)
	.55	0	0	A1(h)
	.6	0	0	A1(i)
	.3	0	-.01	A1(j)
	.3	0	.01	A1(k)
	.3	0	.027	A1(l)
	.3	0	.04	A1(m)
	.3	0	.043	A1(n)
0.125R body				
S/R = 0.224	0.2	0	0	A2(a)
S/R = 0.224	.3	0	0	A2(b)
S/R = 0.275	.1	0	0	A2(c)
↓	.2	-.1	0	A2(d)
	.2	0	0	A2(e)
	.3	0	0	A2(f)
S/R = 0.324	.1	0	0	A2(g)
	.2	.1	0	A2(h)
	.2	-.1	0	A2(i)
	.2	0	0	A2(j)
↓	.3	0	0	A2(k)
0.250R body				
S/R = 0.224	0.1	0	0	A3(a)
	.2	.1	0	A3(b)
	.2	-.1	0	A3(c)
	.2	0	0	A3(d)
	.3	0	0	A3(e)
	.4	0	0	A3(f)
	.5	0	0	A3(g)
S/R = 0.275	.1	0	0	A3(h)
	.2	.1	0	A3(i)
	.2	-.1	0	A3(j)
	.2	0	0	A3(k)
	.3	0	0	A3(l)
S/R = 0.324	.1	0	0	A3(m)
	.2	.1	0	A3(n)
	.2	0	0	A3(o)
↓	.3	0	0	A3(p)
0.375R body				
S/R = 0.224	0.2	0.1	0	A4(a)
	.2	-.1	0	A4(b)
	.2	0	0	A4(c)
	.3	0	0	A4(d)
	.4	0	0	A4(e)
	.5	0	0	A4(f)
S/R = 0.275	.1	0	0	A4(g)
	.2	.1	0	A4(h)
	.2	-.1	0	A4(i)
	.2	0	0	A4(j)
S/R = 0.324	.1	0	0	A4(k)
	.2	.1	0	A4(l)
	.2	-.1	0	A4(m)
↓	.2	0	0	A4(n)
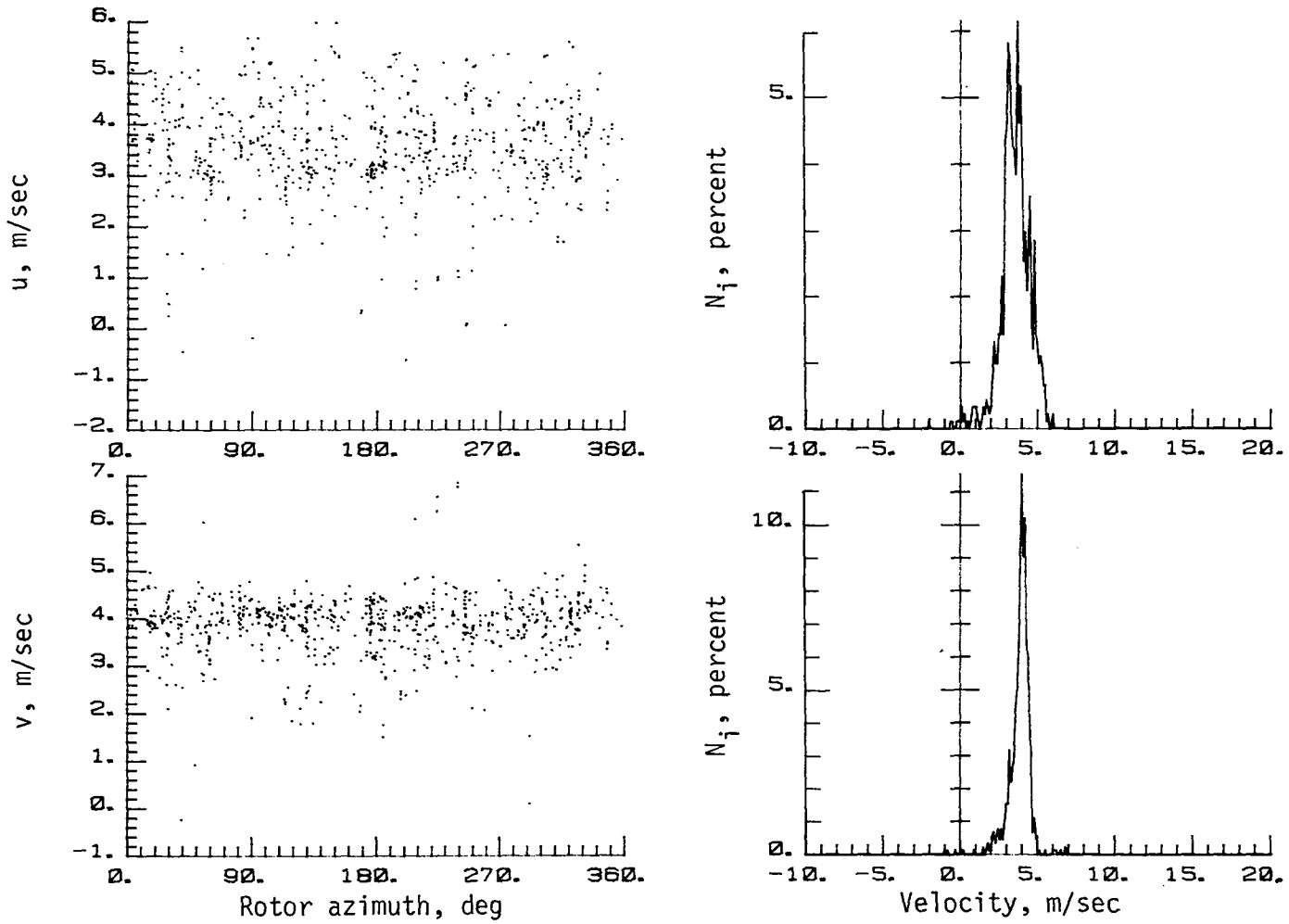
(a)   x/R = 0.1;   y/R = 0;   z/R = 0.

Figure A1.- LV data for rotor-only test.
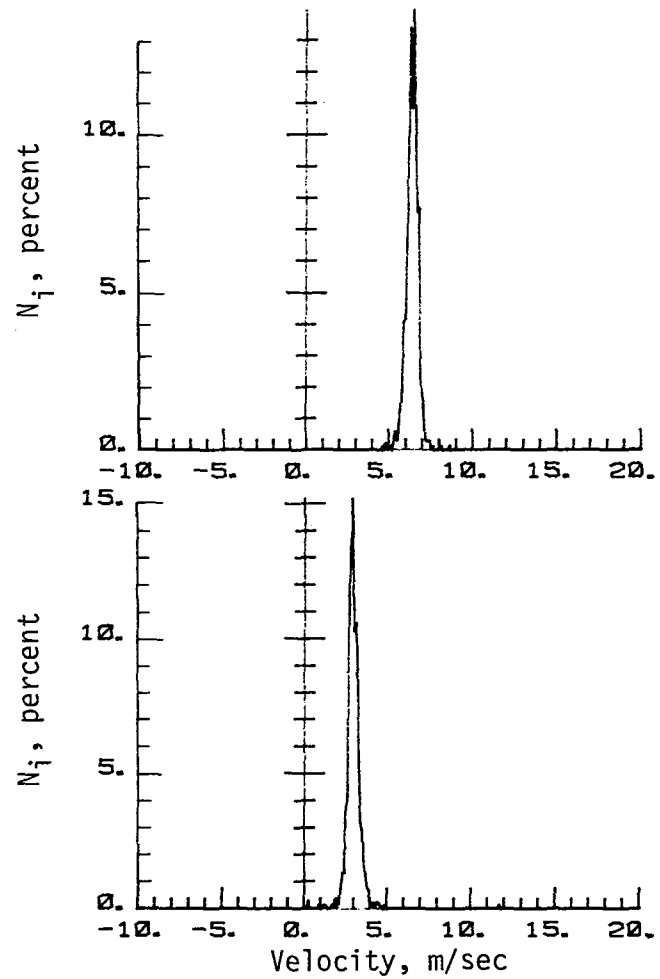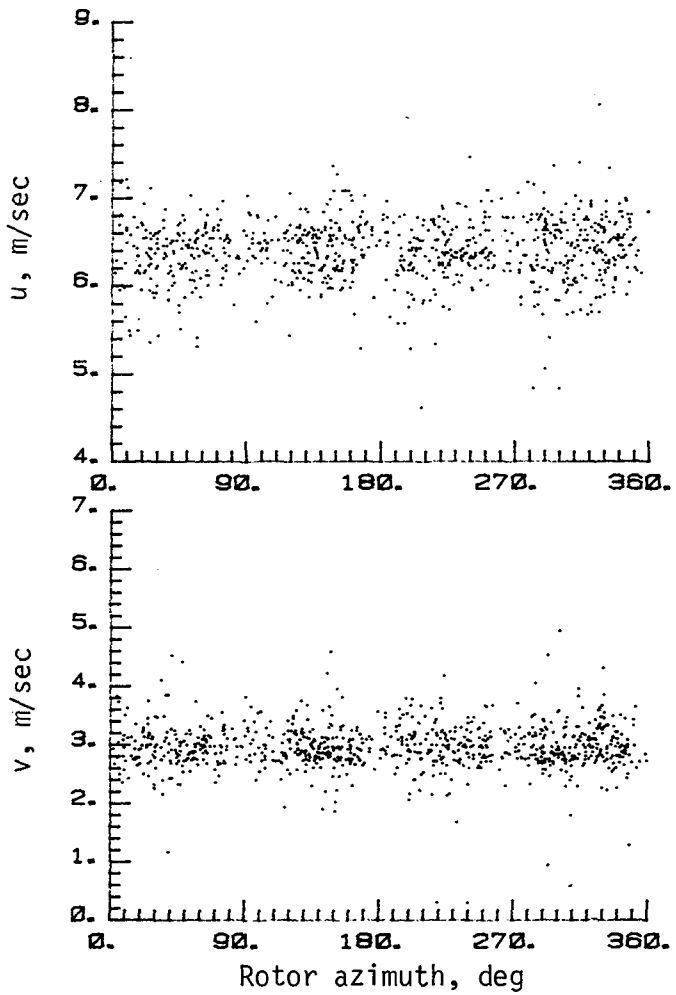
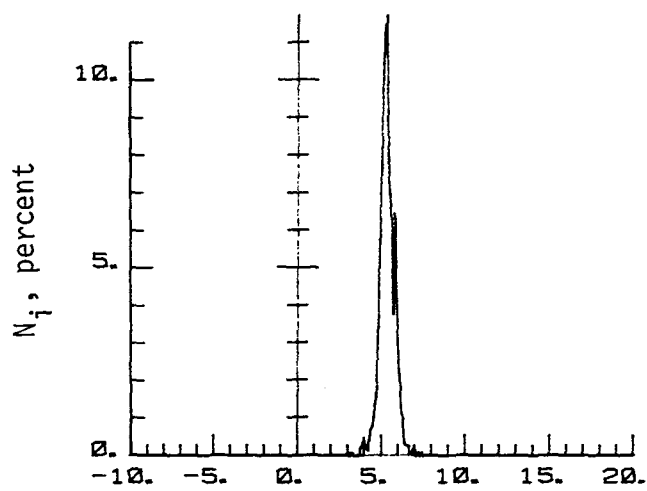(b)   x/R = 0.2;   y/R = 0.1;   z/R = 0.

Figure A1.- Continued.
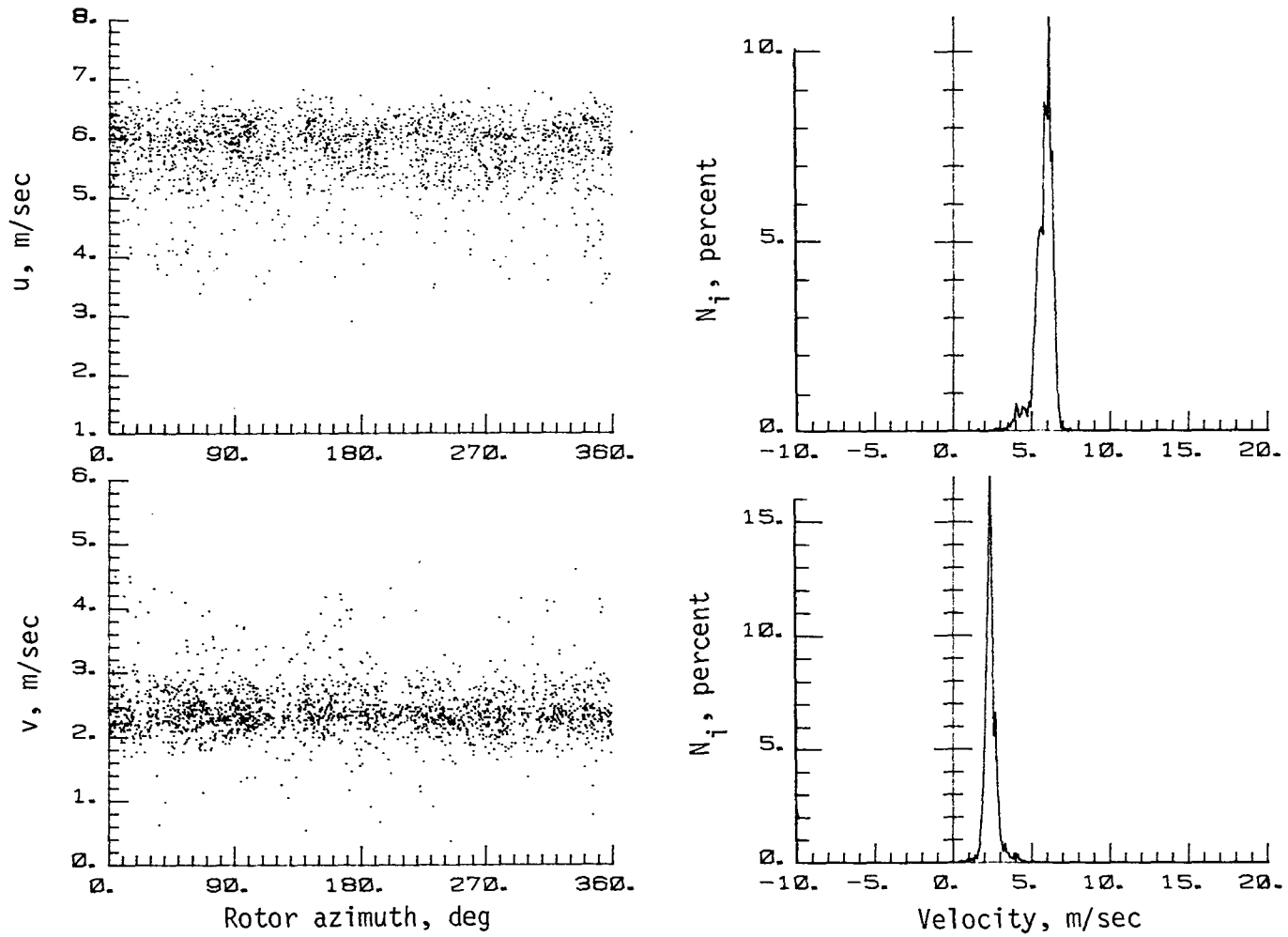
(c) $x/R = 0.2$; $y/R = -0.1$; $z/R = 0$.

Figure A1.- Continued.
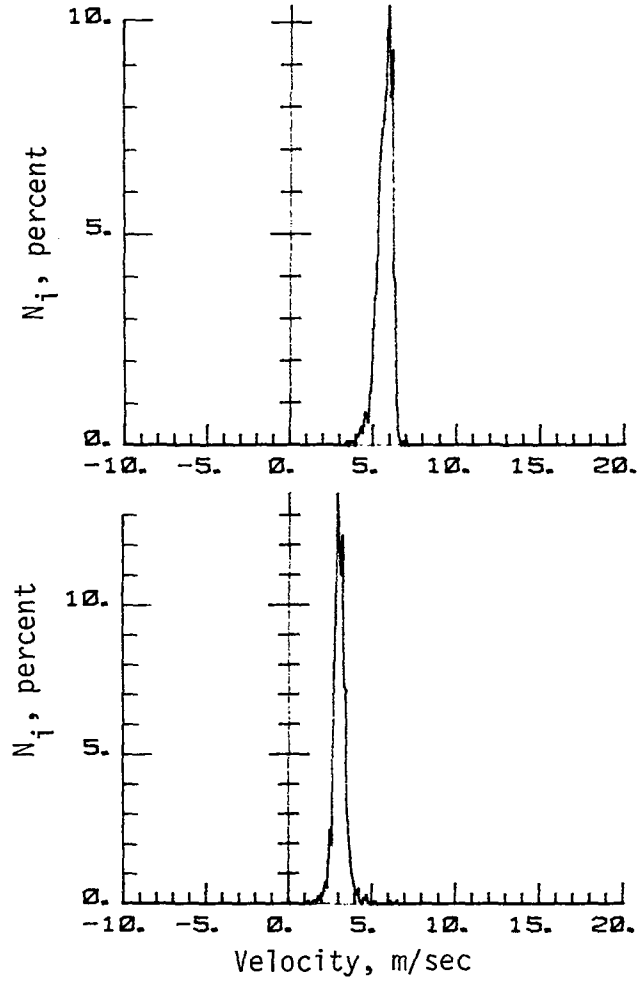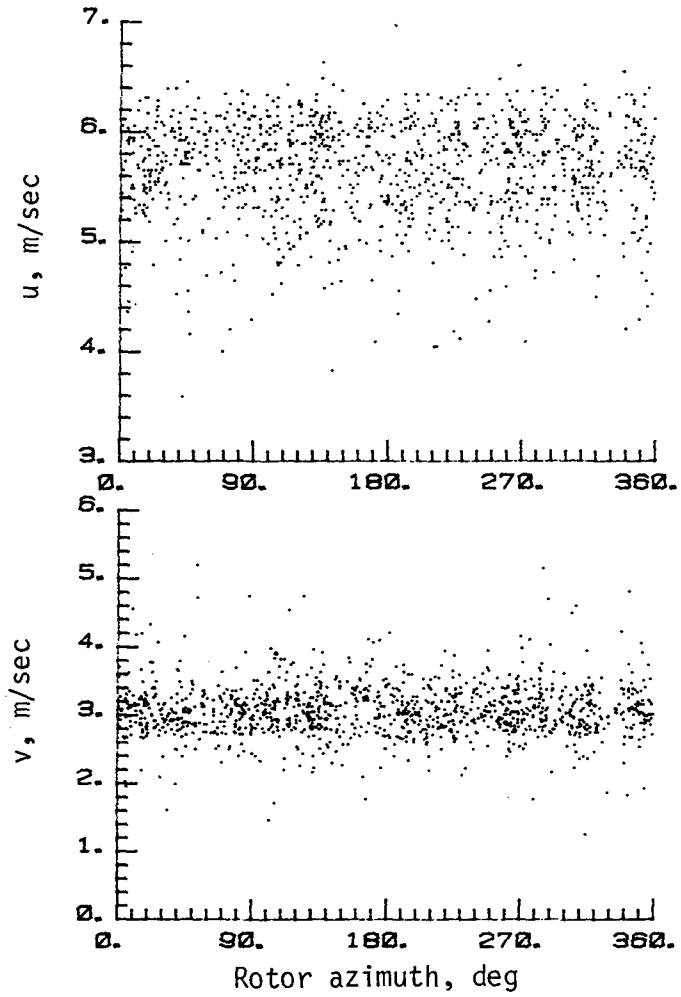
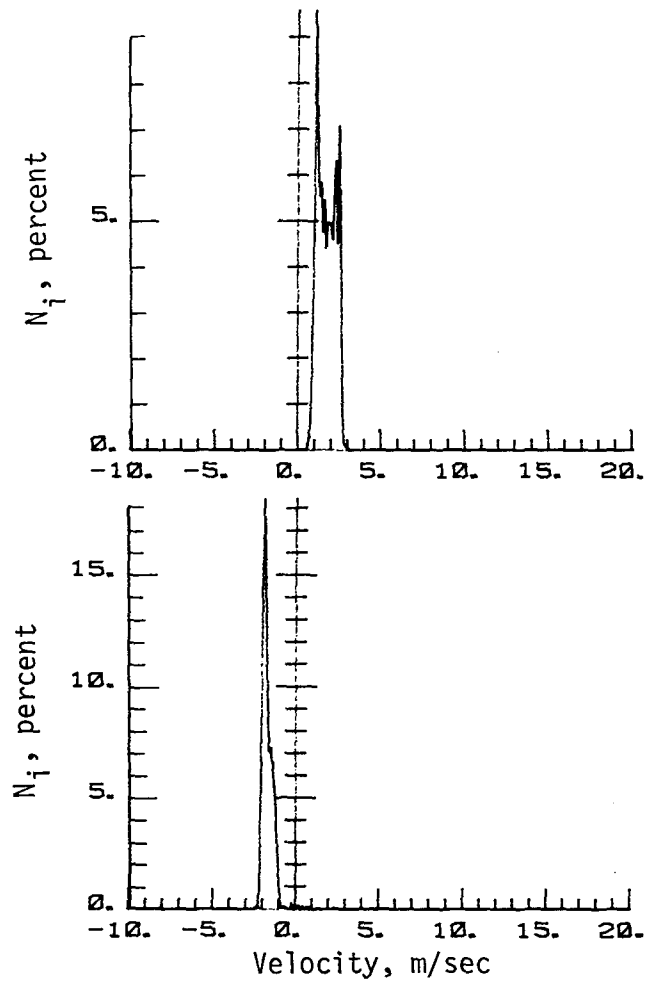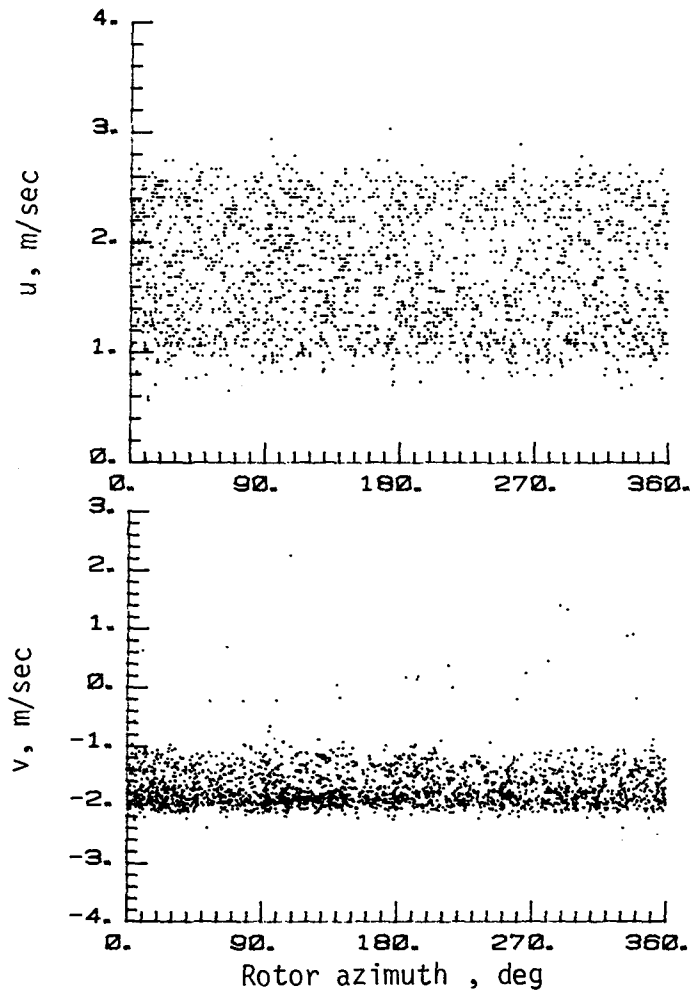(d)   x/R = 0.2;   y/R = 0;   z/R = 0.

Figure A1.- Continued.
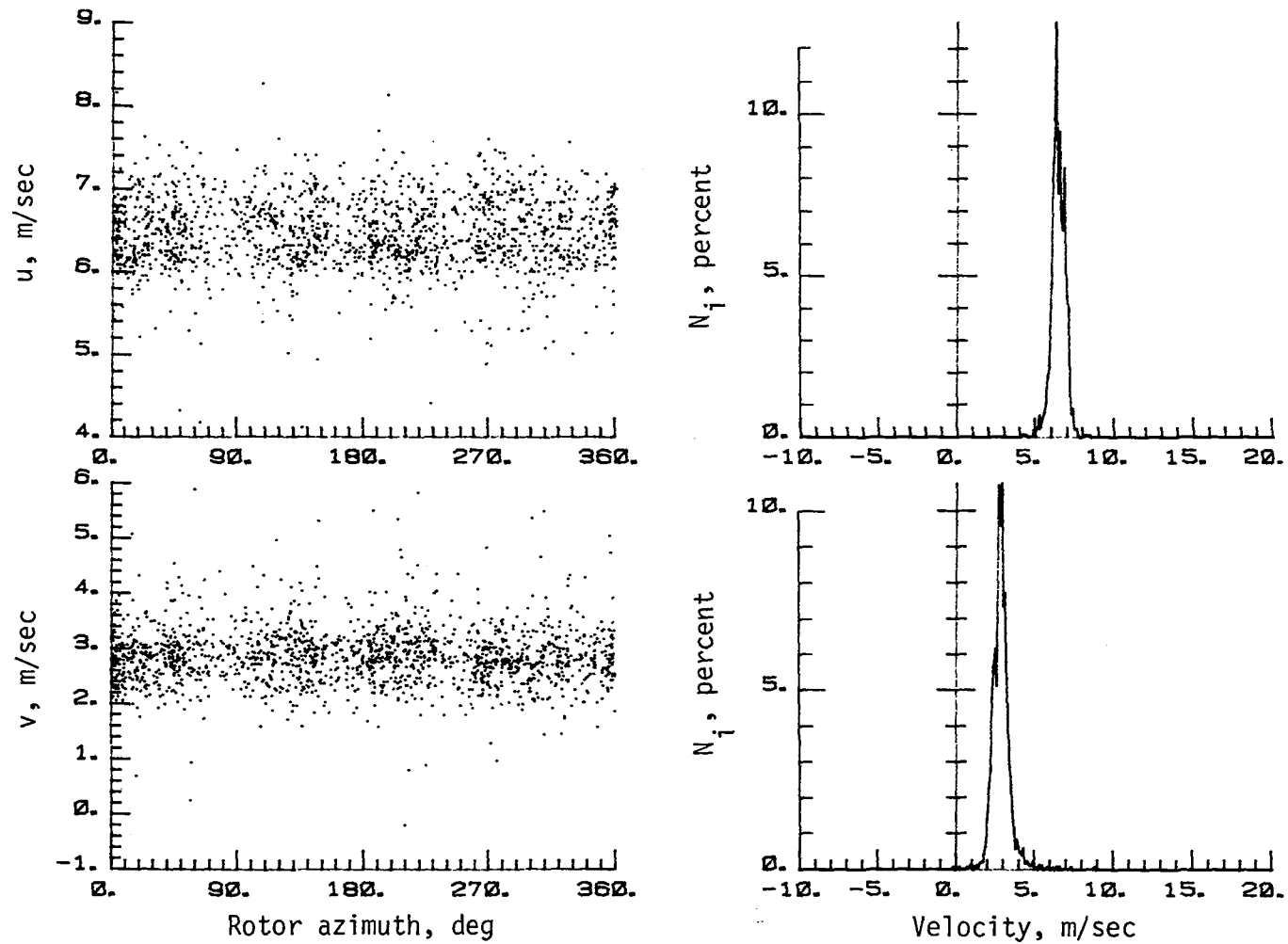
(e) x/R = 0.3;   y/R = 0;   z/R = 0.

Figure A1.- Continued.
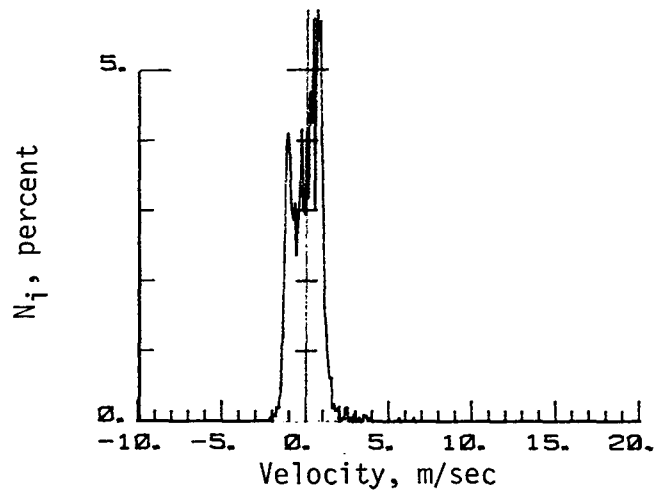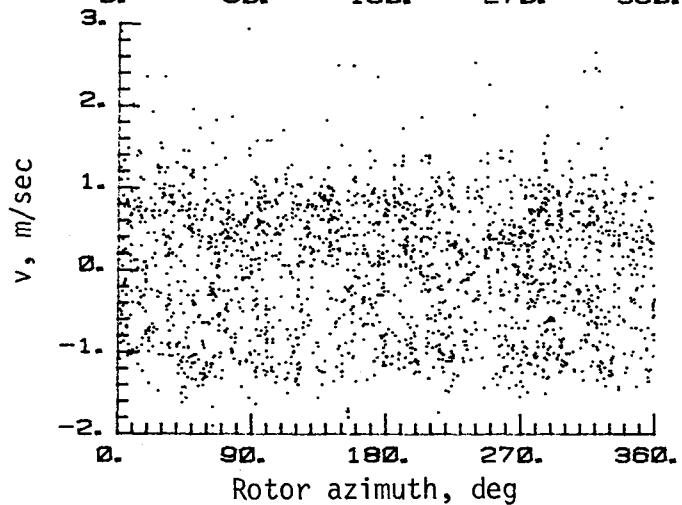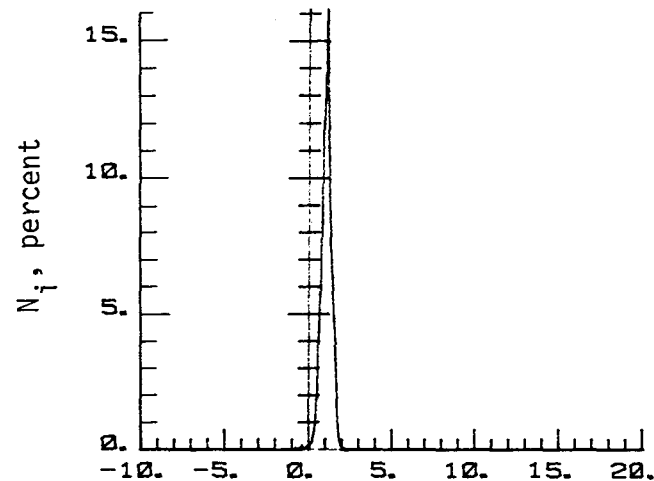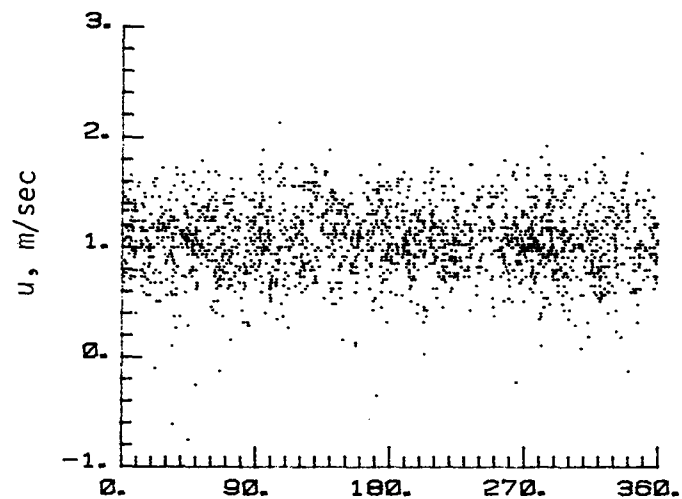
(f) x/R = 0.45; y/R = 0; z/R = 0.

Figure A1.- Continued.
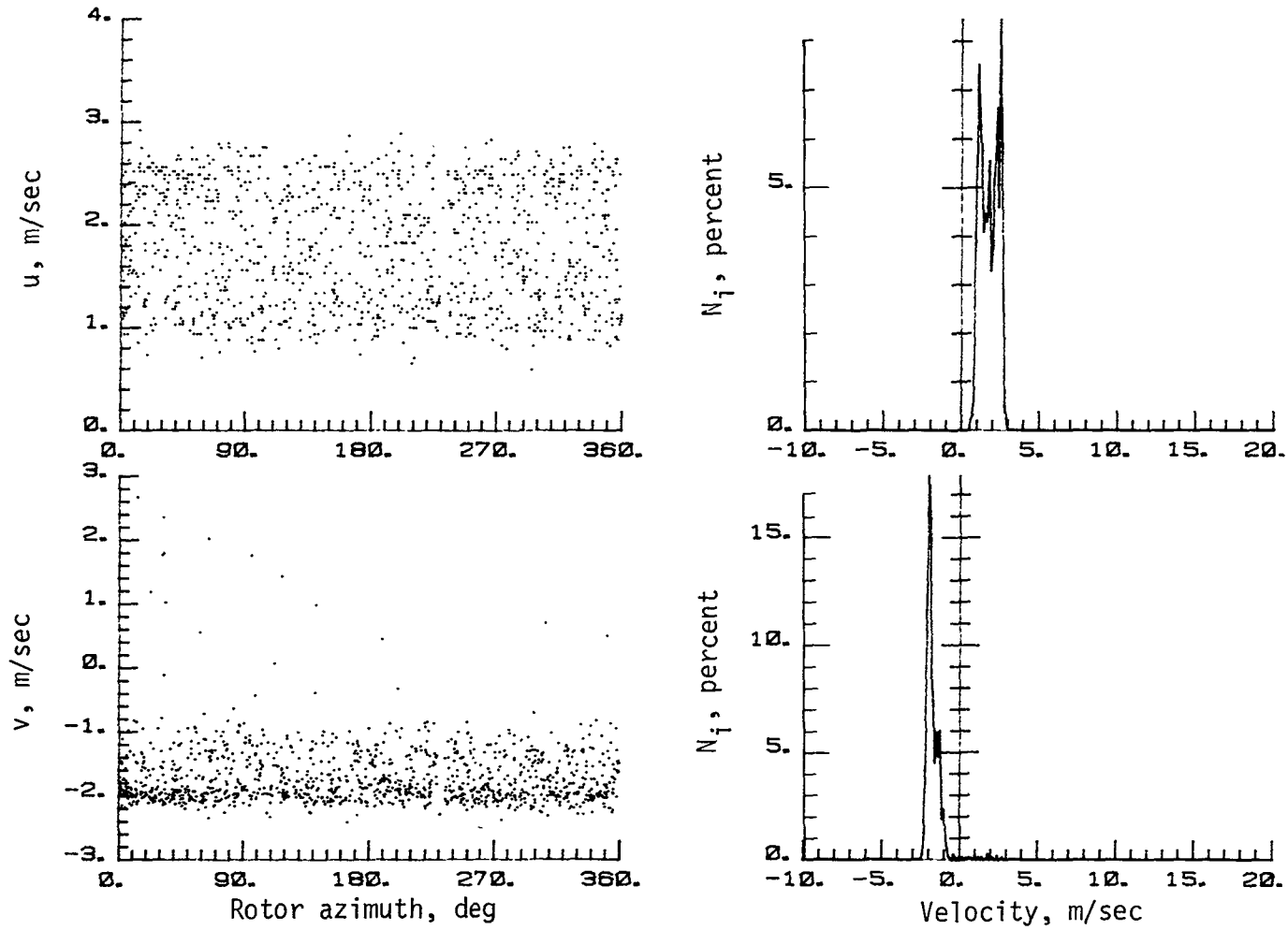
(g)   x/R = 0.5;   y/R = 0;   z/R = 0.

Figure A1.- Continued.
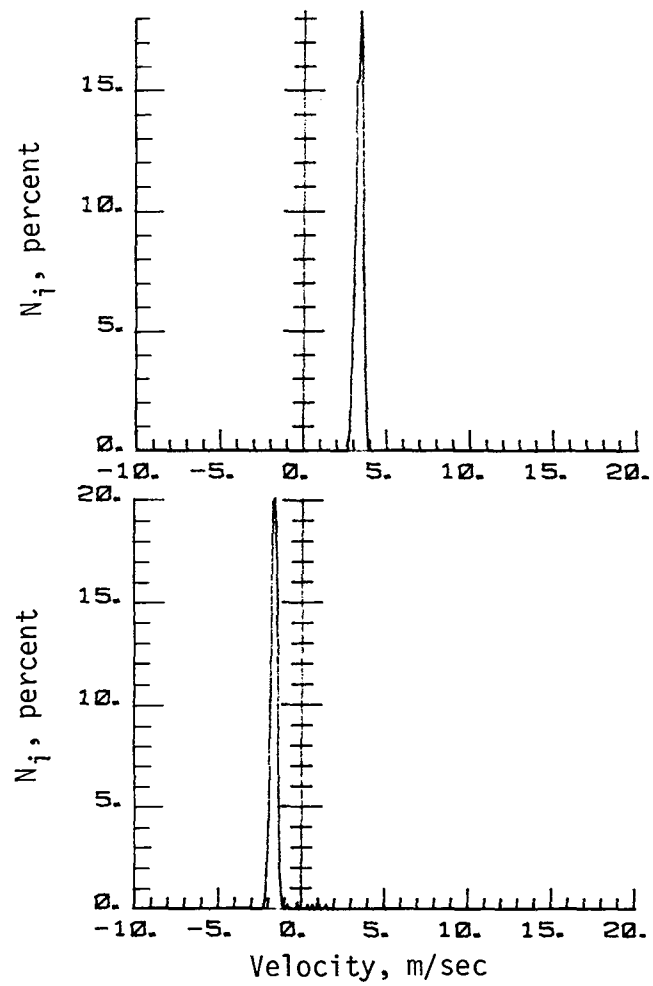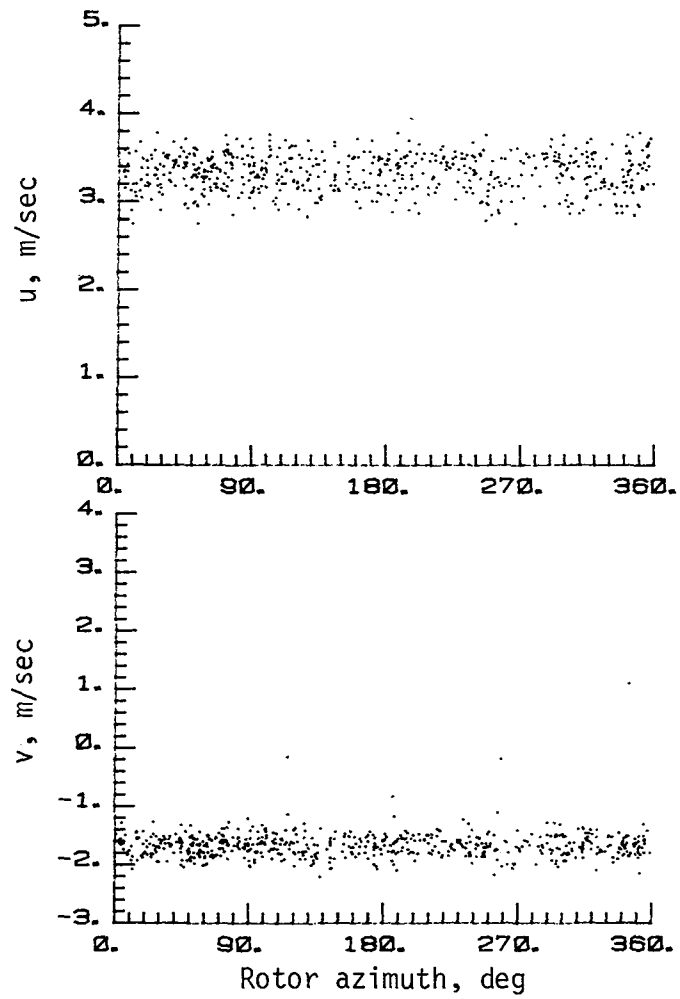
(h)   x/R = 0.55;   y/R = 0;   z/R = 0.

Figure A1.- Continued.
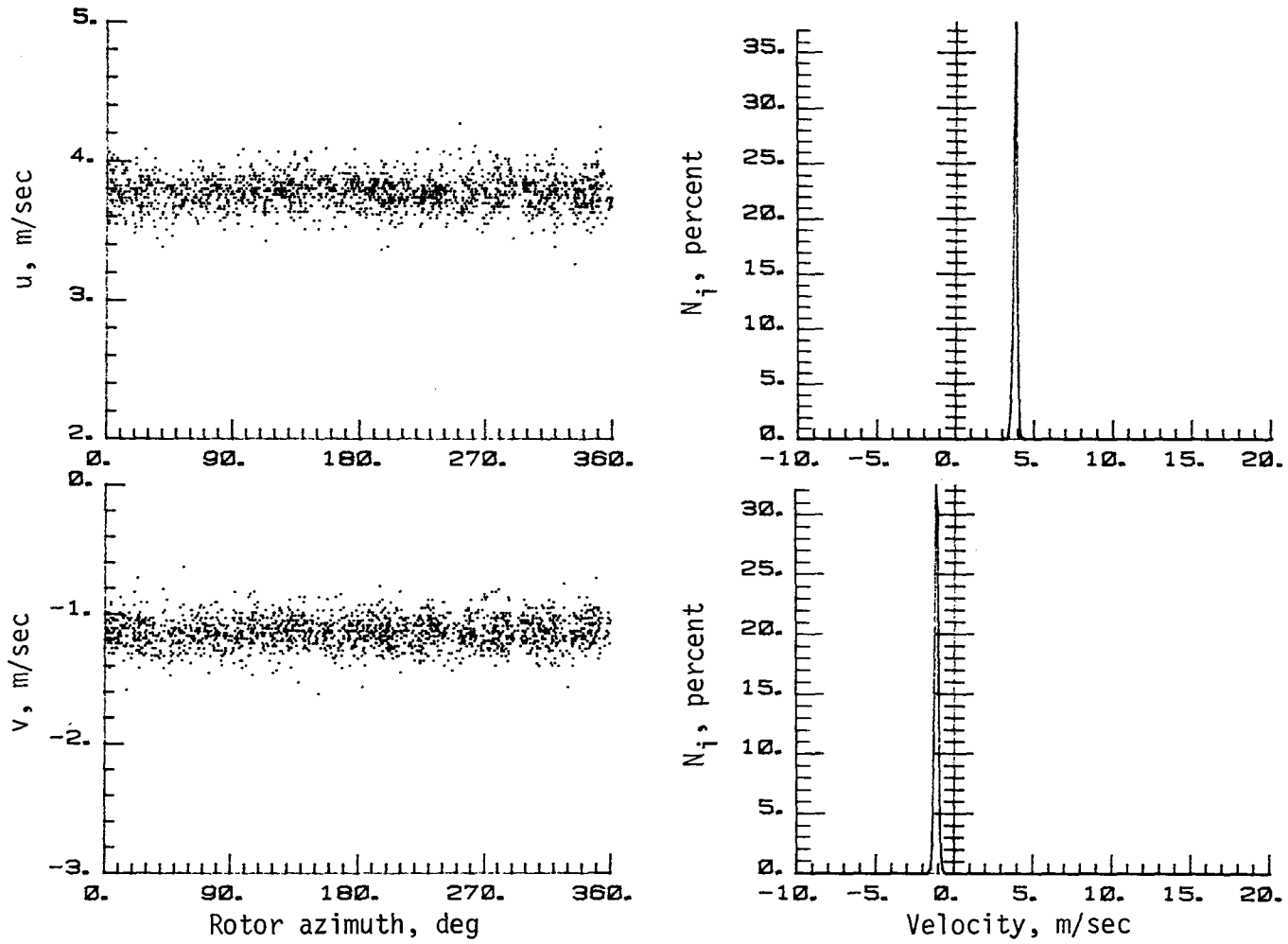
(i)   x/R = 0.6;   y/R = 0;   z/R = 0.

Figure A1.- Continued.
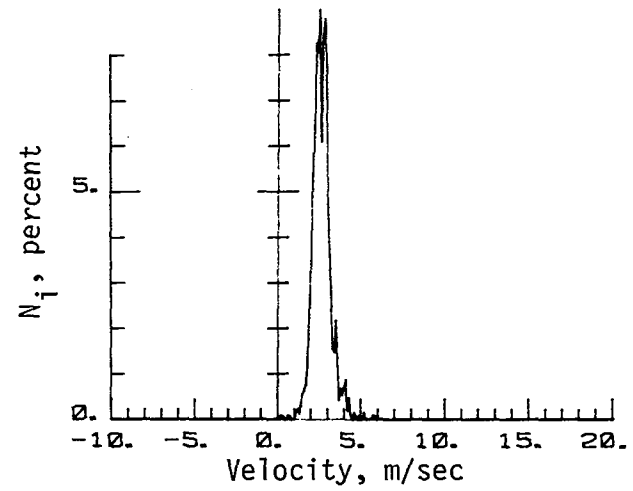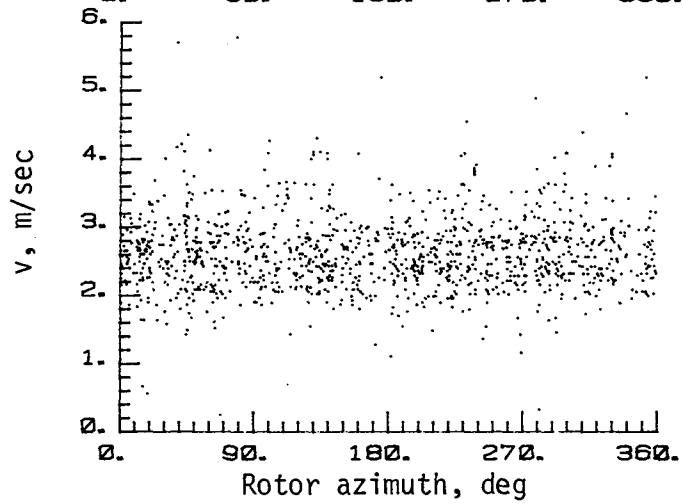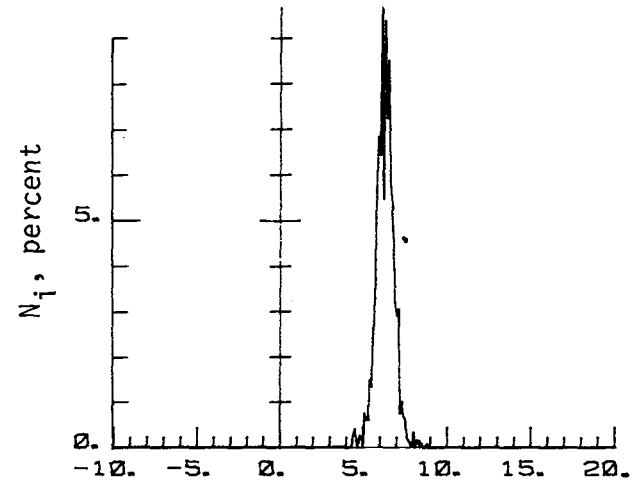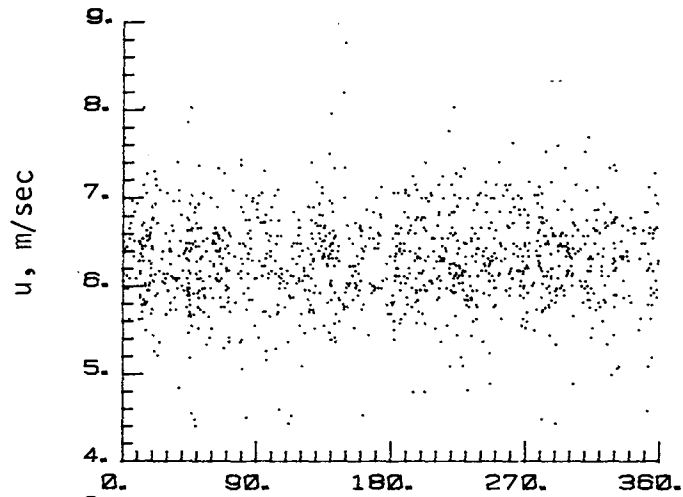
(j)   x/R = 0.3;   y/R = 0;   z/R = -0.01.

Figure A1.- Continued.
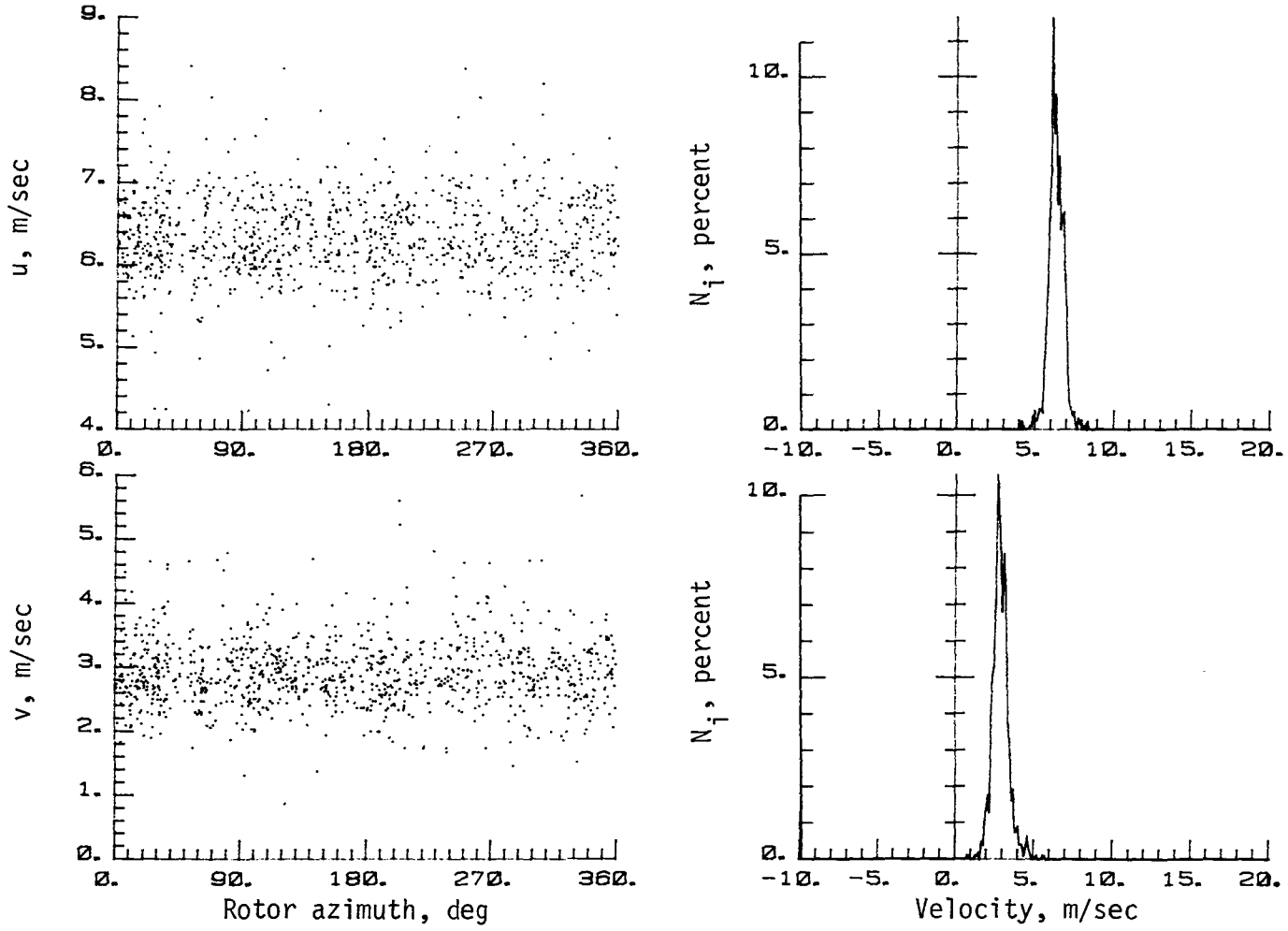
(k)   x/R = 0.3;   y/R = 0;   z/R = 0.01.

Figure A1.- Continued.
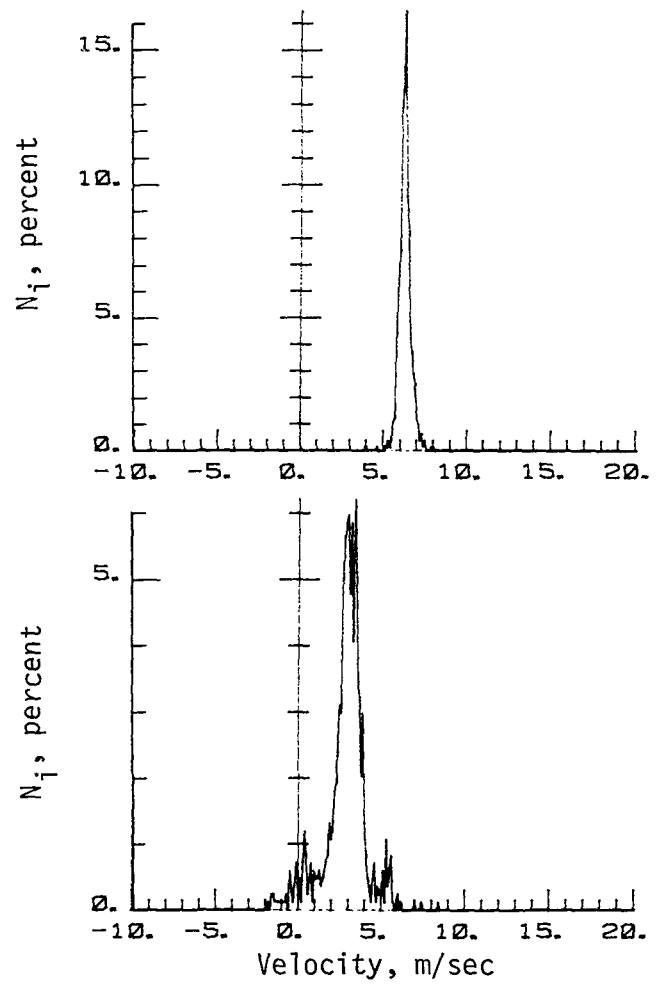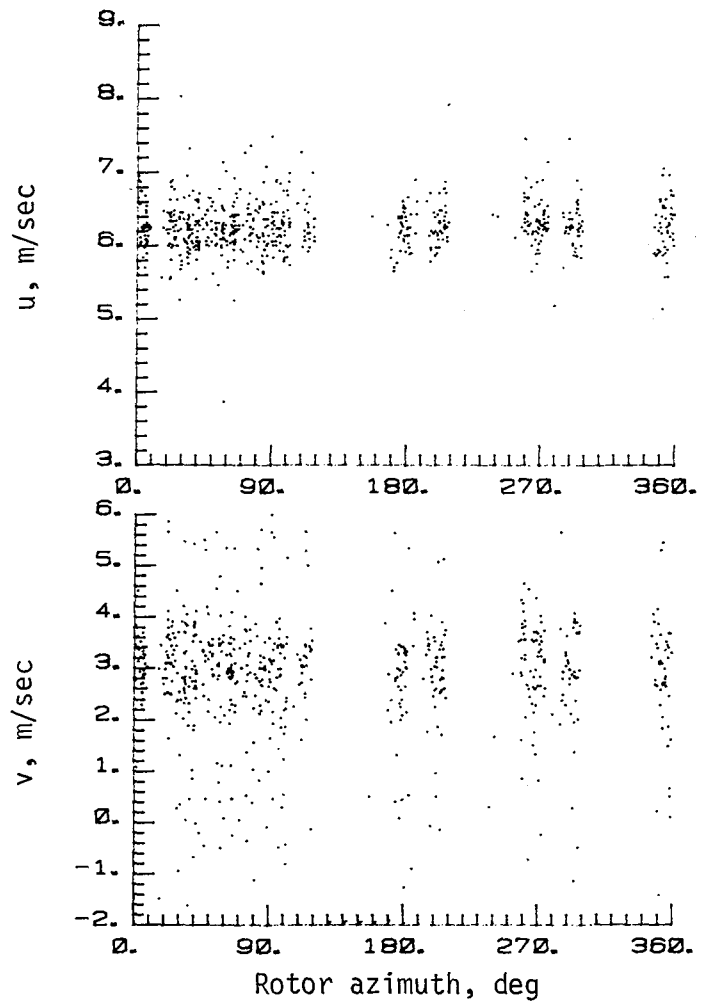
(1)   x/R = 0.3;   y/R = 0;   z/R = 0.027.

Figure A1.- Continued.
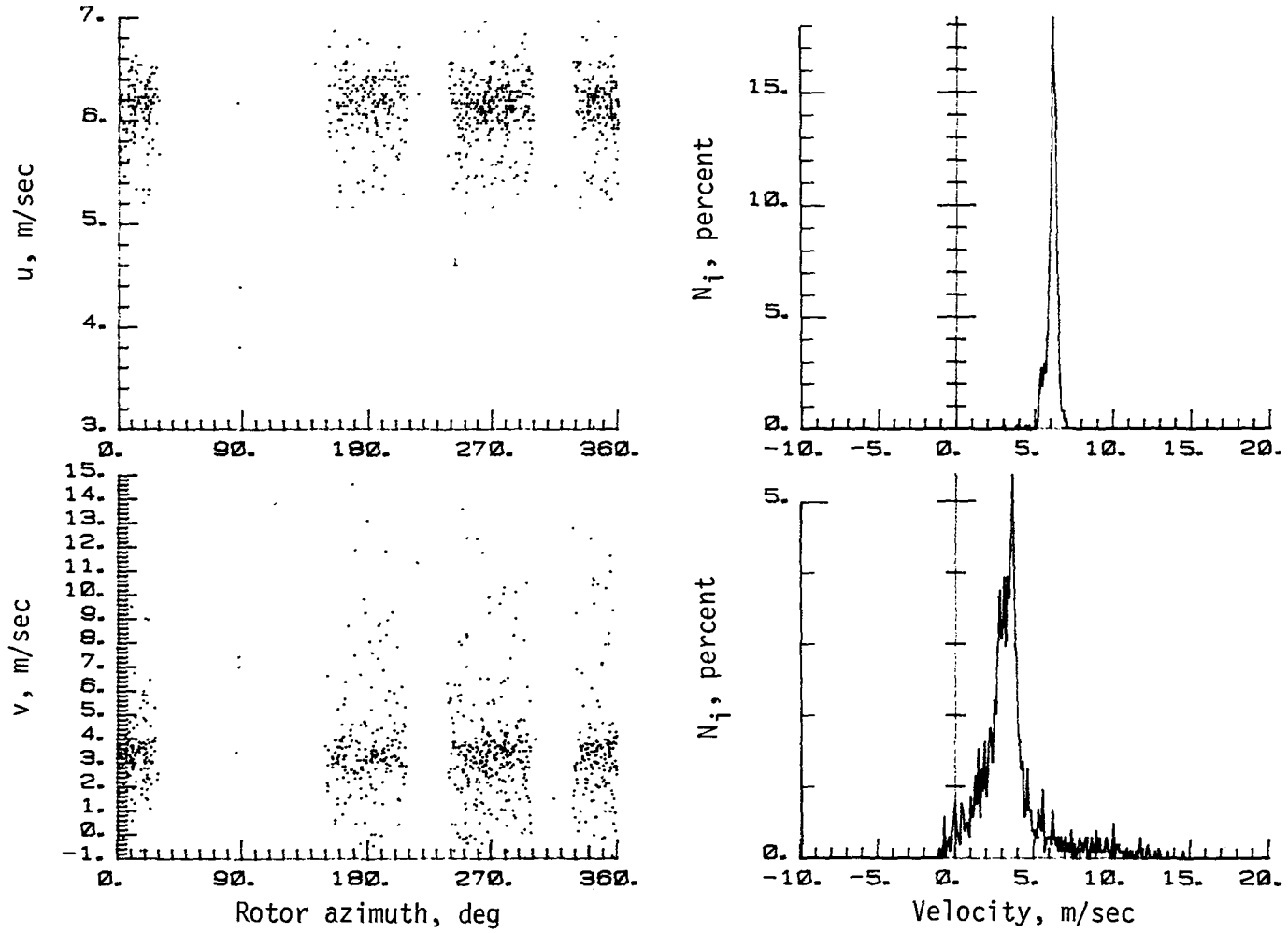
(m)   x/R = 0.3;   y/R = 0;   z/R = 0.04.

Figure A1.- Continued.
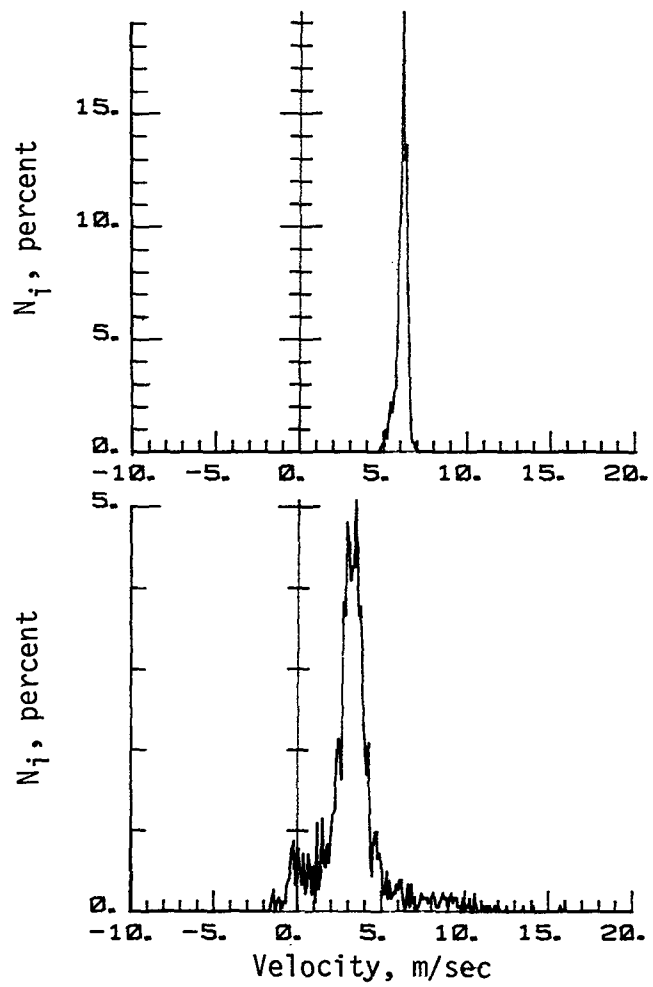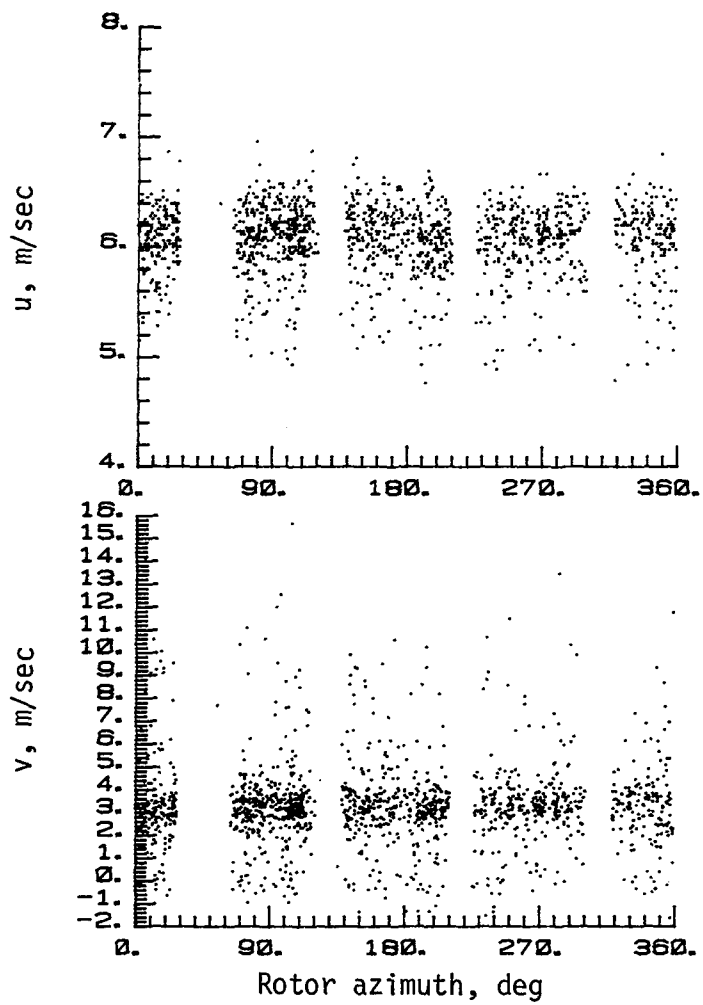
(n)   x/R = 0.3;   y/R = 0;   z/R = 0.043.

Figure A1.- Concluded.
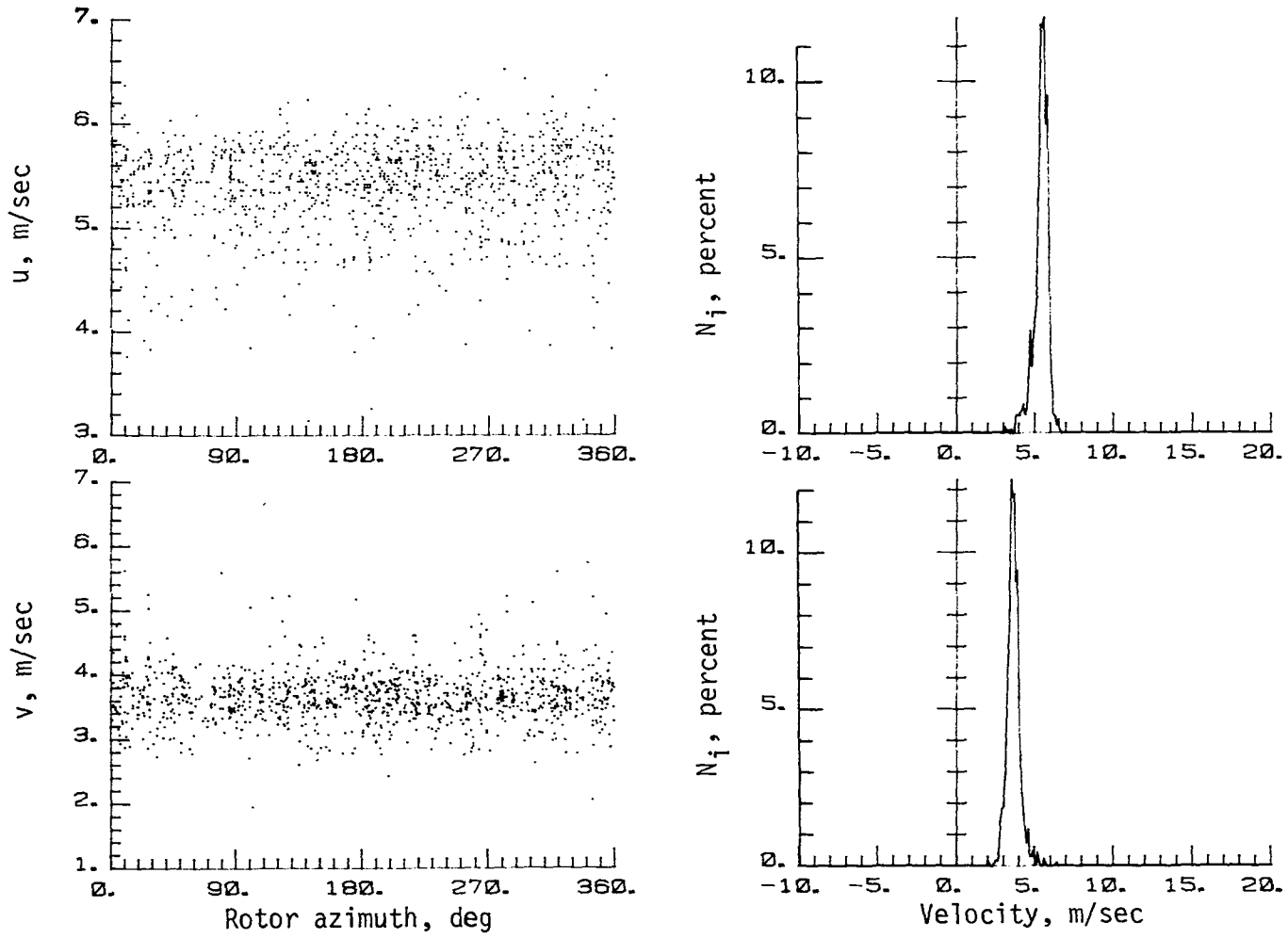
(a)   S/R = 0.224;   x/R = 0.2;   y/R = 0;   z/R = 0.

Figure A2.- LV data for rotor with 0.125R body.
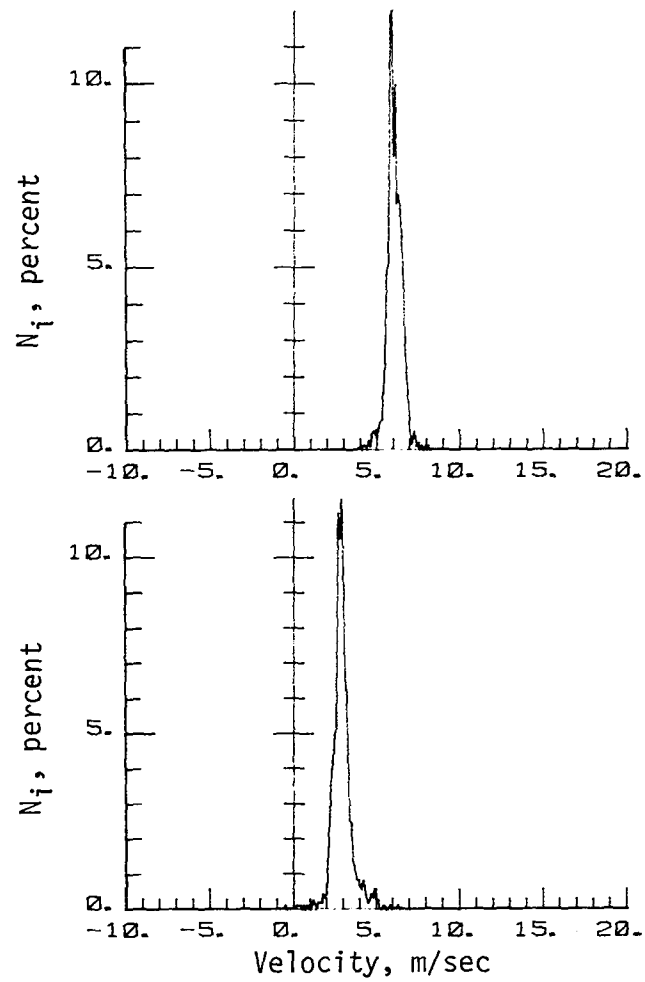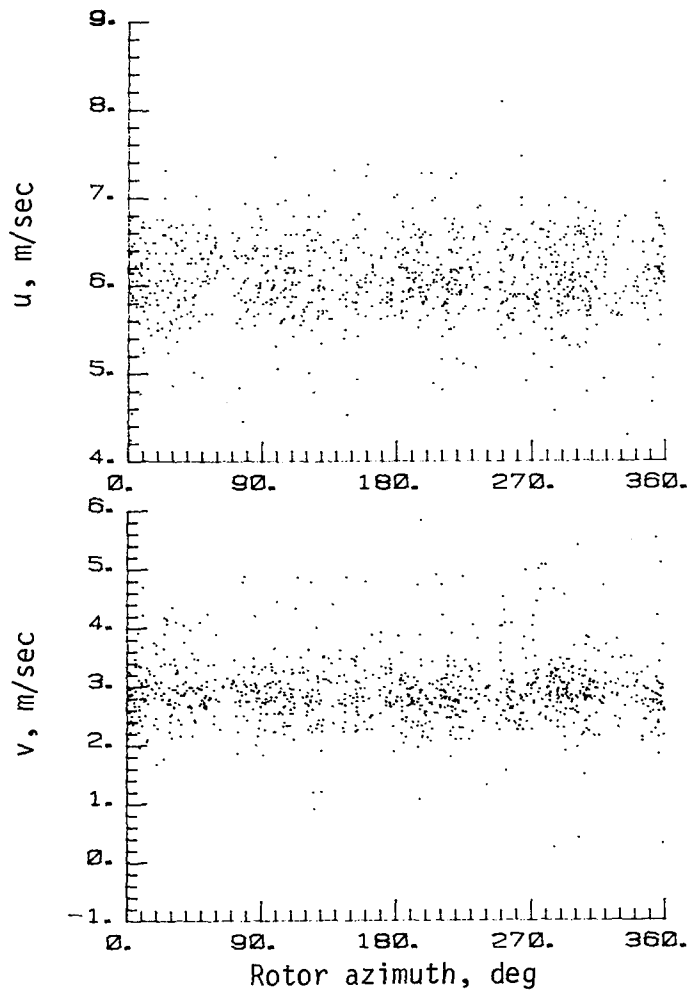
(b)   S/R = 0.224;   x/R = 0.3;   y/R = 0;   z/R = 0.

Figure A2.- Continued.
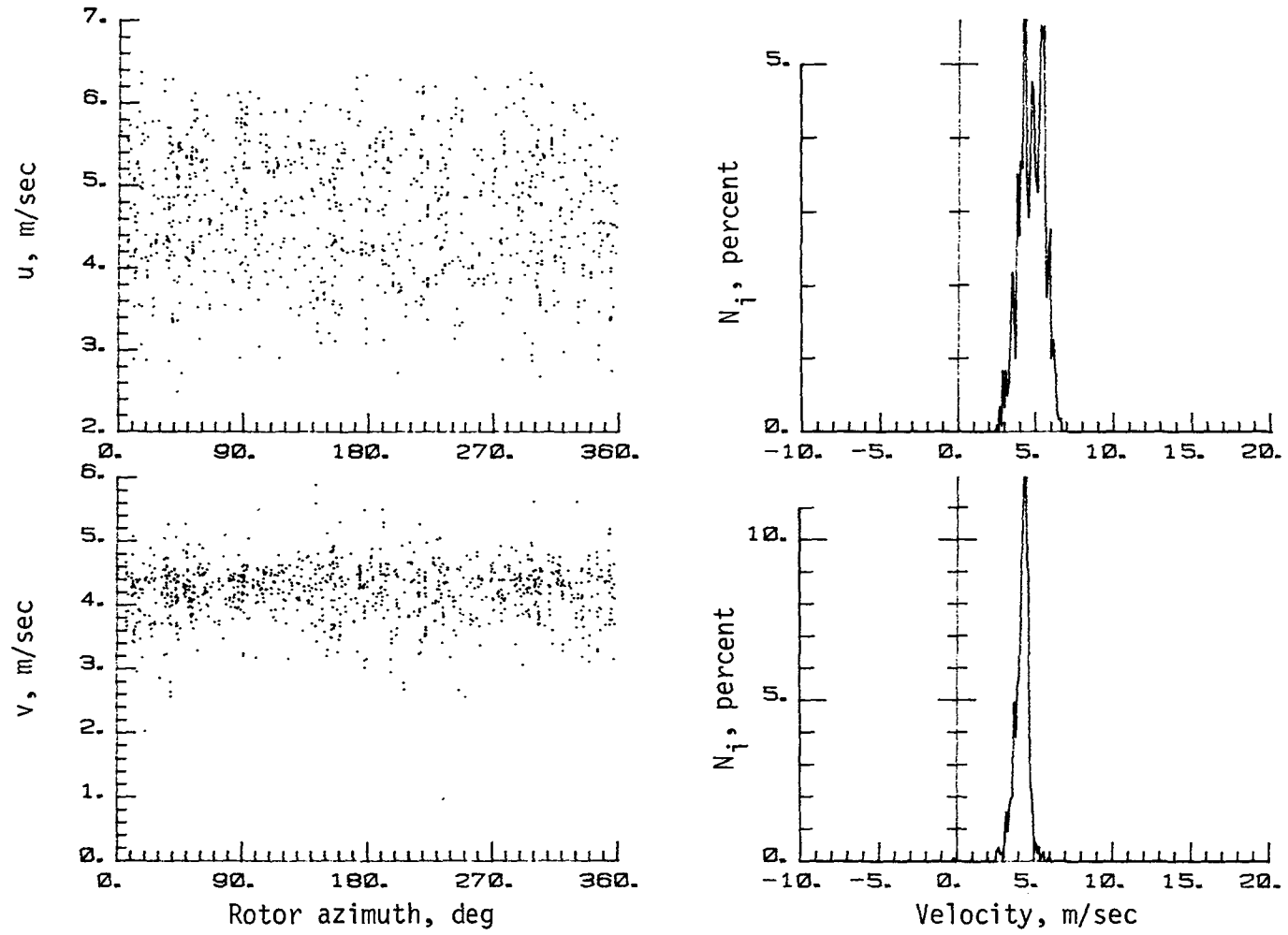
(c)   S/R = 0.275;   x/R = 0.1;   y/R = 0;   z/R = 0.

Figure A2.- Continued.
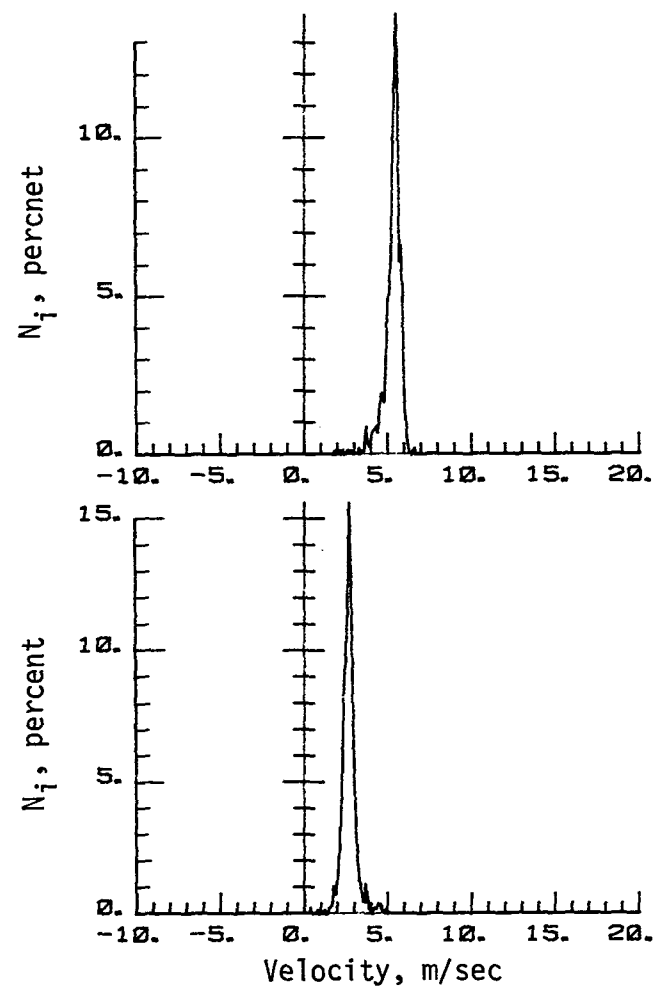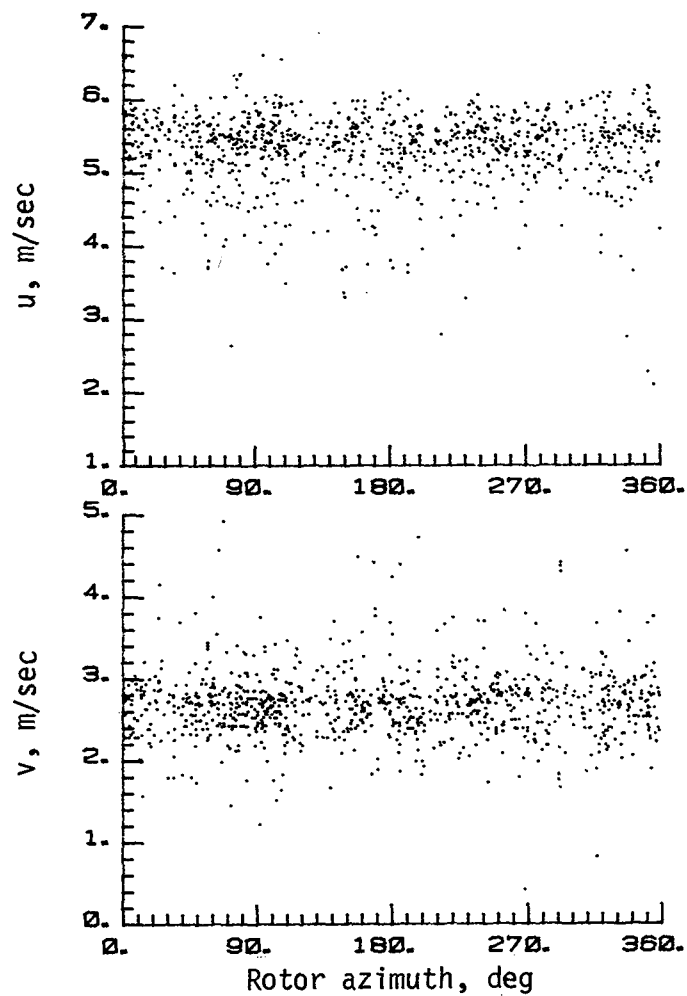
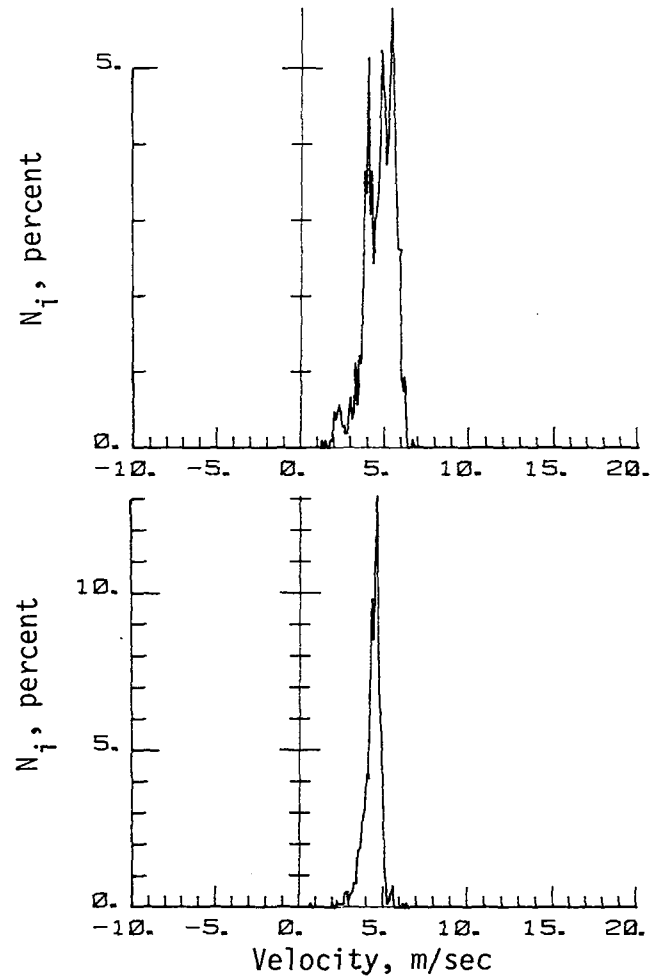(d)   S/R = 0.275;   x/R = 0.2;   y/R = -0.1;   z/R = 0.

Figure A2.- Continued.
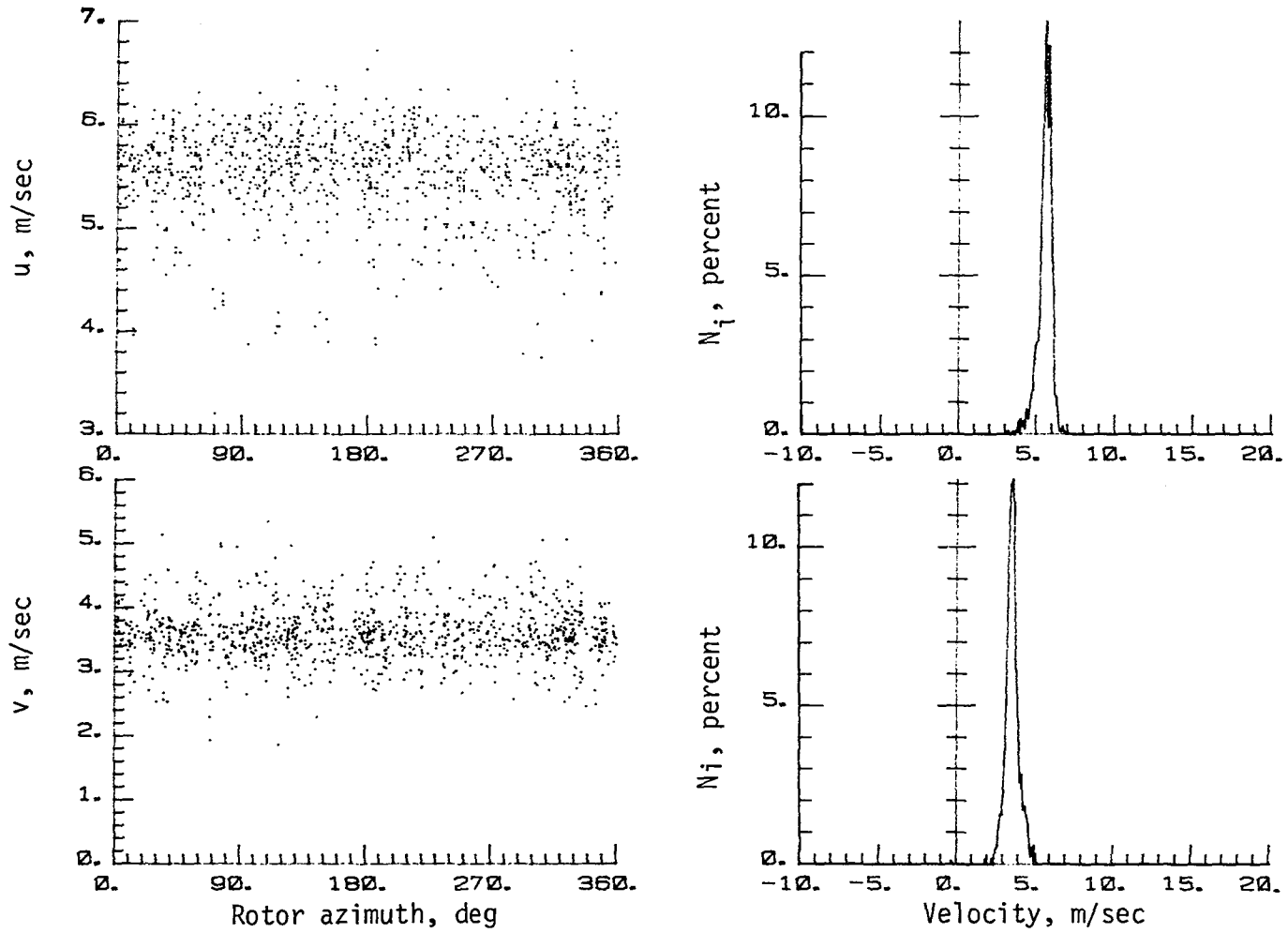
(e)   S/R = 0.275;   x/R = 0.2;   y/R = 0;   z/R = 0.

Figure A2.- Continued.
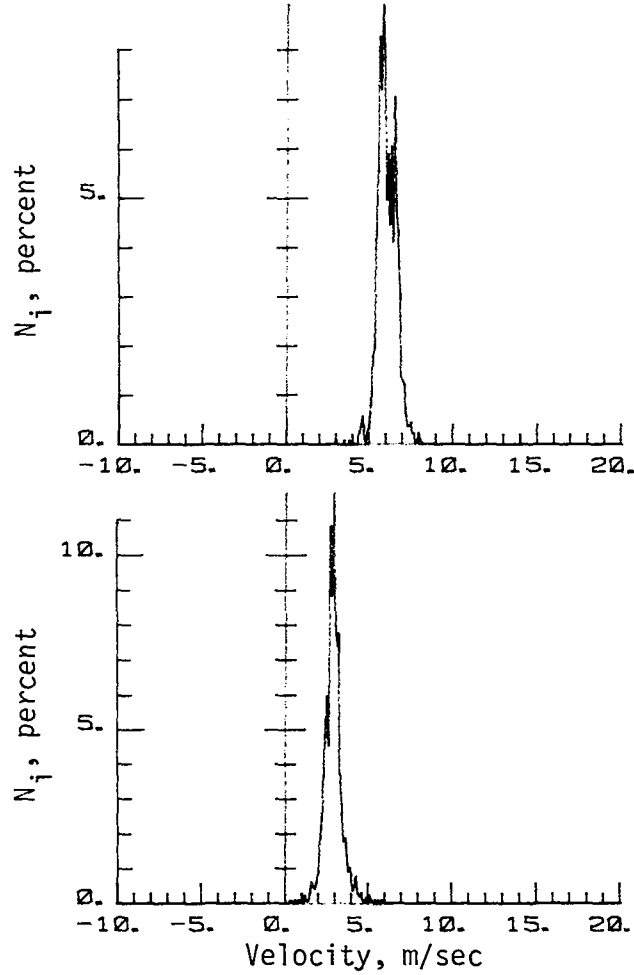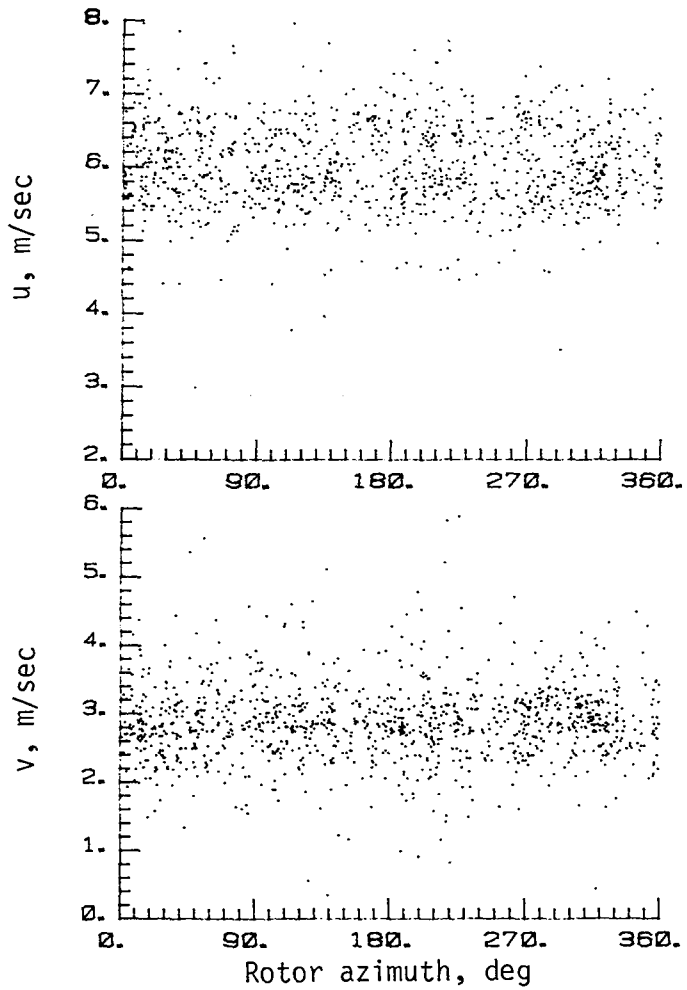
(f)   S/R = 0.275;   x/R = 0.3;   y/R = 0;   z/R = 0.

Figure A2.- Continued.
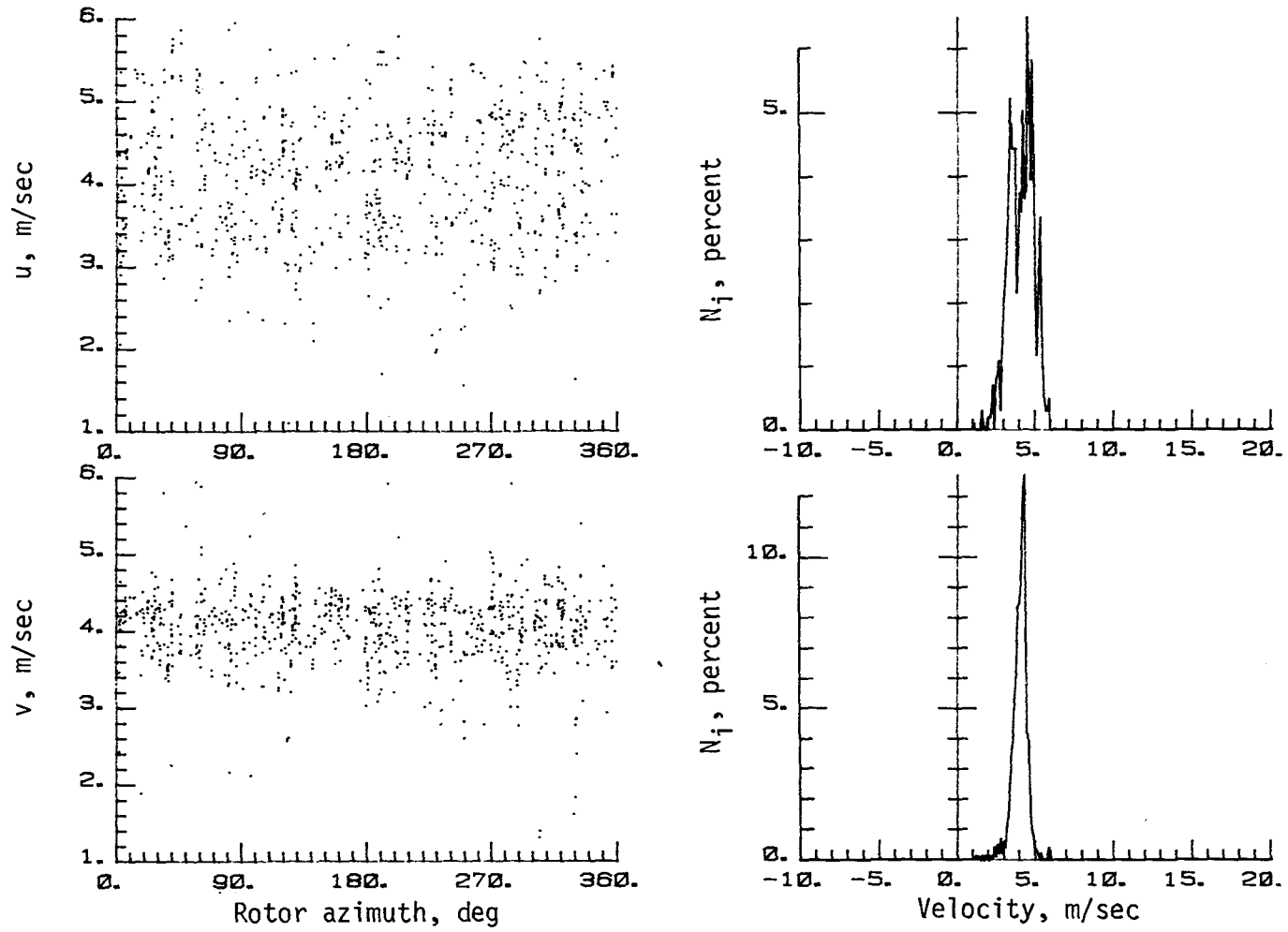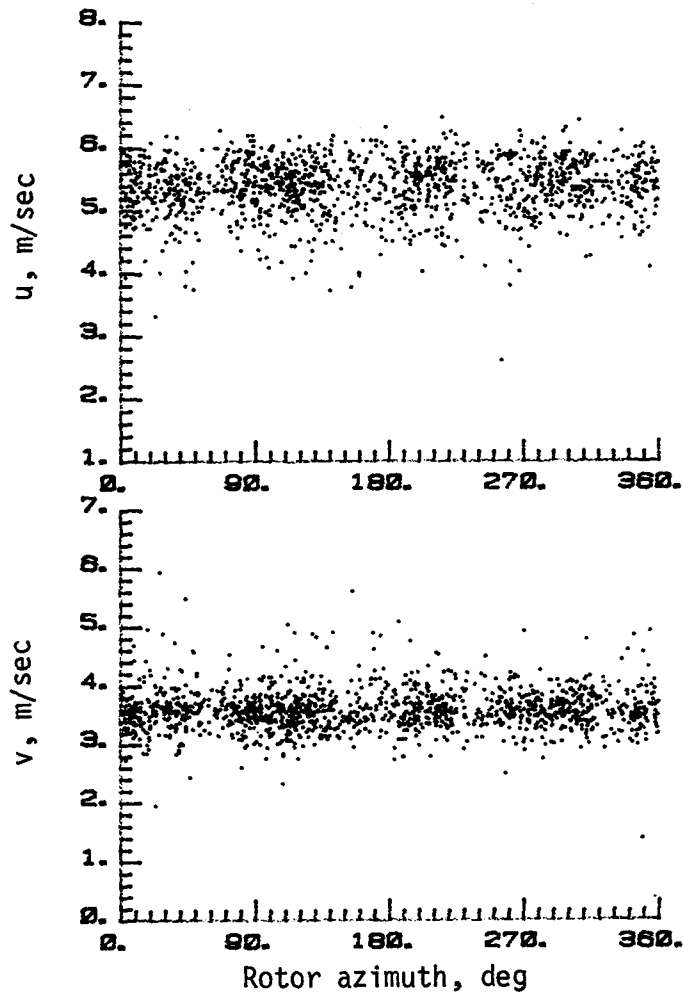
(g)   S/R = 0.324;   x/R = 0.1;   y/R = 0;   z/R = 0.

Figure A2.- Continued.
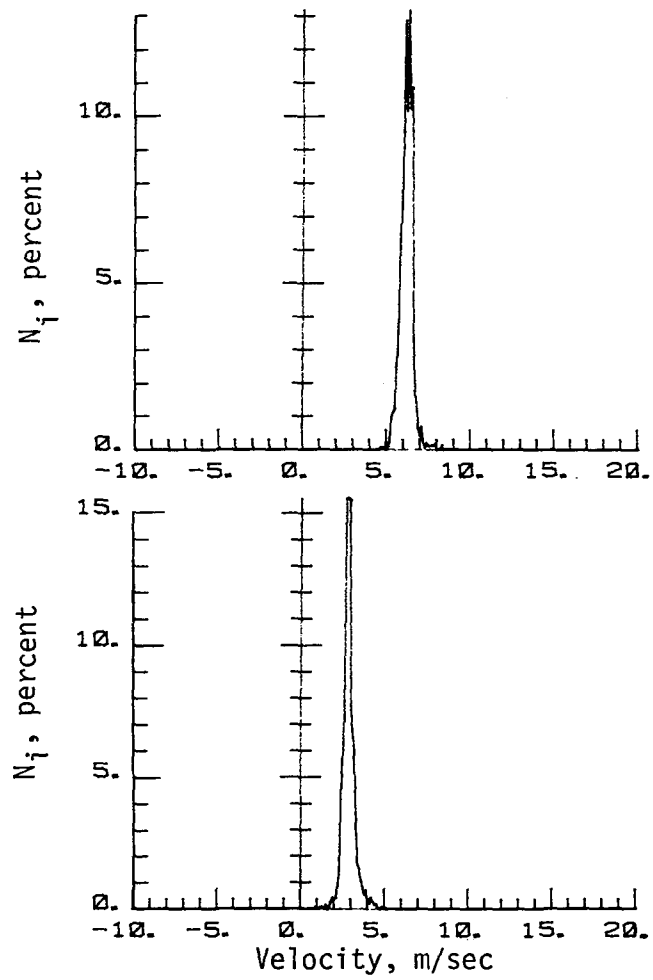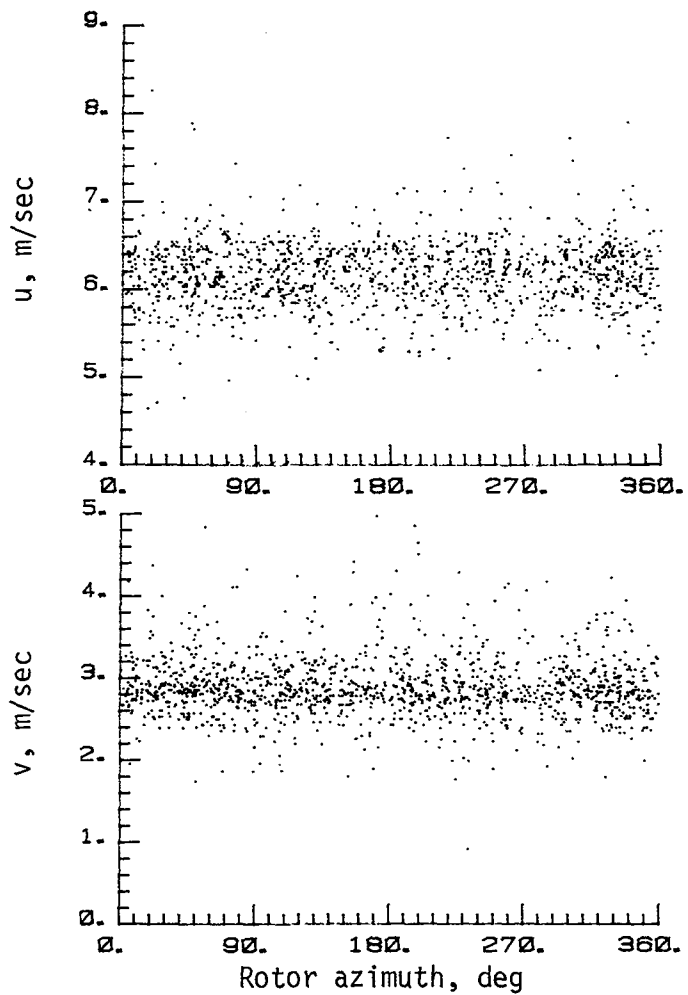
(h) S/R = 0.324;   x/R = 0.2;   y/R = 0.1;   z/R = 0.

Figure A2.- Continued.
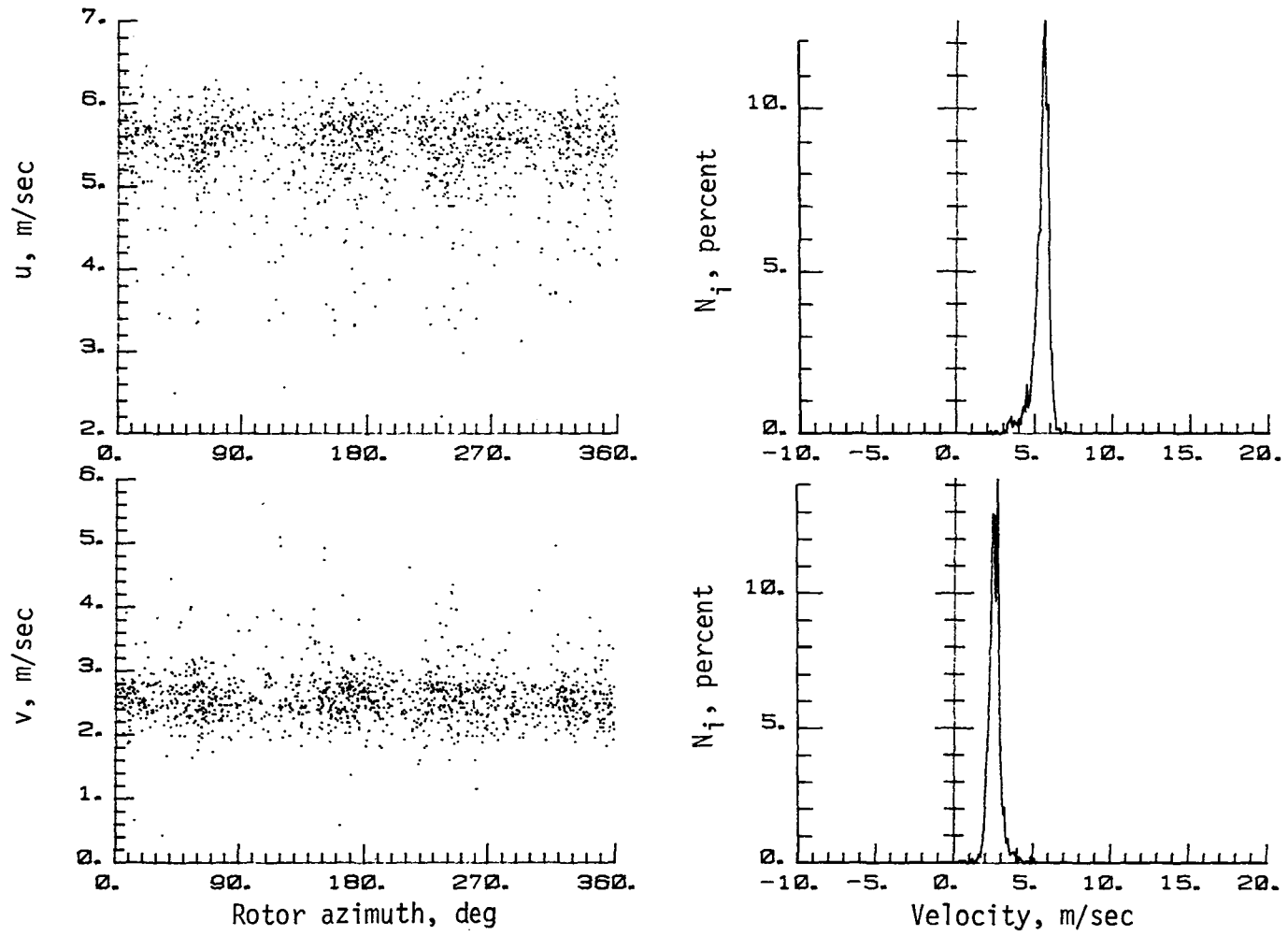
(i) S/R = 0.324; x/R = 0.2; y/R = -0.1; z/R = 0.

Figure A2.- Continued.
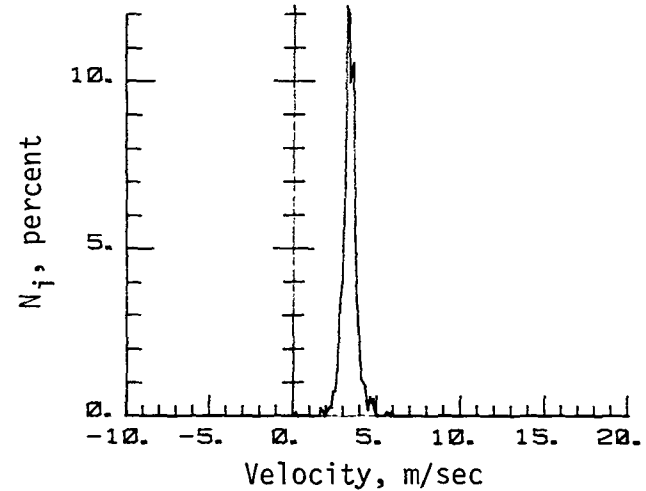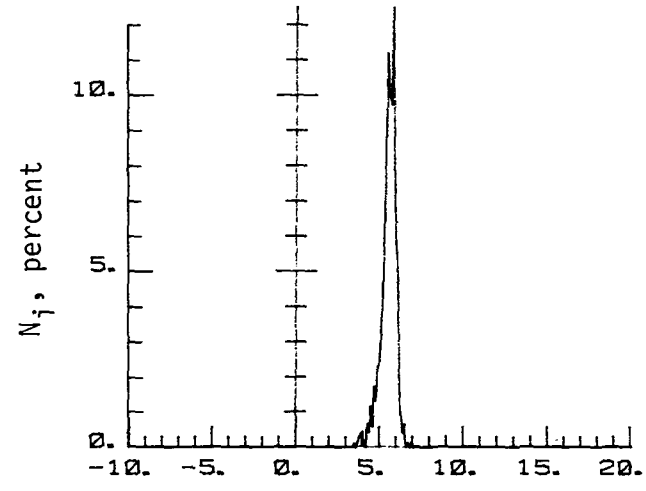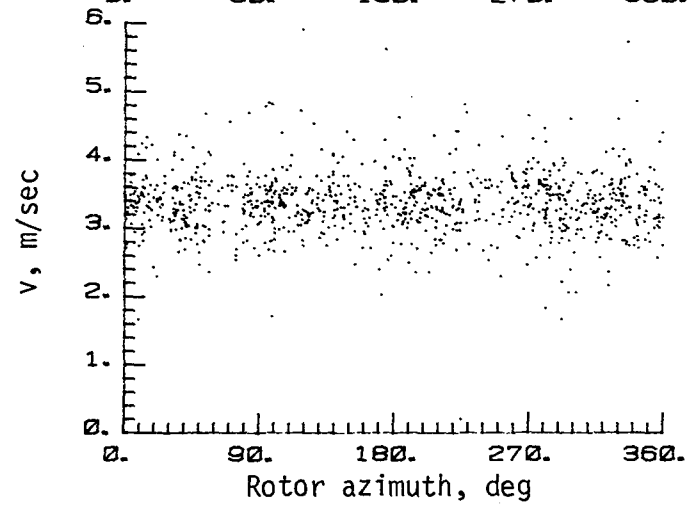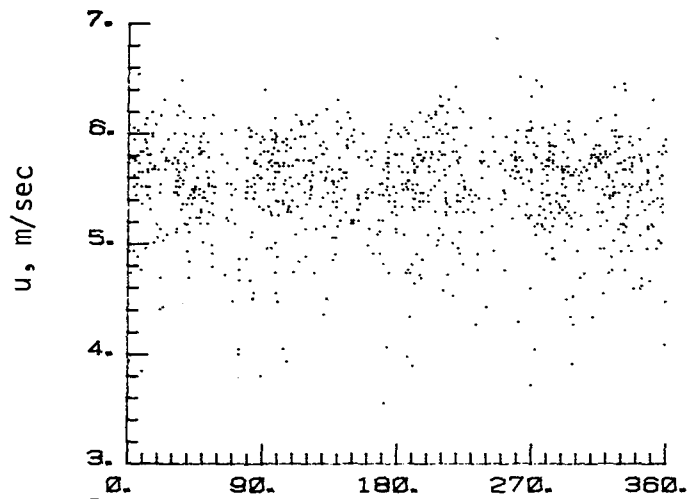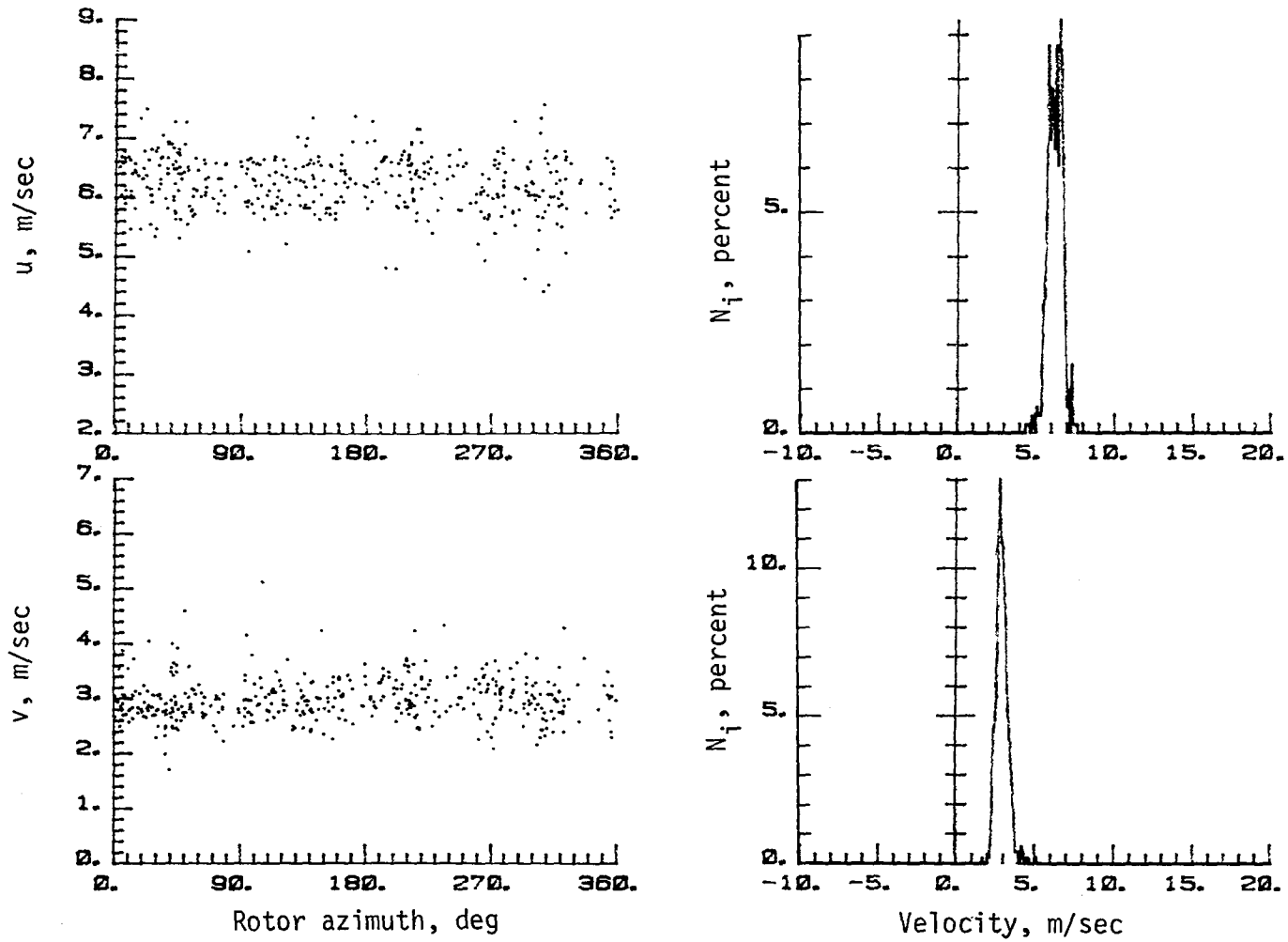
(j) S/R = 0.324;   x/R = 0.2;   y/R = 0;   z/R = 0.

Figure A2.- Continued.
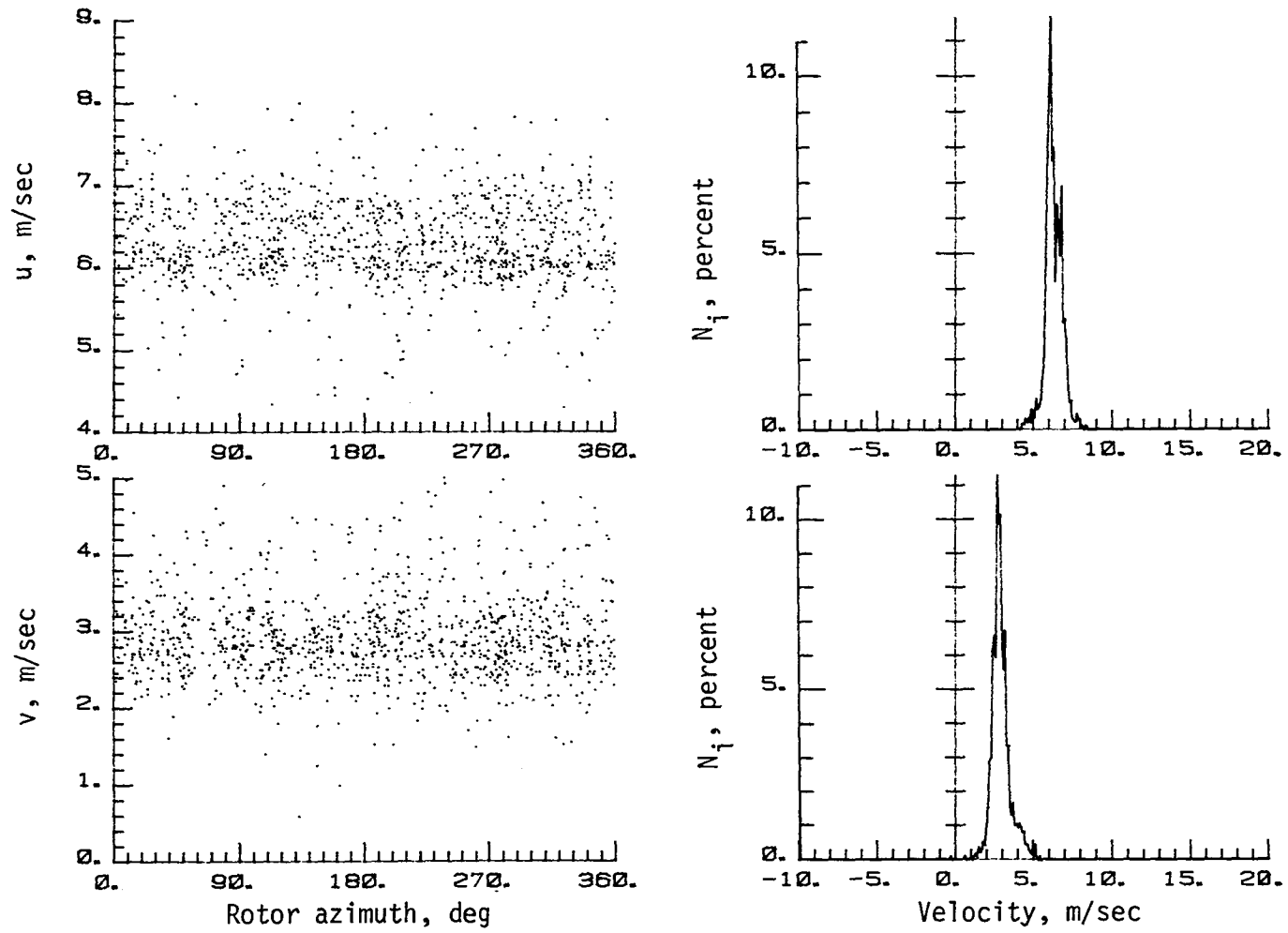
(k)   S/R = -.324;   x/R = 0.3;   y/R = 0;   z/R = 0.

Figure A2.- Concluded.
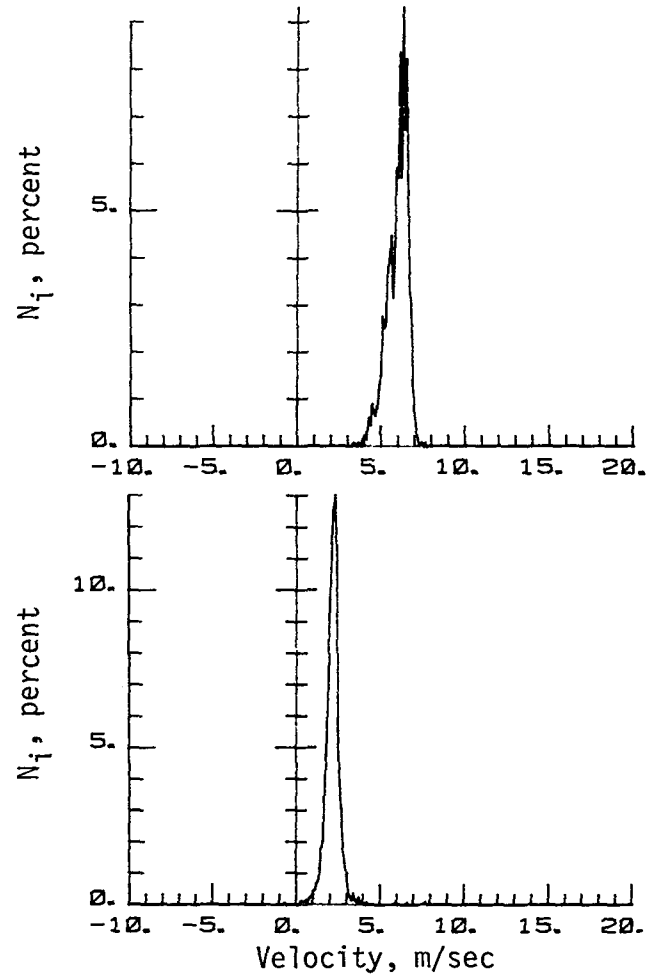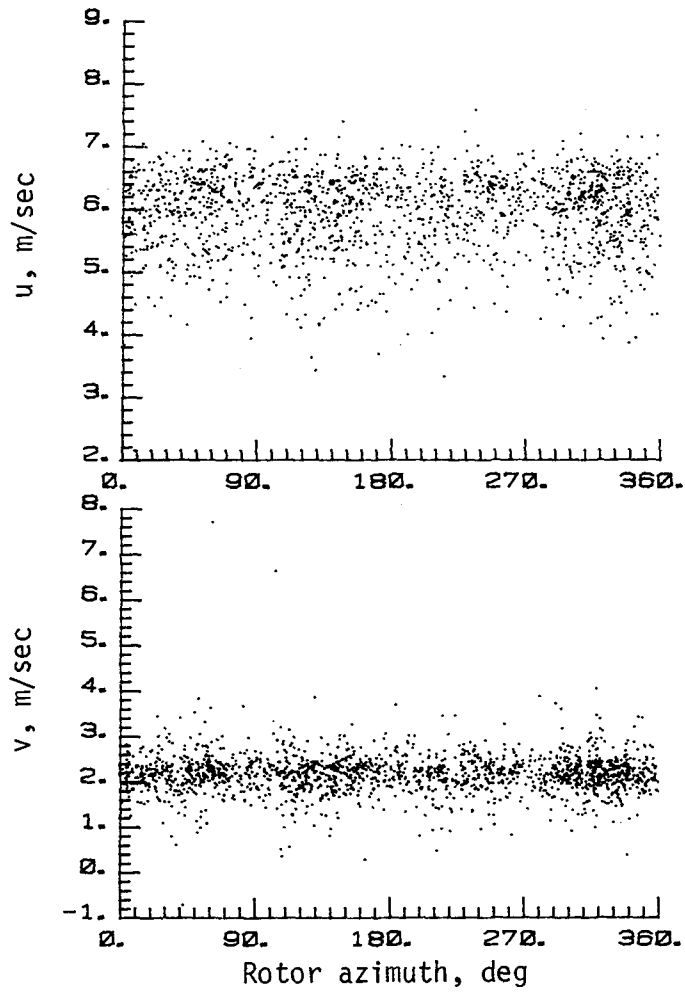
(a)   S/R = 0.224;   x/R = 0.1;   y/R = 0;   z/R = 0.

Figure A3.- LV data for rotor with 0.250R body.
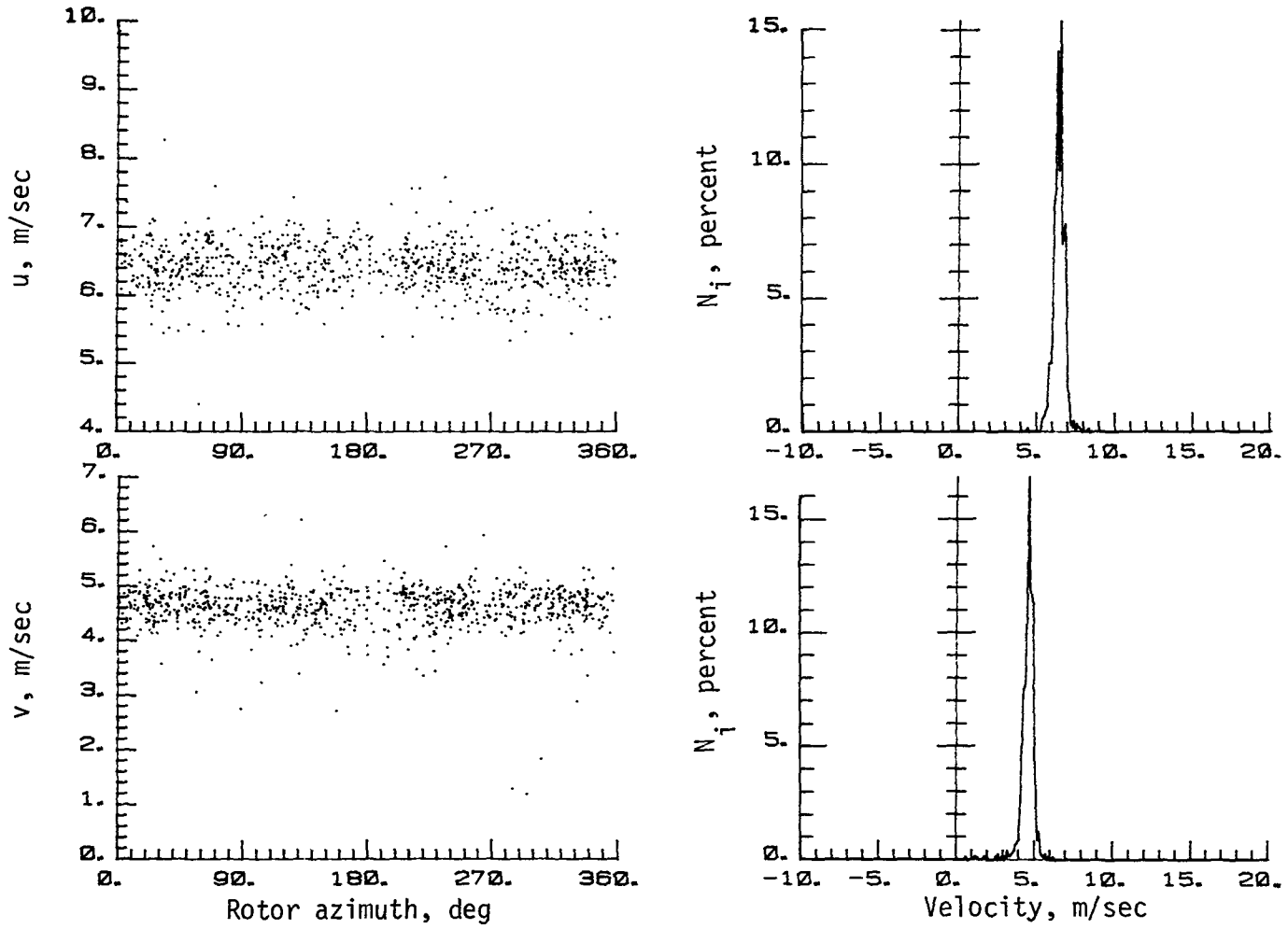
(b)   S/R = 0.224;   x/R = 0.2;   y/R = 0.1;   z/R = 0.

Figure A3.- Continued.
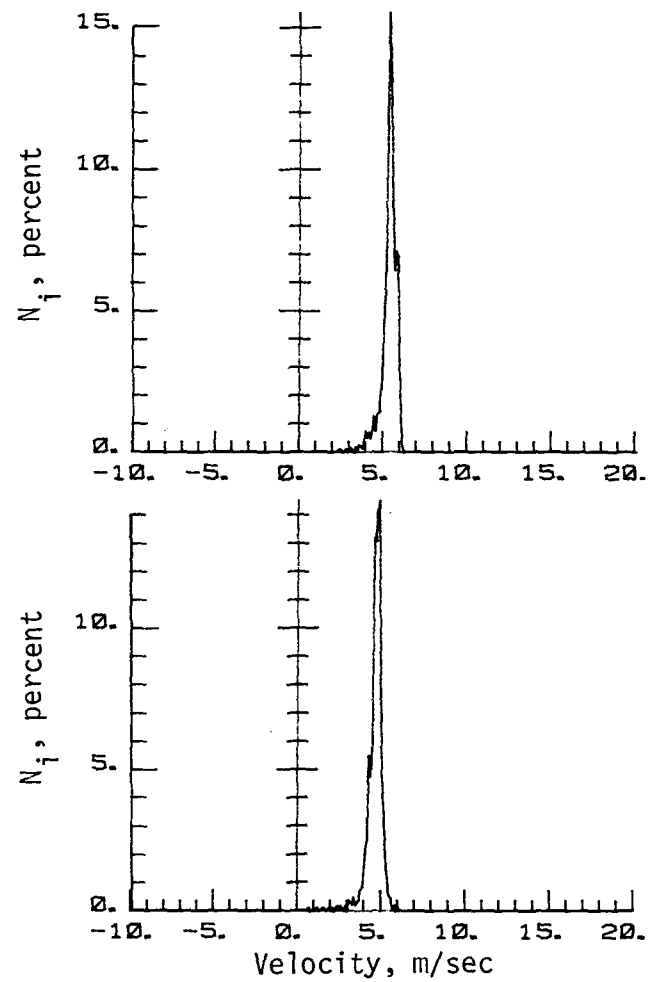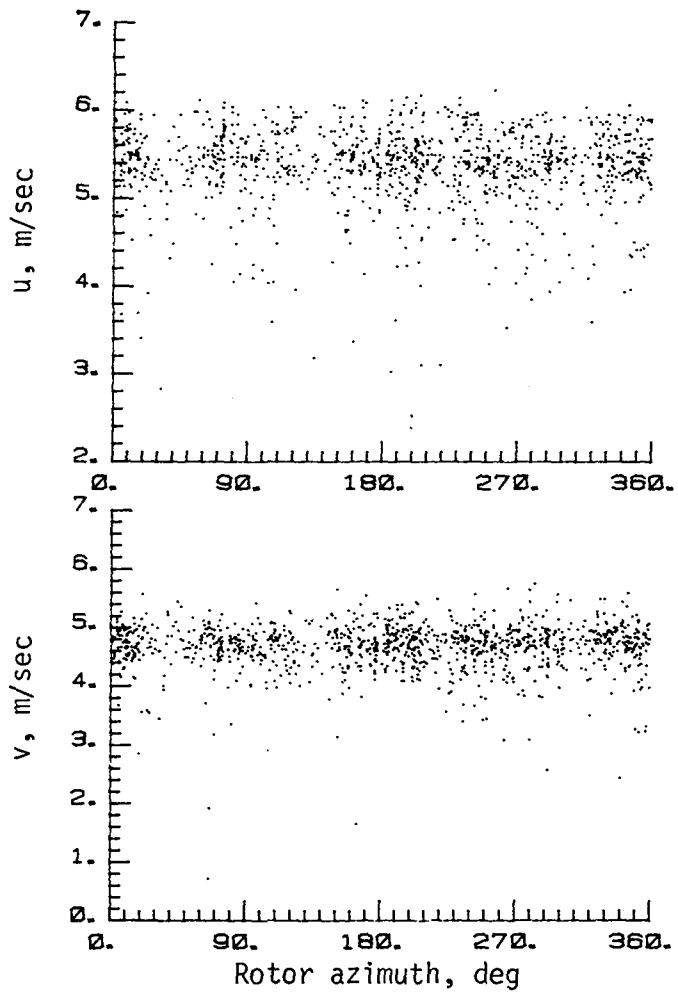
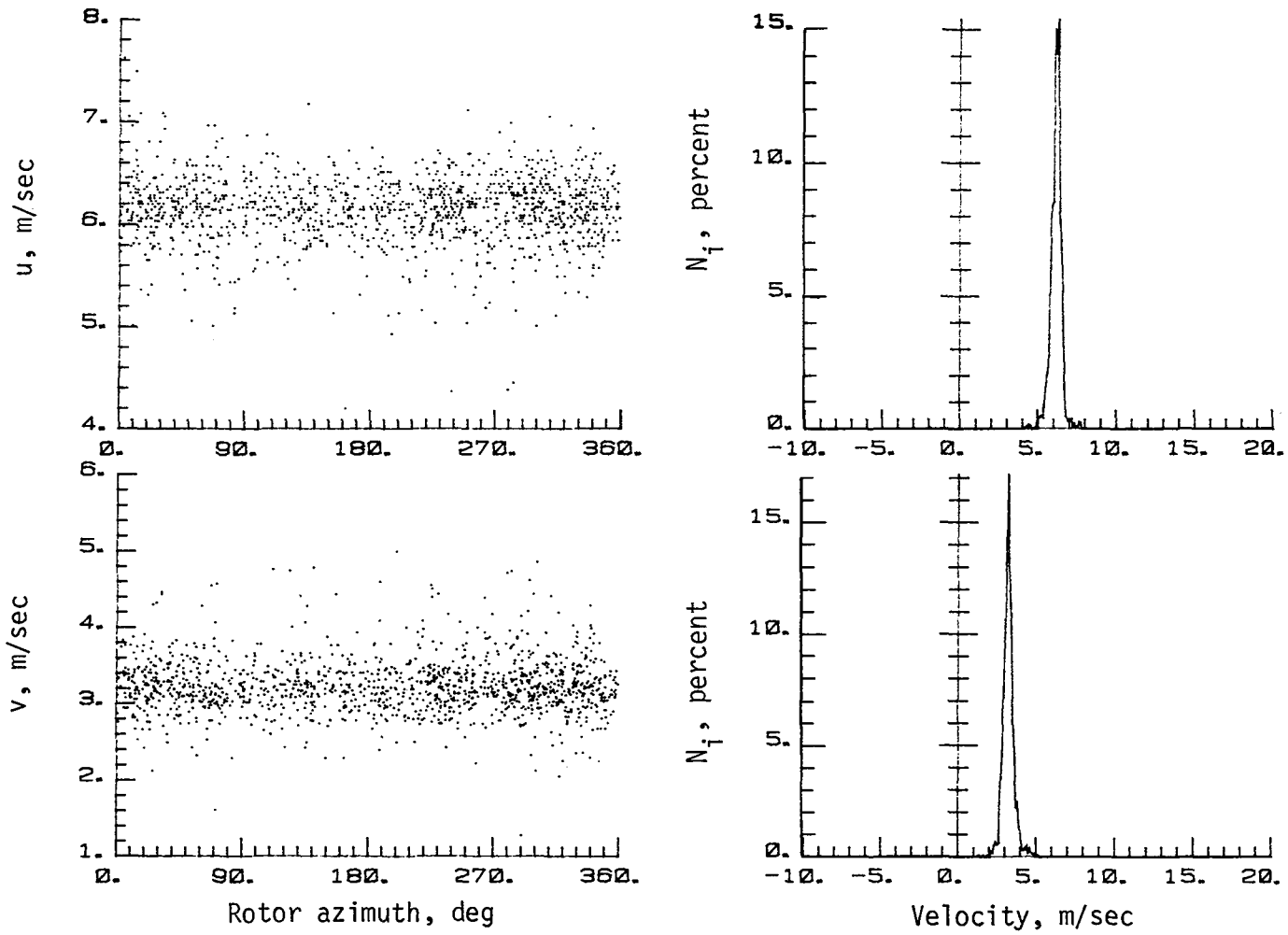(c)   S/R = 0.224;   x/R = 0.2;   y/R = -0.1;   z/R = 0.

Figure A3.- Continued.
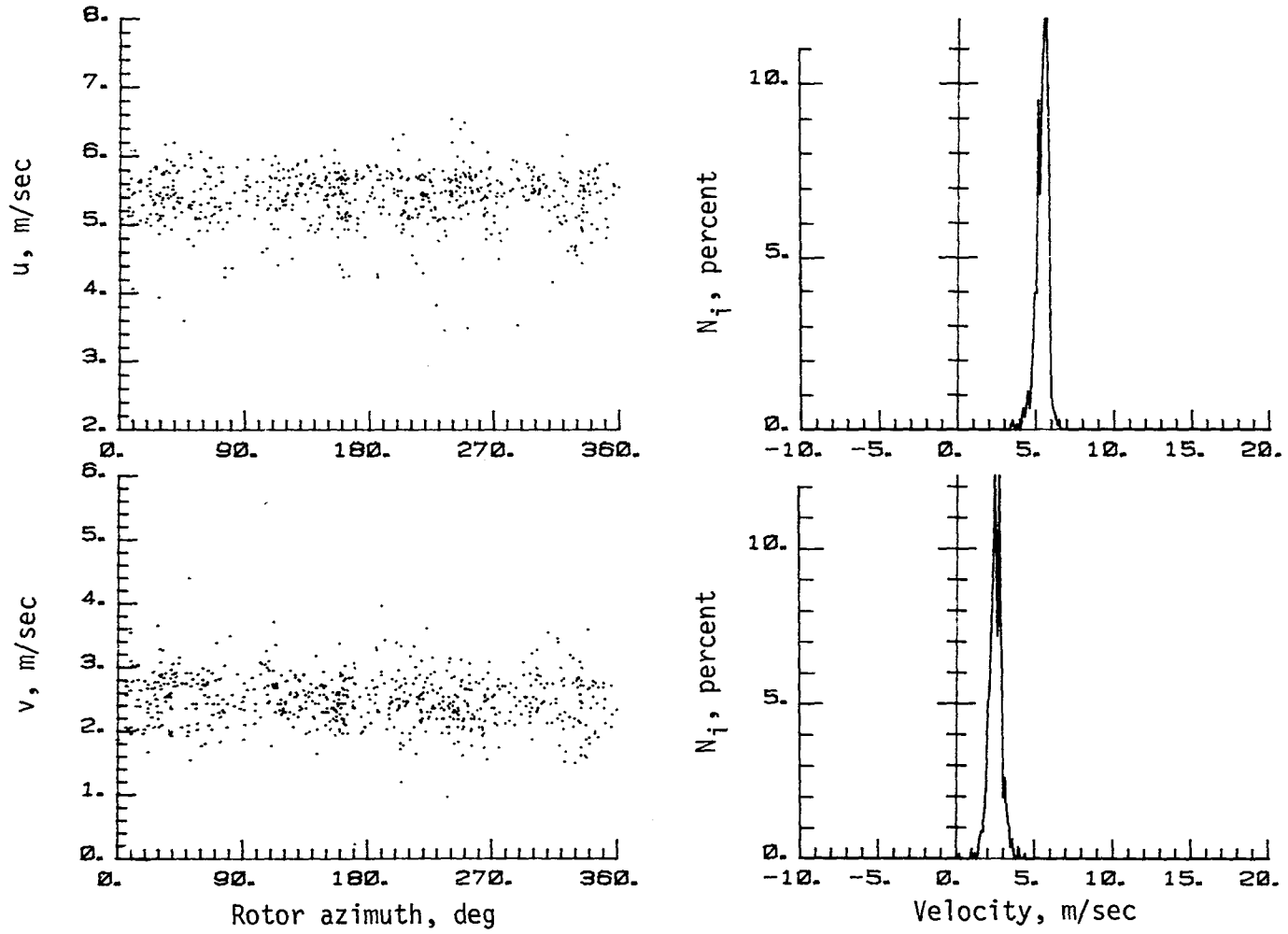
(d)   S/R = 0.224;   x/R = 0.2;   y/R = 0;   z/R = 0.

Figure A3.- Continued.
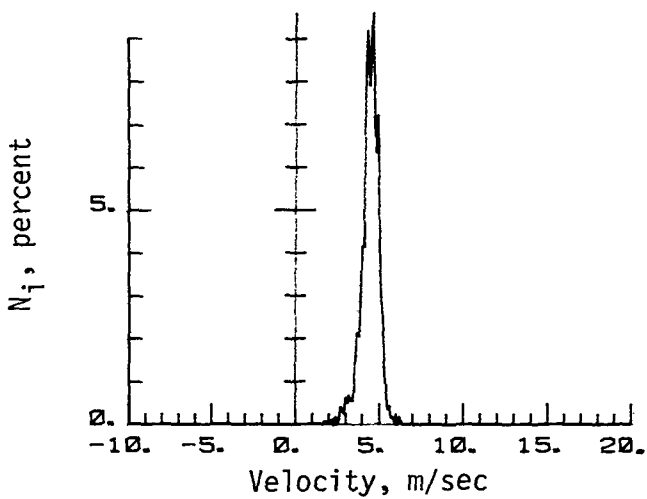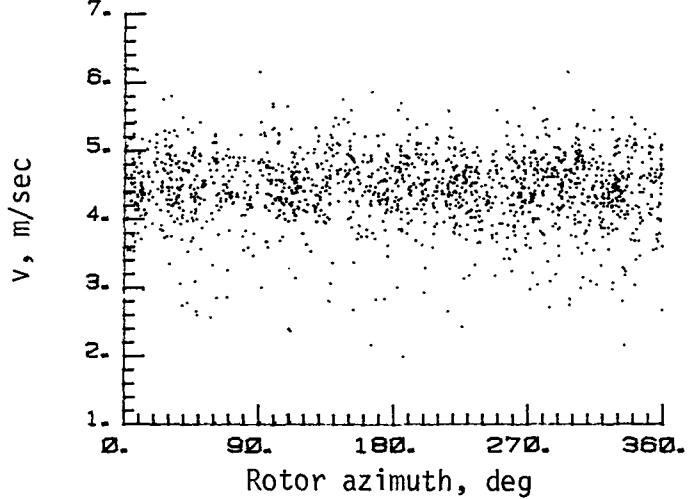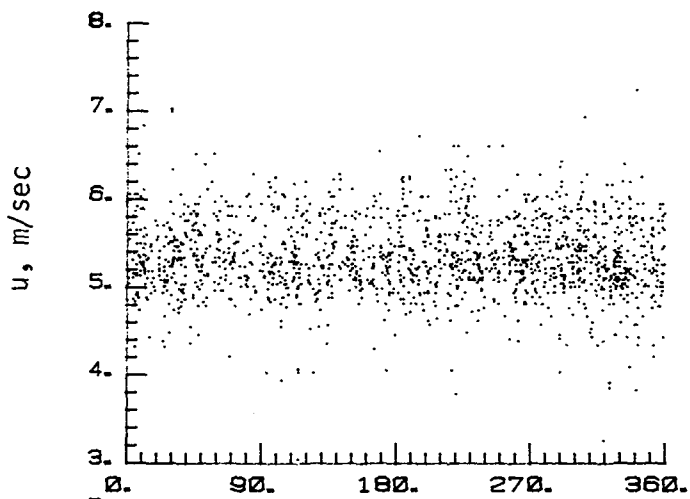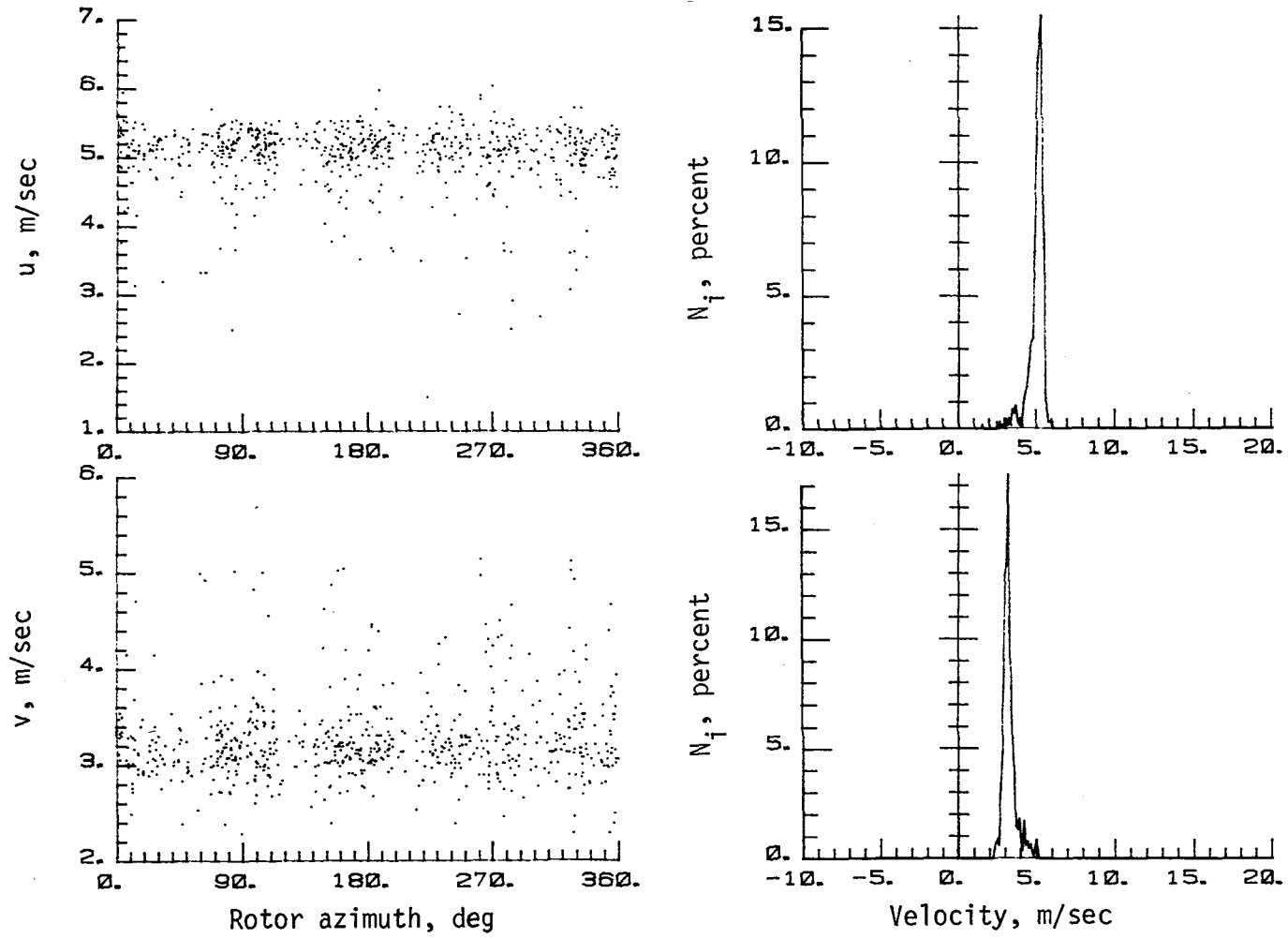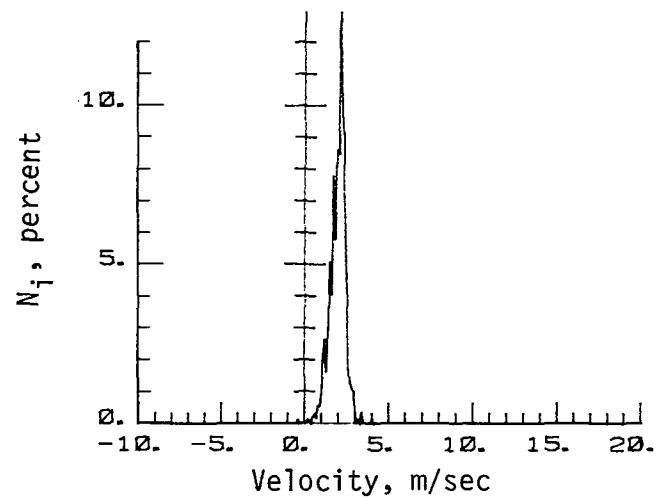
(e) S/R = 0.224; x/R = 0.3; y/R = 0; z/R = 0.

Figure A3.- Continued.
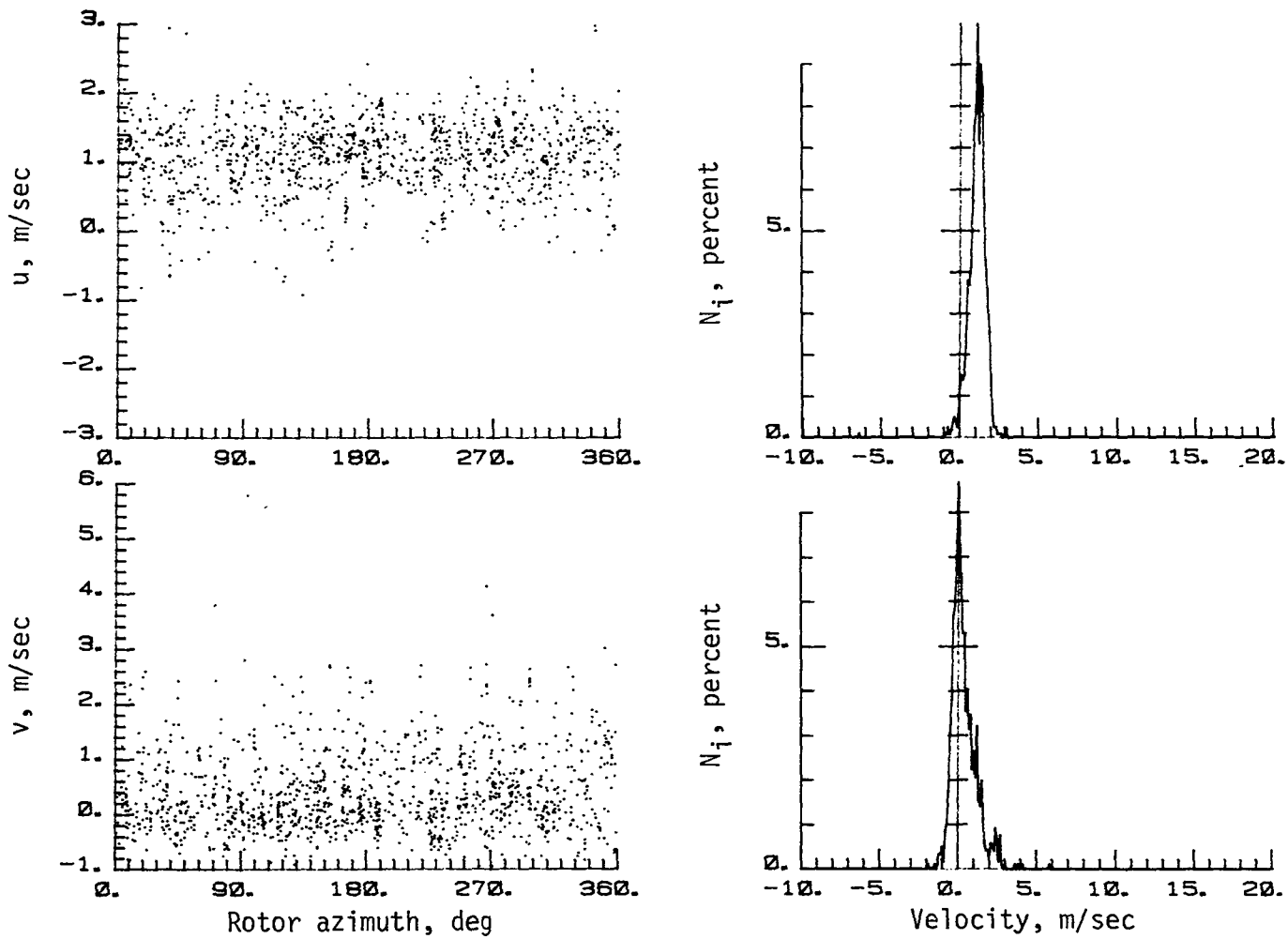
(f)   S/R = 0.224;   x/R = 0.4;   y/R = 0;   z/R = 0.

Figure A3.- Continued.

(g)   S/R = 0.224;   x/R = 0.5;   y/R = 0;   z/R = 0.

Figure A3.- Continued.
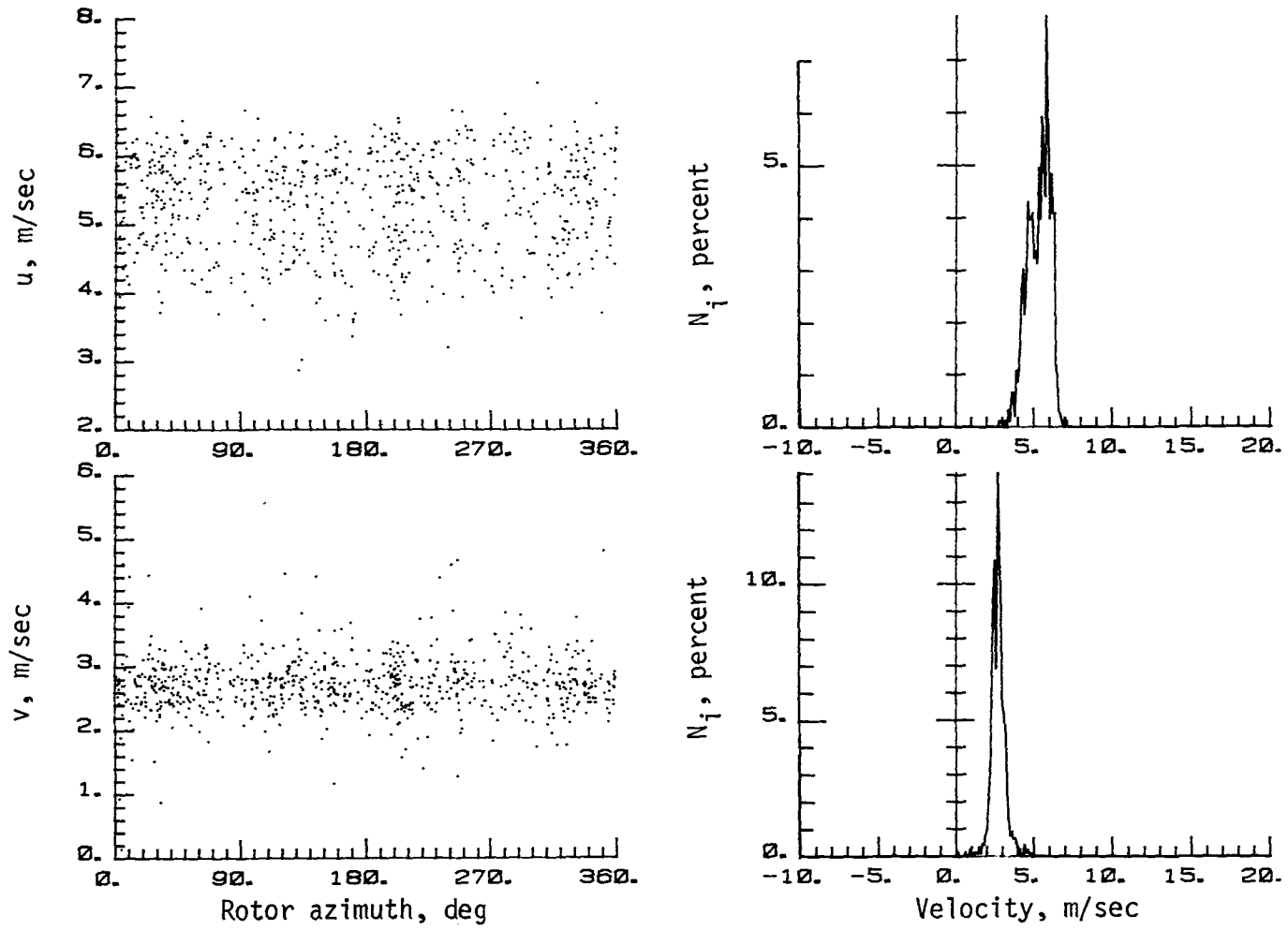
(h)   S/R = 0.275;   x/R = 0.1;   y/R = 0;   z/R = 0.

Figure A3.- Continued.
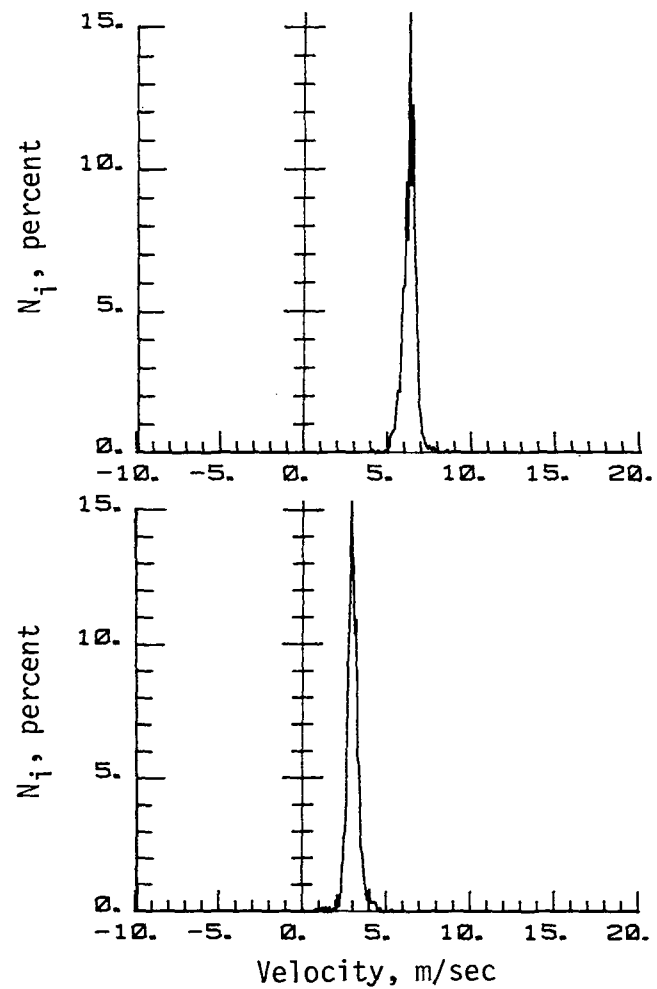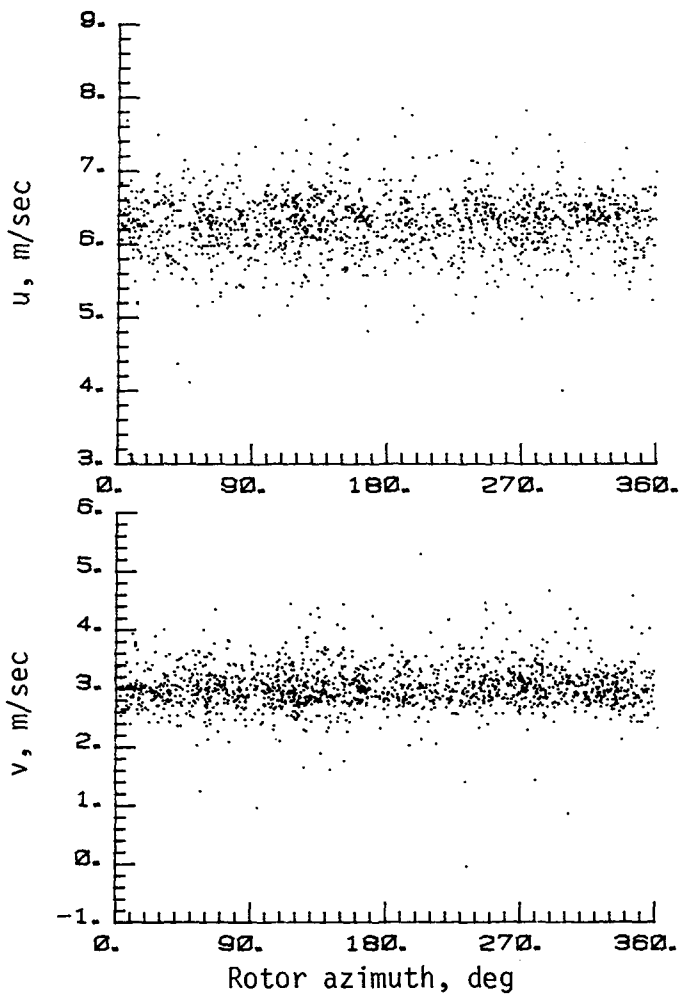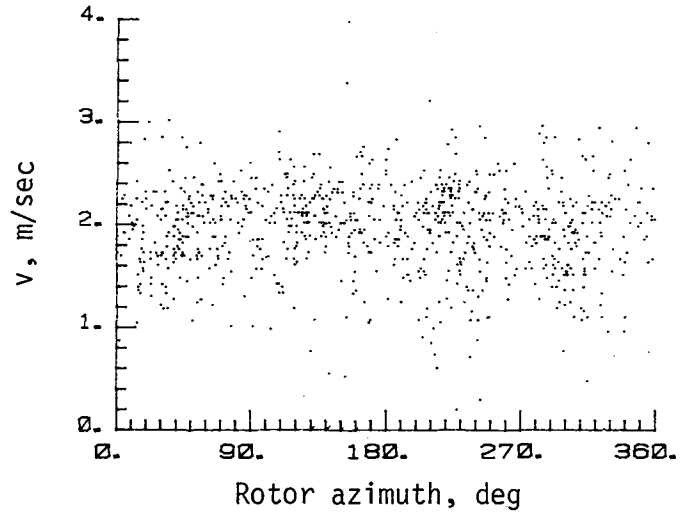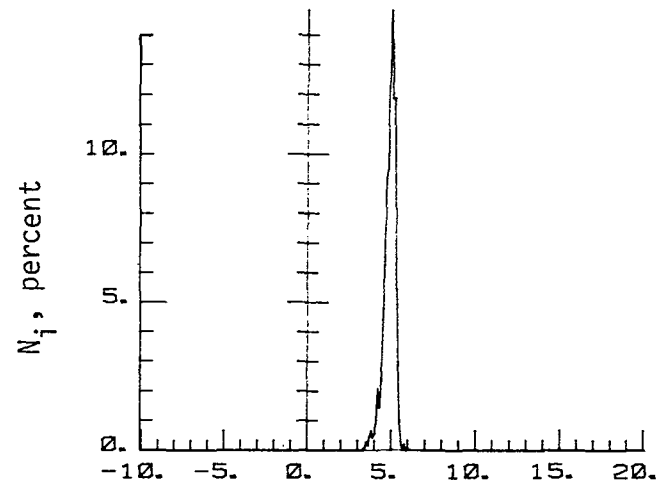
(i)   S/R = 0.275;   x/R = 0.2;   y/R = 0.1;   z/R = 0.

Figure A3.- Continued.
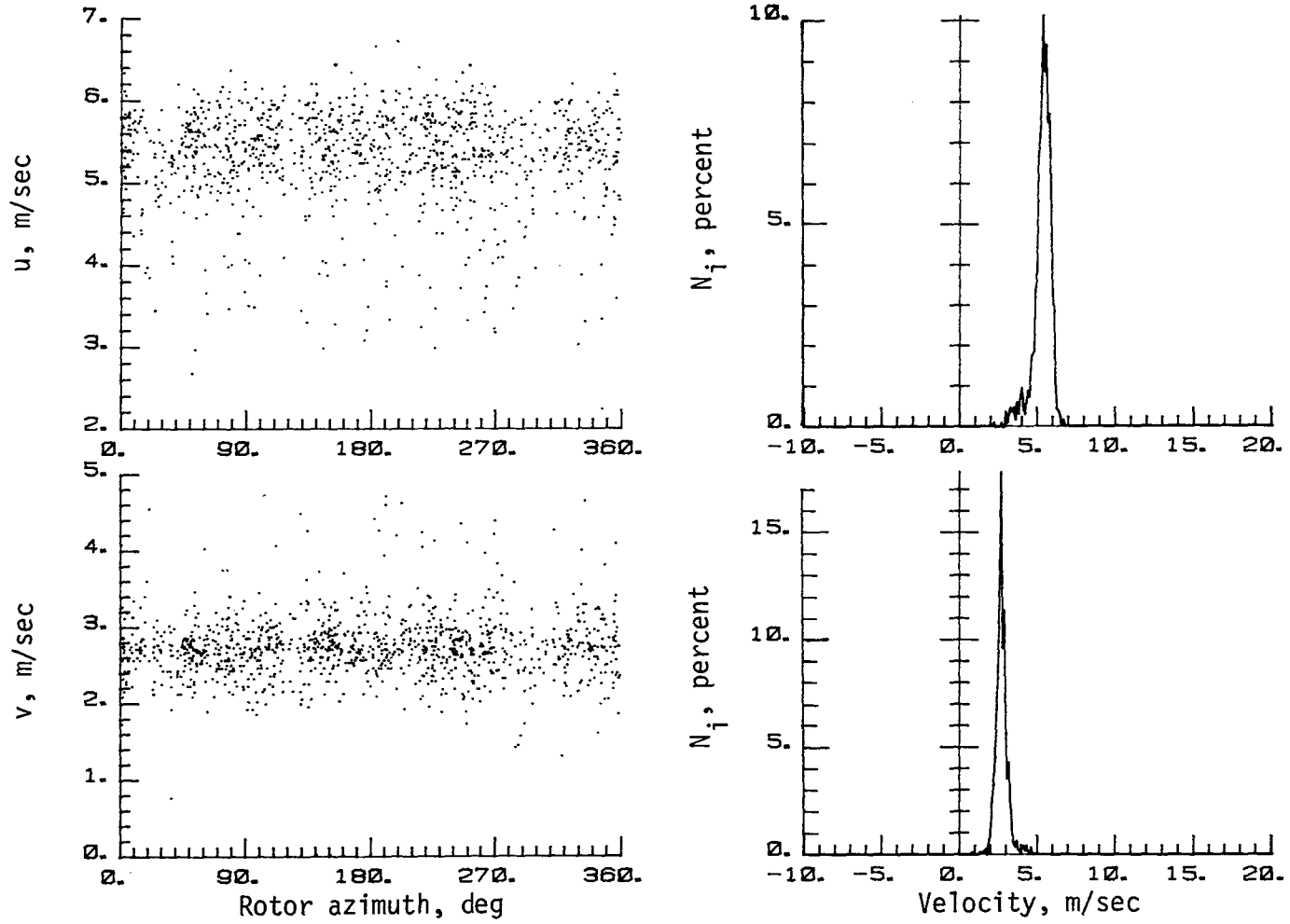
(j) S/R = 0.275; x/R = 0.2; y/R = -0.1; z/R = 0.

Figure A3.- Continued.
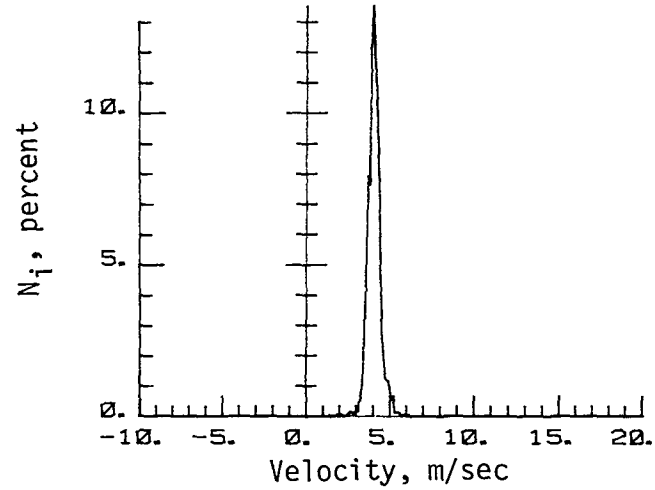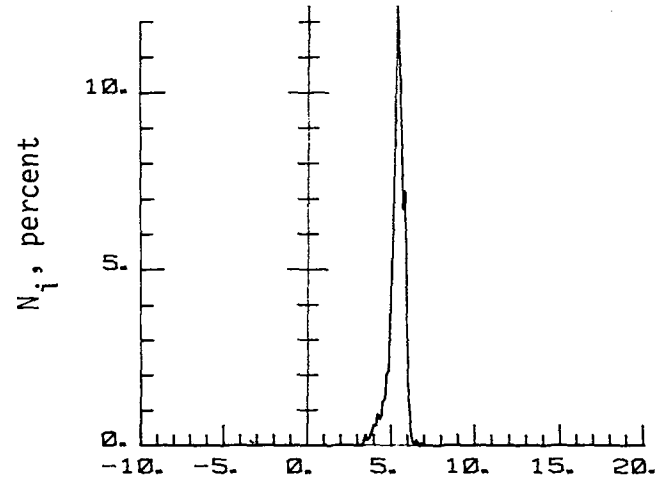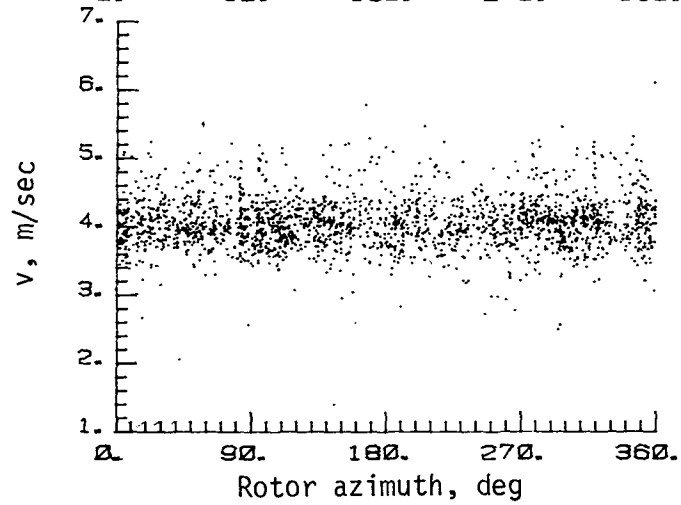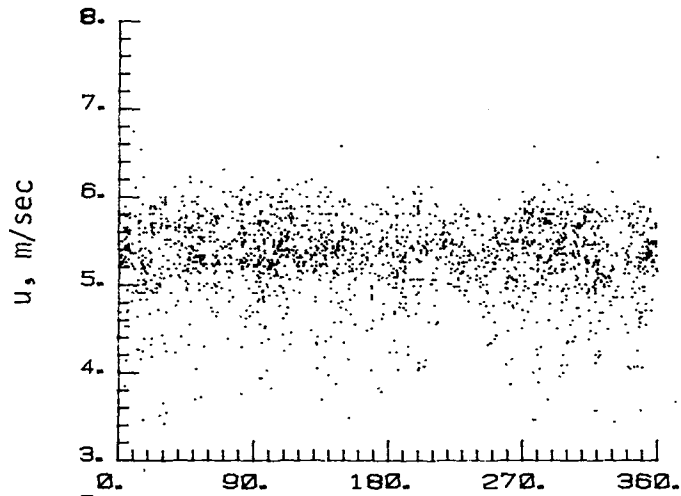
(k)   S/R = 0.275;   x/R = 0.2;   y/R = 0;   z/R = 0.

Figure A3.- Continued.
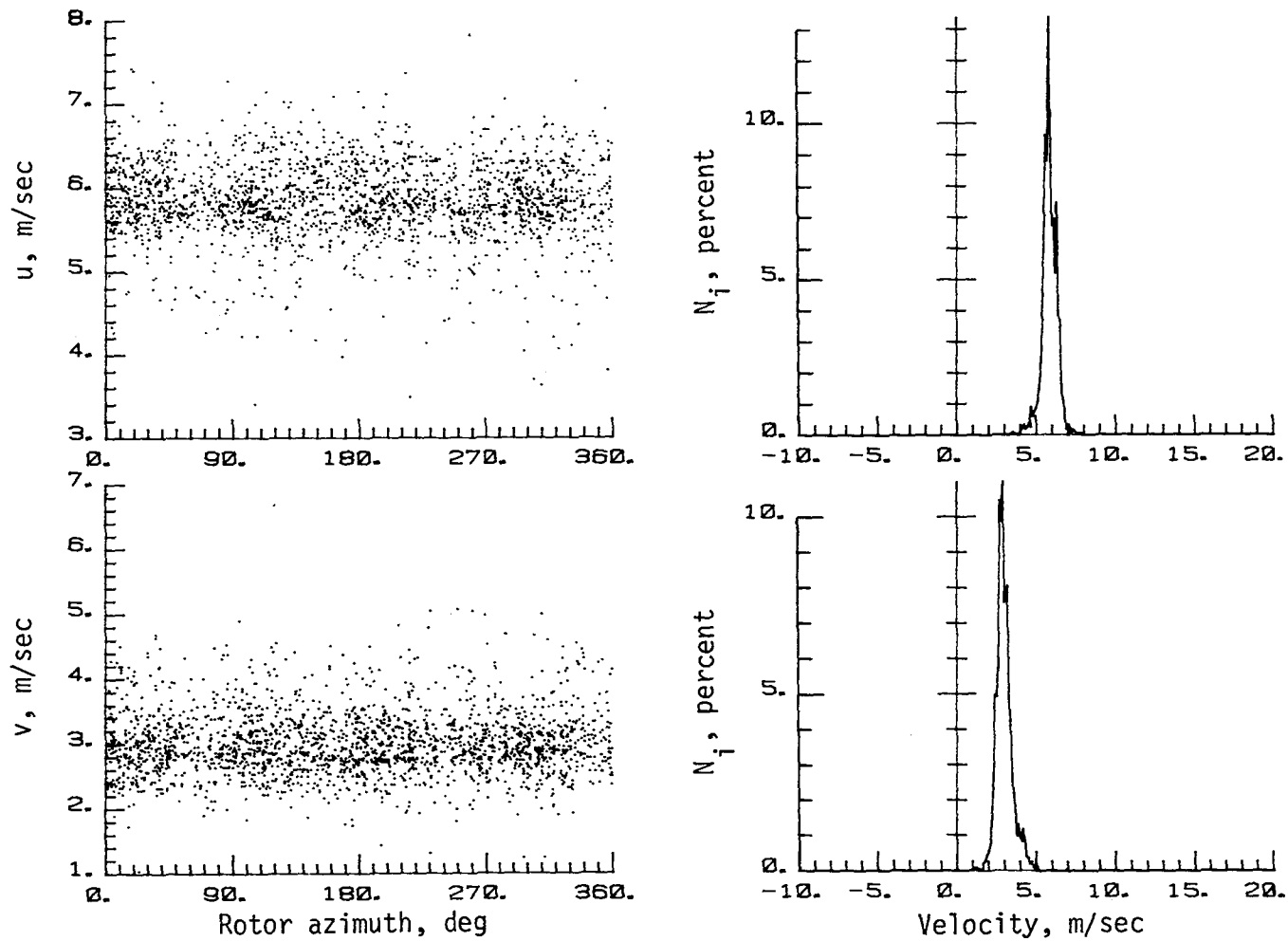
(1)   S/R = 0.275;   x/R = 0.3;   y/R = 0;   z/R = 0.

Figure A3.- Continued.
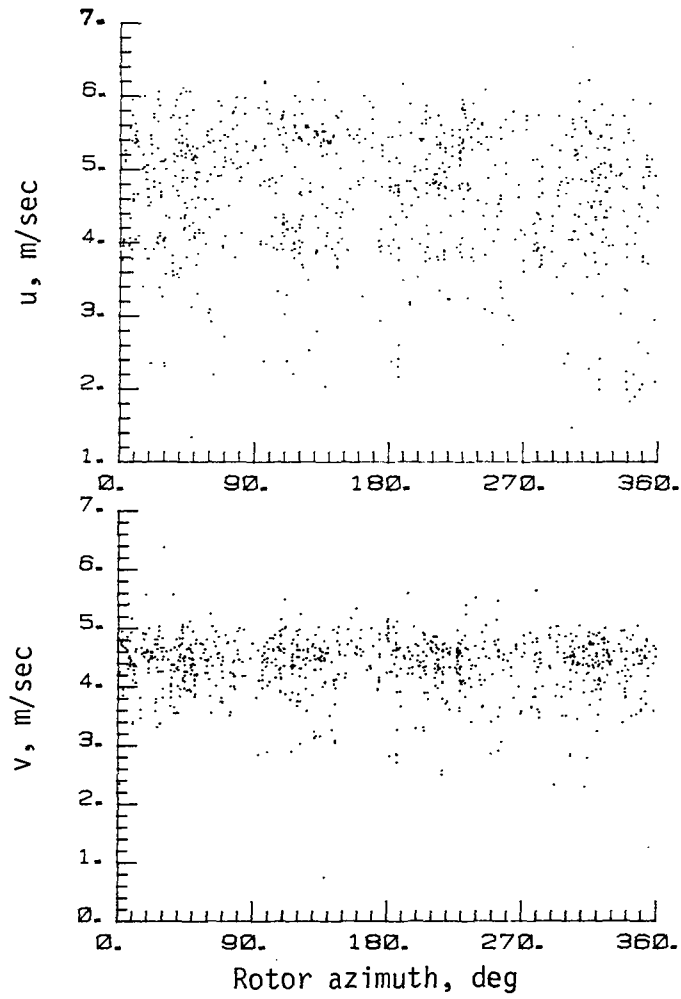
(m)   S/R = 0.324;   x/R = 0.1;   y/R = 0;   z/R = 0.

Figure A3.- Continued.
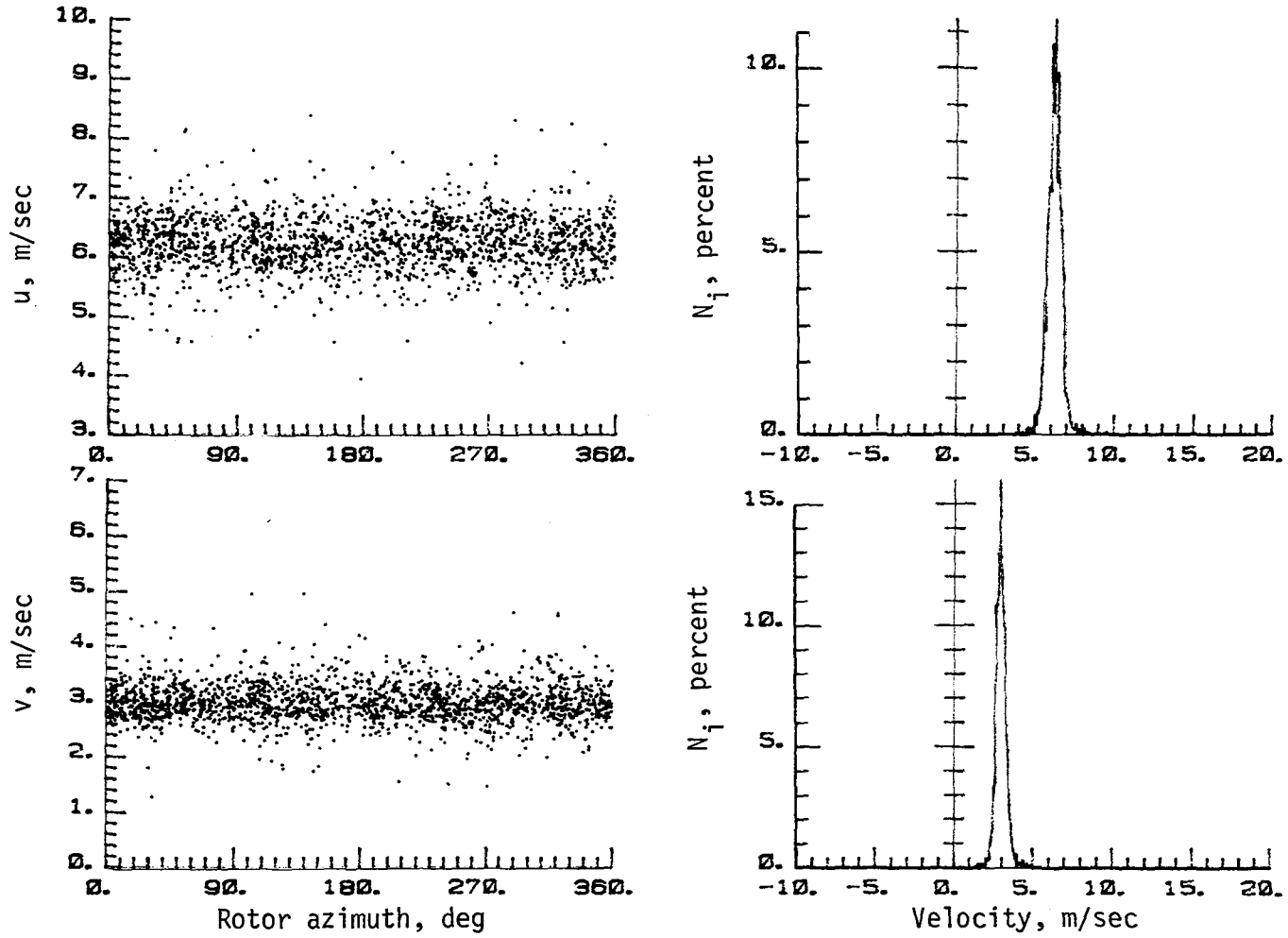
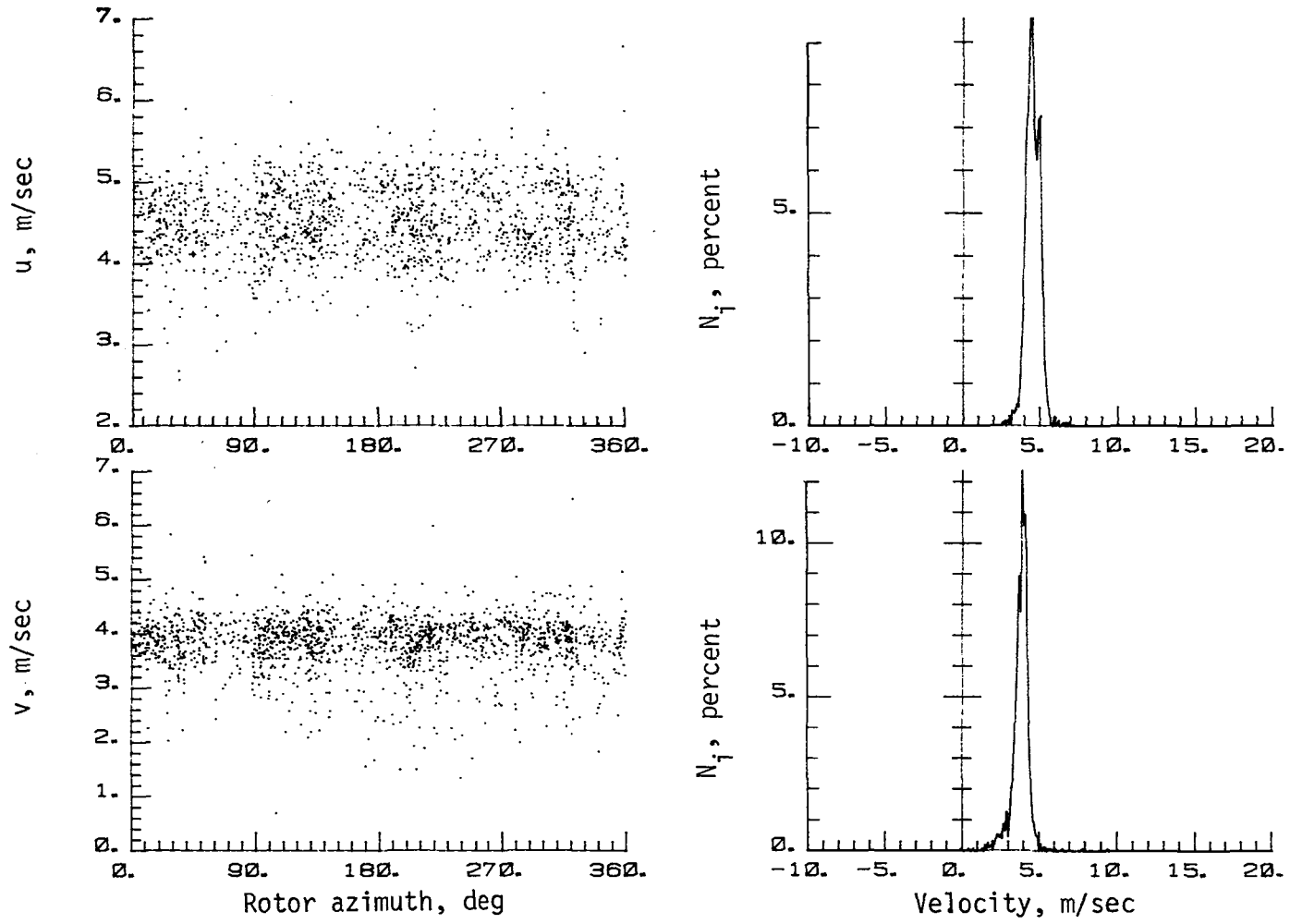(n)   S/R = 0.324;   x/R = 0.2;   y/R = 0.1;   z/R = 0.

Figure A3.- Continued.
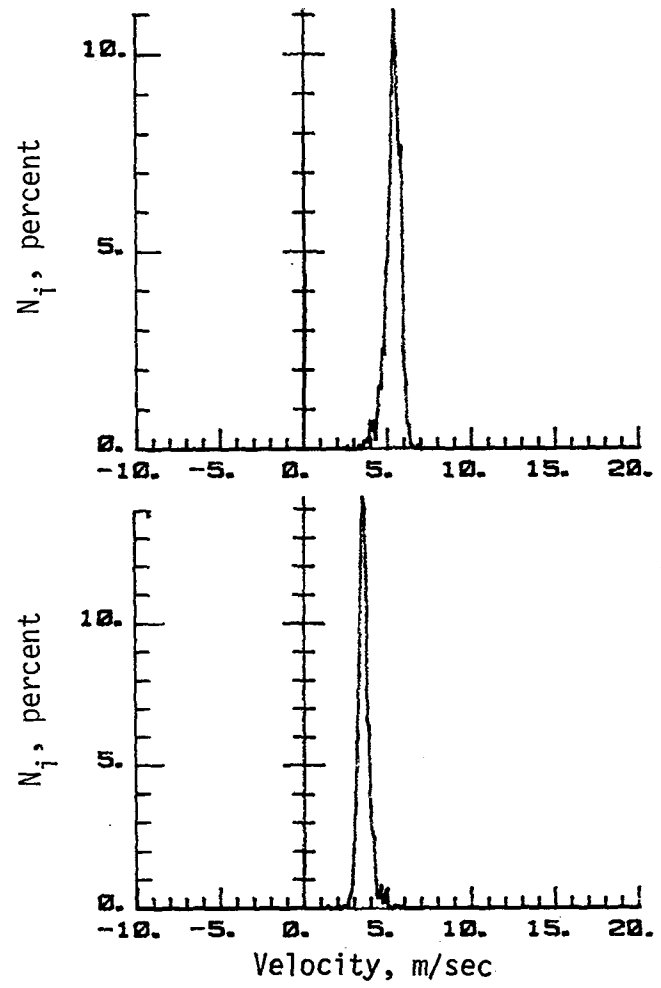
(o)   S/R = 0.324;   x/R = 0.2;   y/R = 0;   z/R = 0.

Figure A3.- Continued.

(p) S/R = 0.324; x/R = 0.3; y/R = 0; z/R = 0.

Figure A3.- Concluded.

(a) S/R = 0.224; x/R = 0.2; y/R = 0.1; z/R = 0.

Figure A4.- LV data for rotor with 0.375R body.

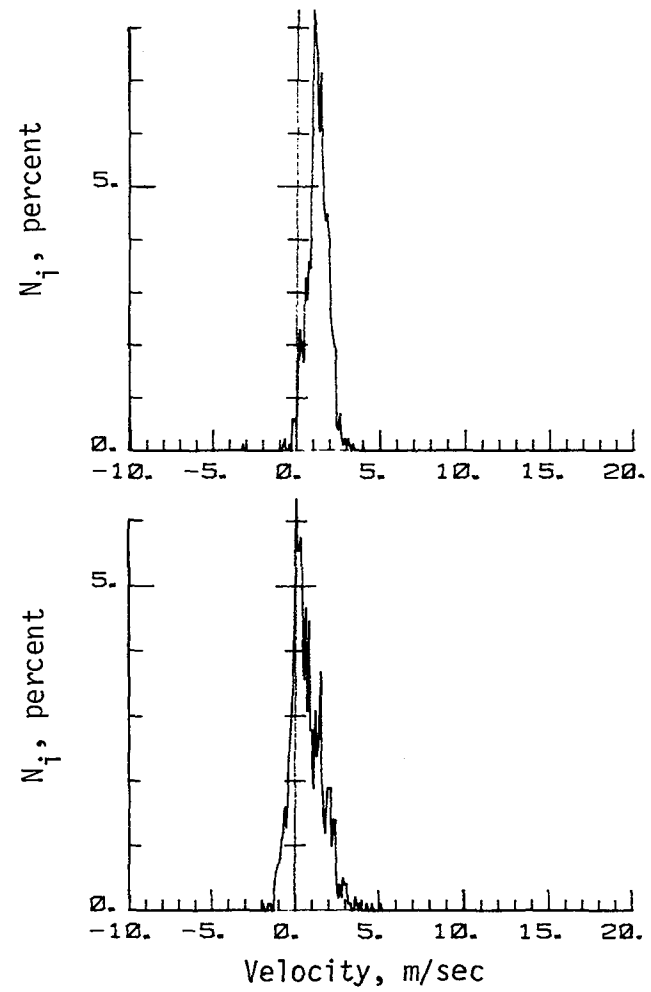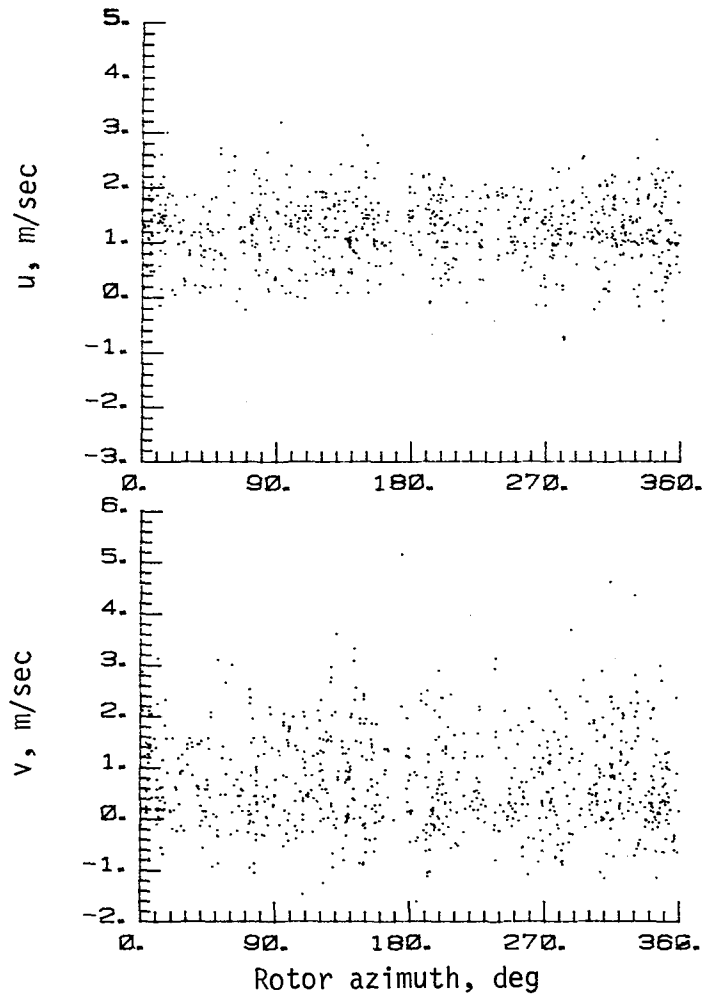(b)   S/R = 0.224;   x/R = 0.2;   y/R = -0.1;   z/R = 0.

Figure A4.- Continued.
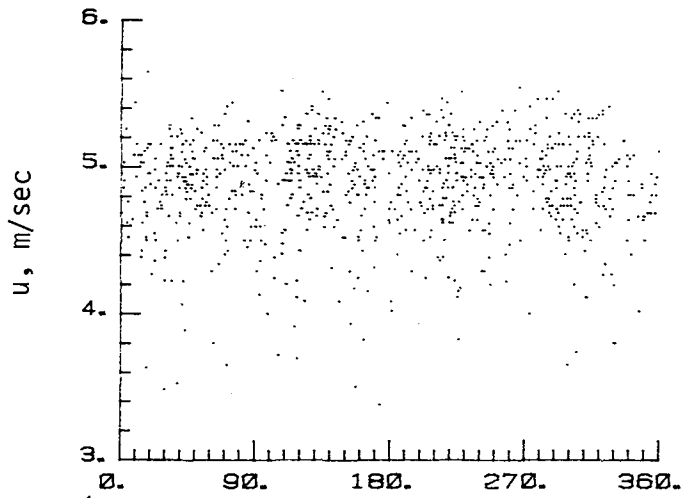
(c)   S/R = 0.224;   x/R = 0.2;   y/R = 0;   z/R = 0.

Figure A4.- Continued.
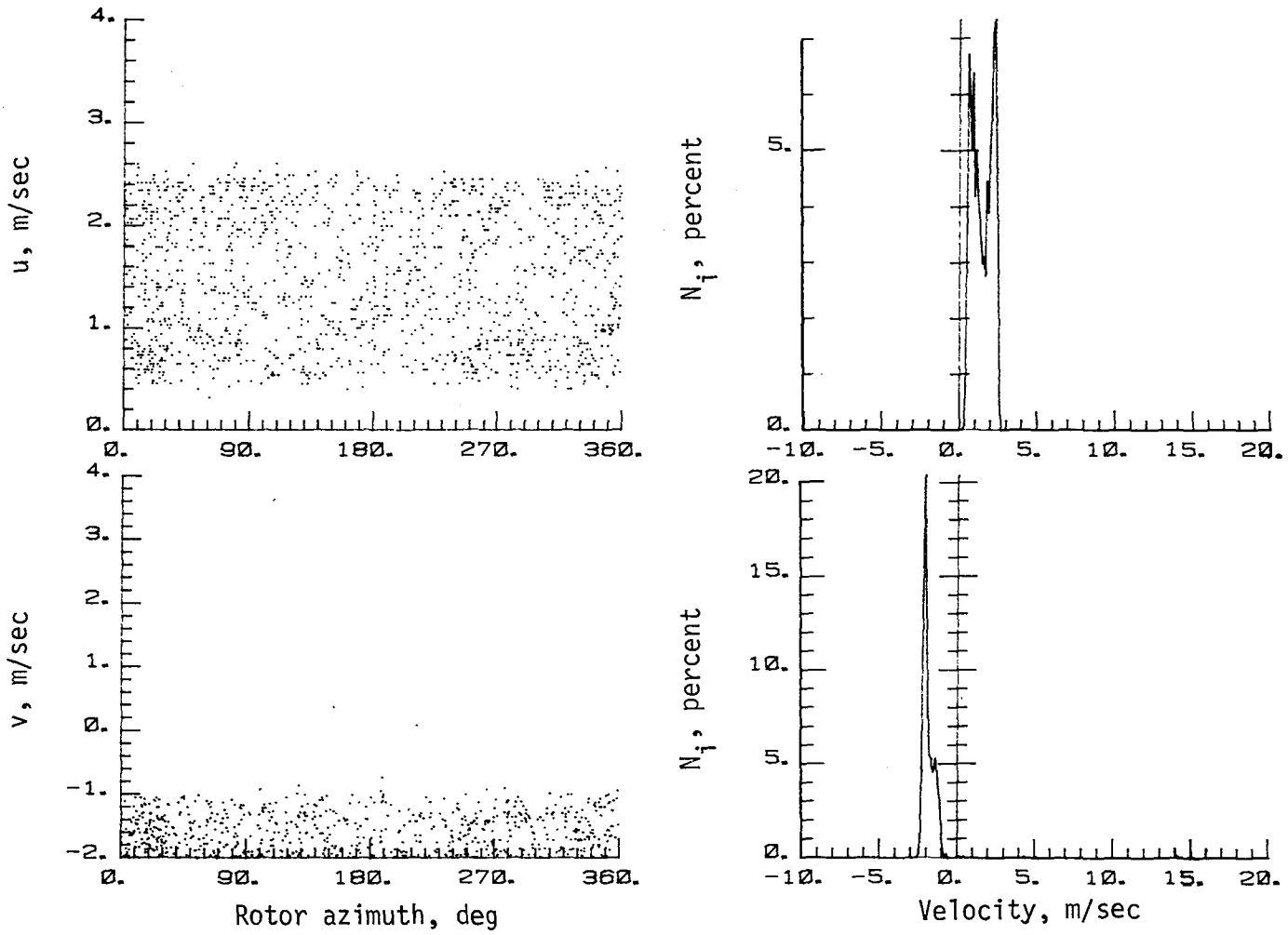
(d) S/R = 0.224; x/R = 0.3; y/R = 0; z/R = 0.

Figure A4.- Continued.
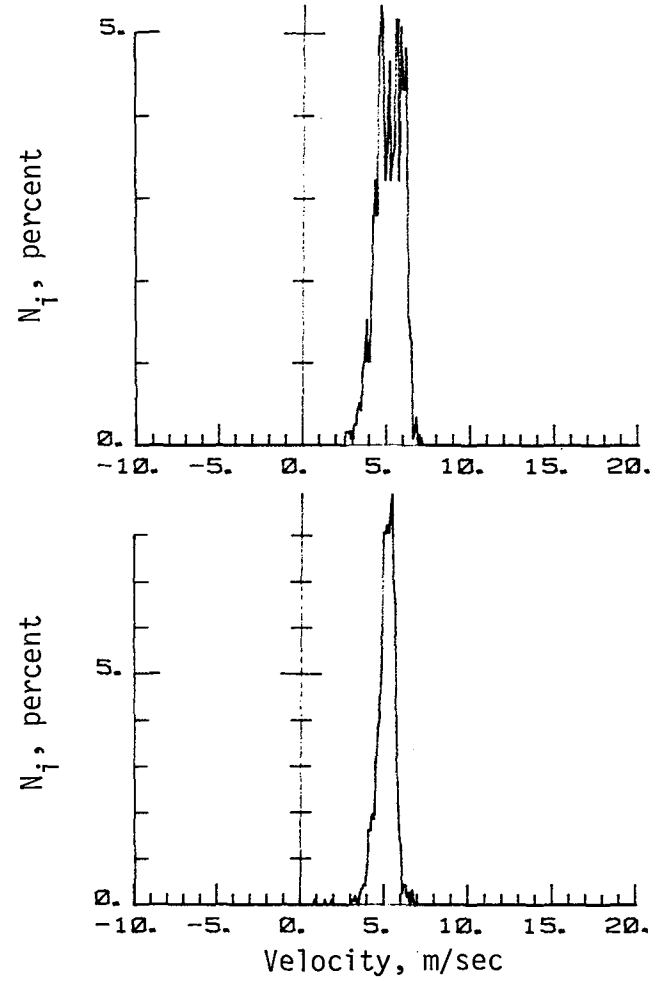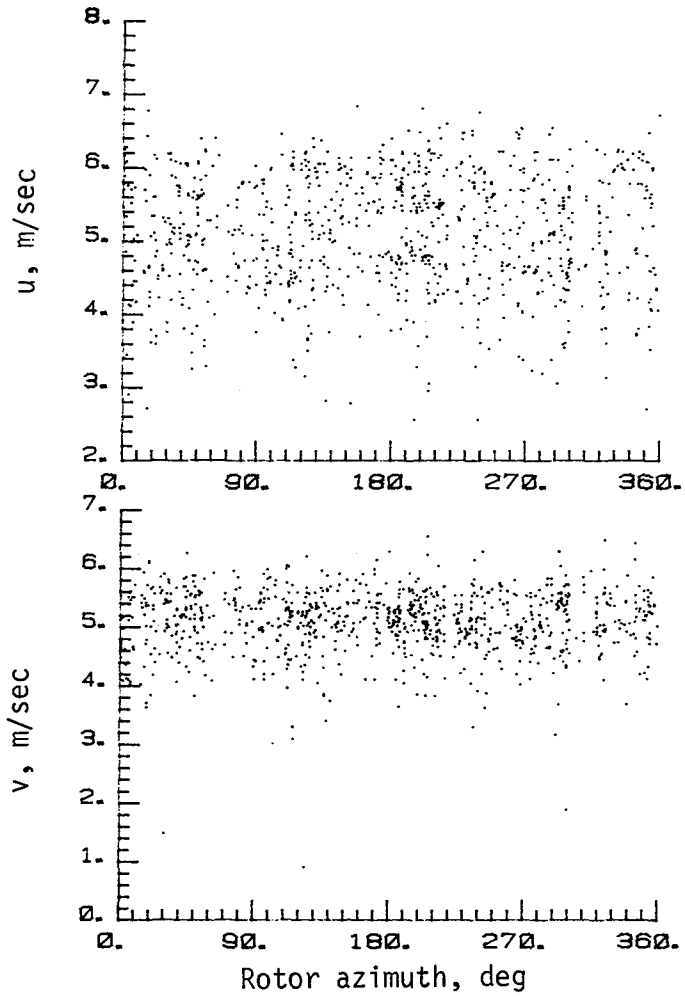
(e) S/R = 0.224;   x/R = 0.4;   y/R = 0;   z/R = 0.

Figure A4.- Continued.

(f)   S/R = 0.224;   x/R = 0.5;   y/R = 0;   z/R = 0.

Figure A4.- Continued.

(g) S/R = 0.275; x/R = 0.1; y/R = 0; z/R = 0.

Figure A4.- Continued.

(h)   S/R = 0.275;   x/R = 0.2;   y/R = 0.1;   z/R = 0.

Figure A4.- Continued.

(i)   S/R = 0.275;   x/R = 0.2;   y/R = -0.1;   z/R = 0.

Figure A4.- Continued.

(j) S/R = 0.275;   x/R = 0.2;   y/R = 0;   z/R = 0.

Figure A4.- Continued.

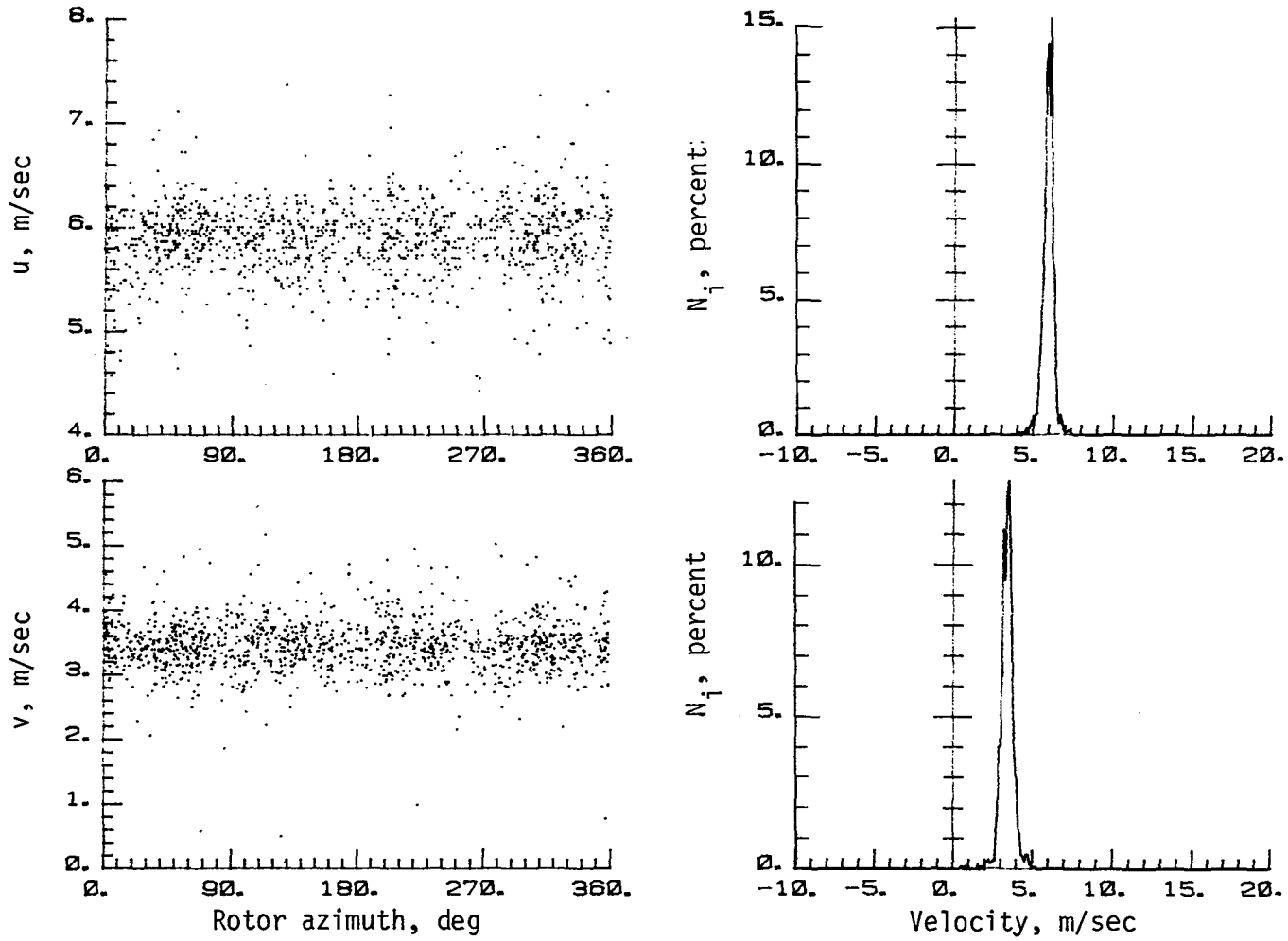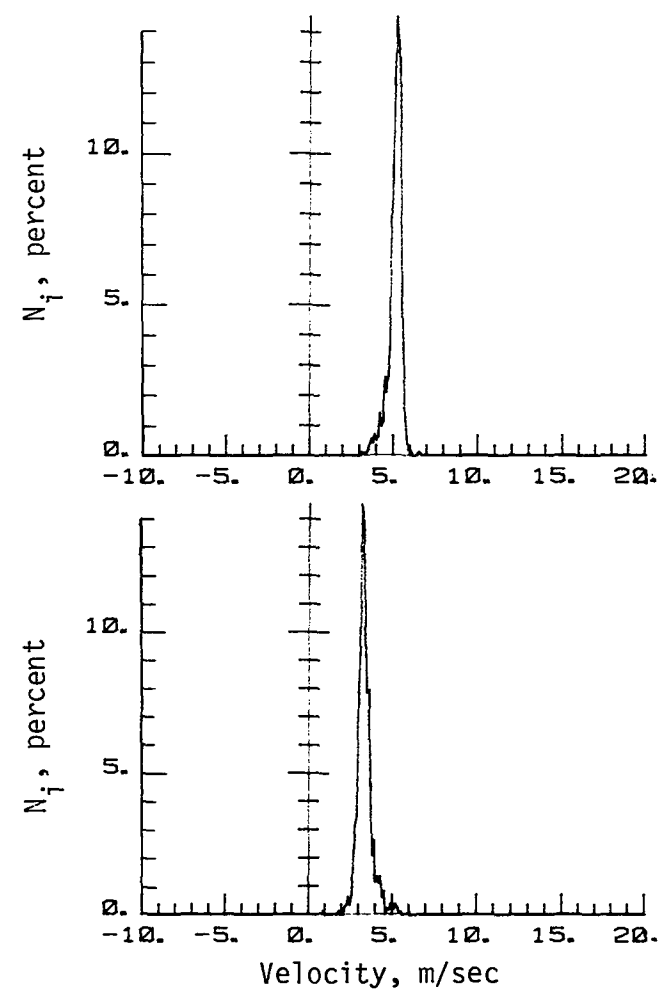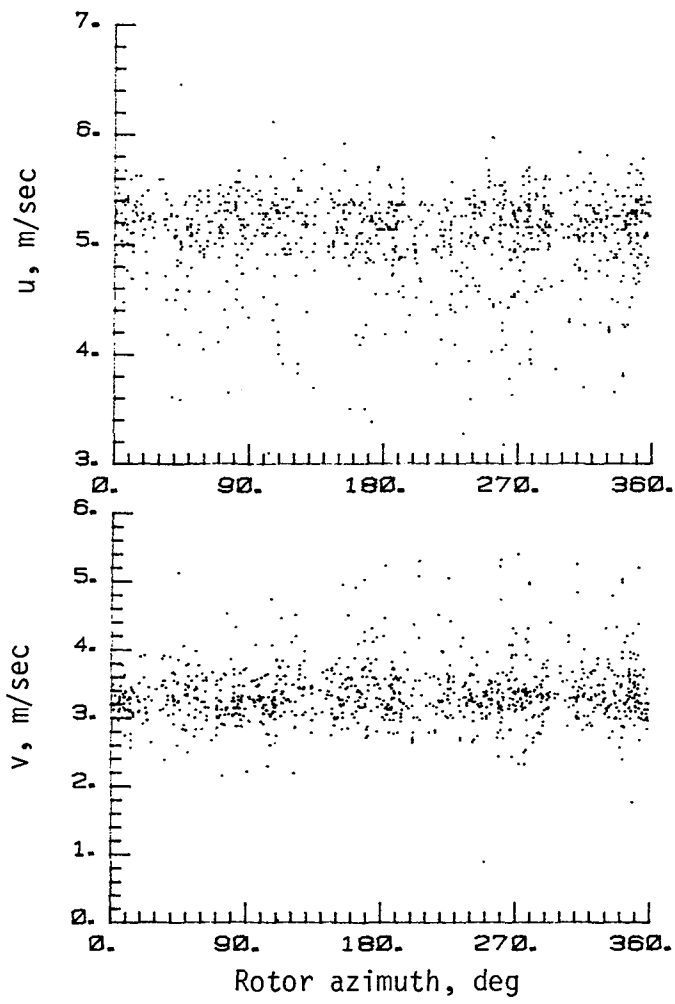(k) S/R = 0.324; x/R = 0.1; y/R = 0; z/R = 0.

Figure A4.- Continued.
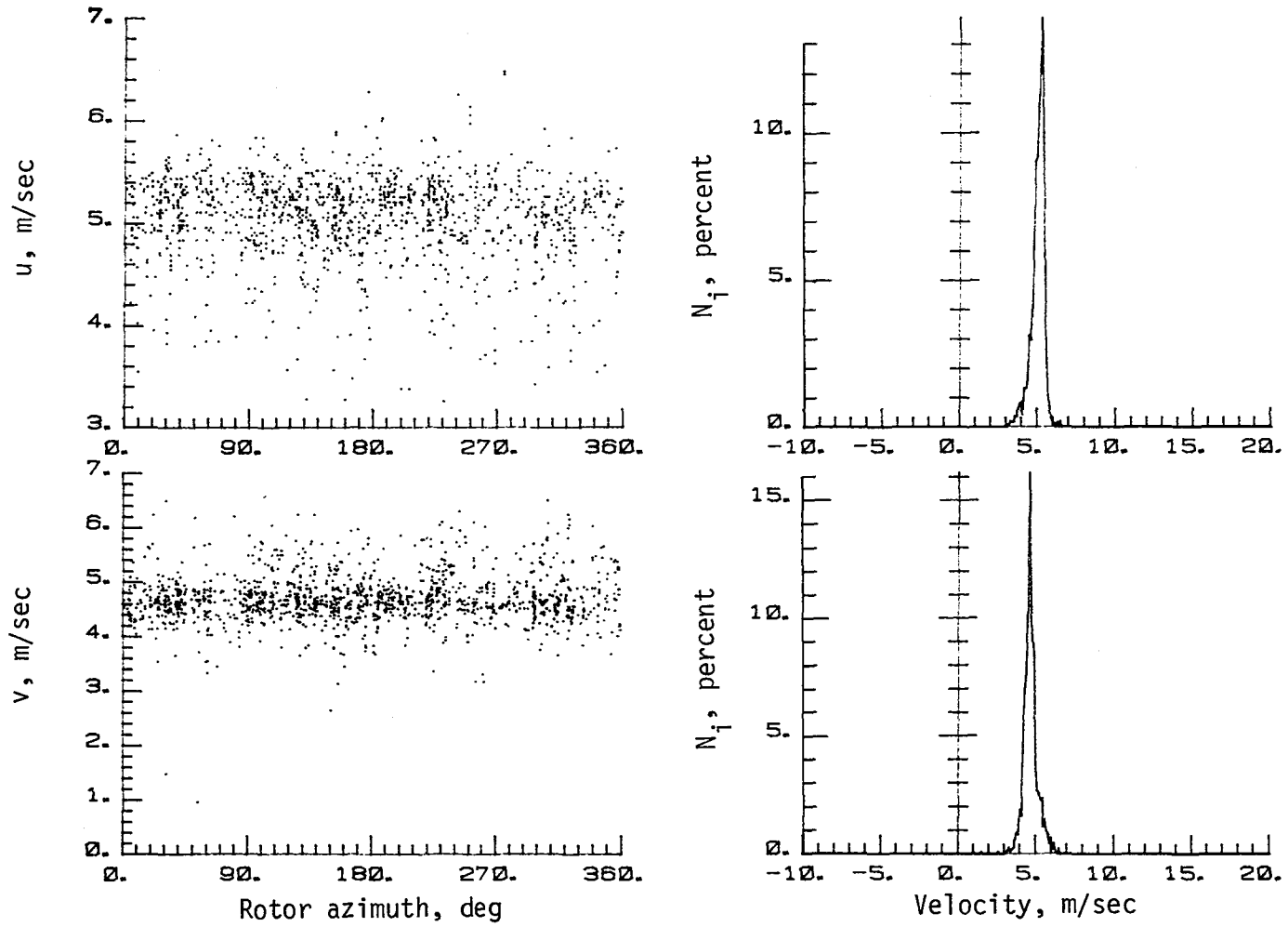
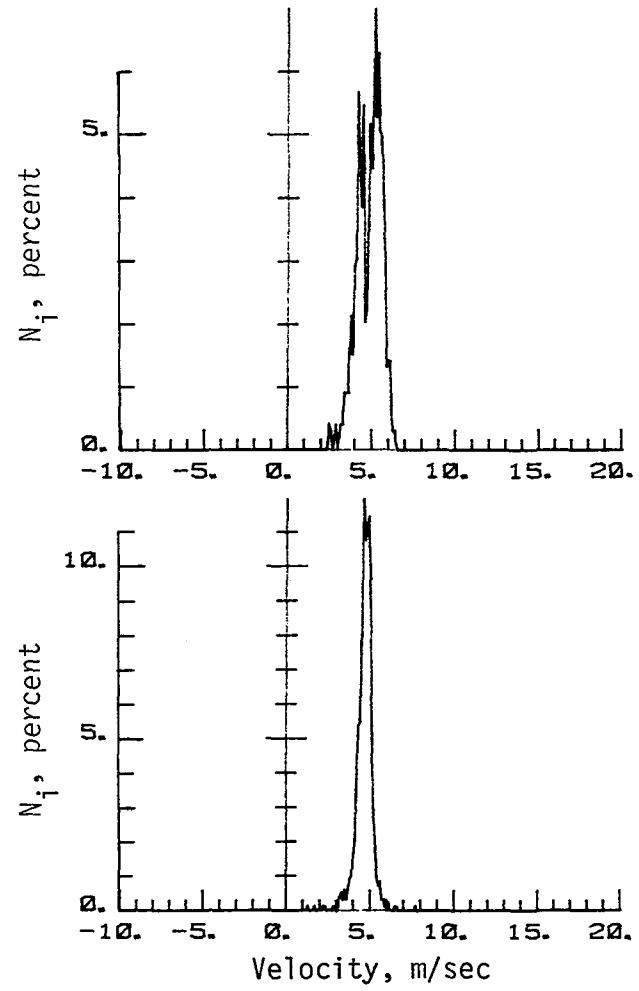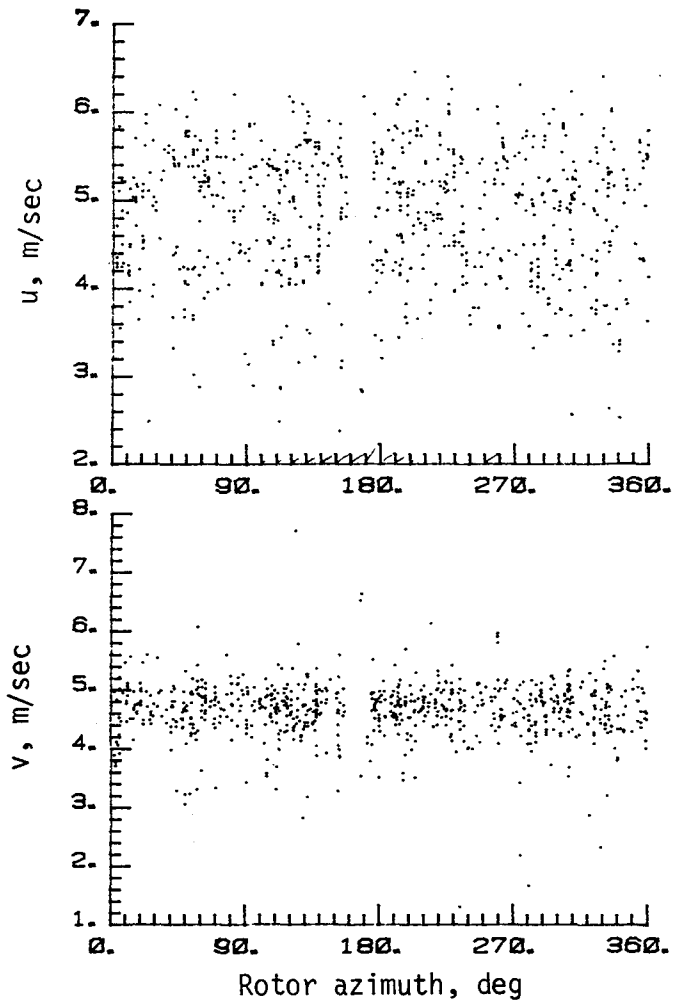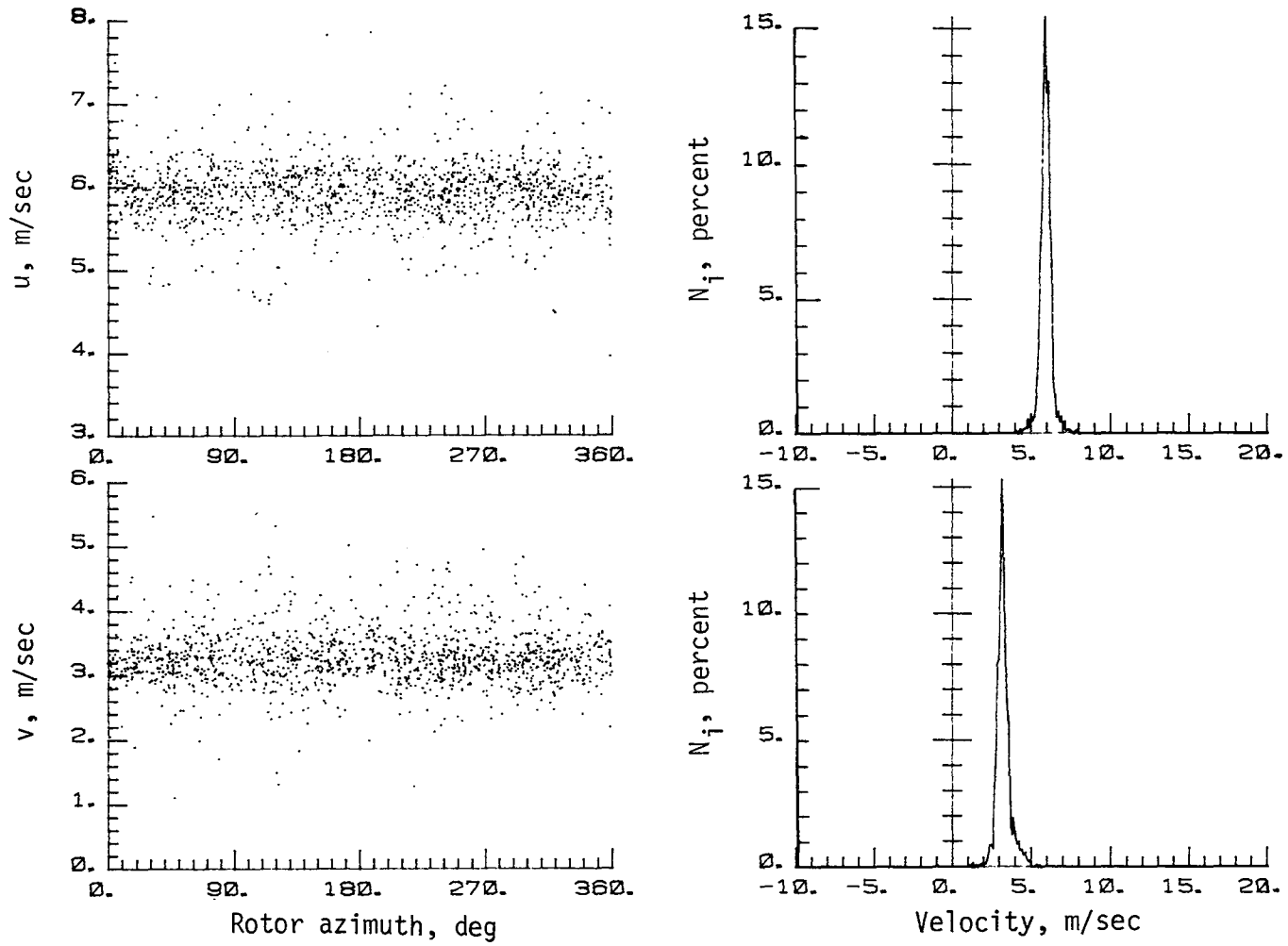(1)   S/R = 0.324;   x/R = 0.2;   y/R = 0.1;   z/R = 0.

Figure A4.- Continued.

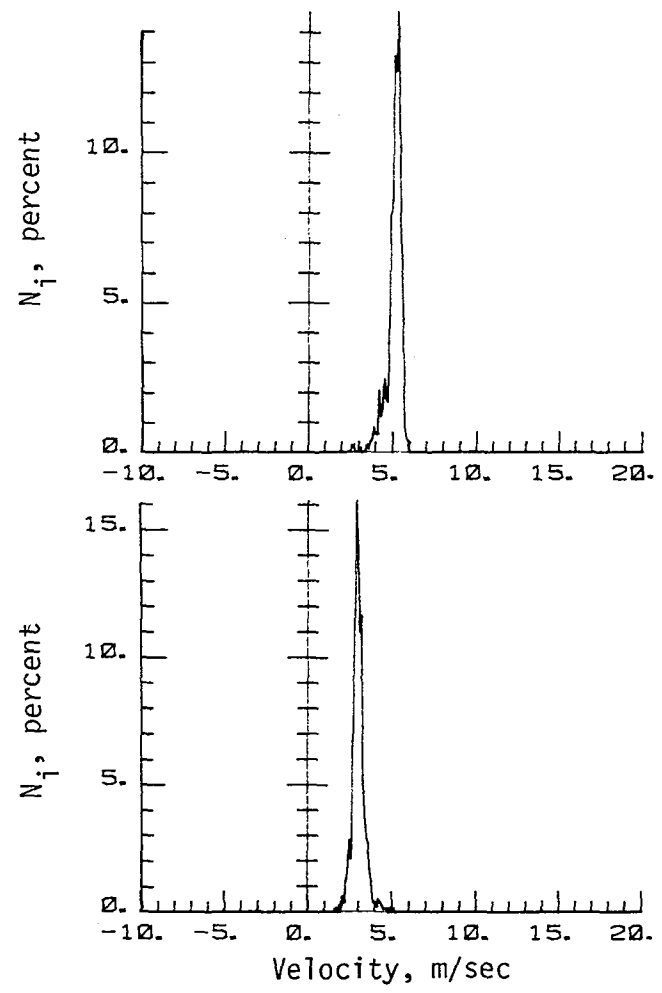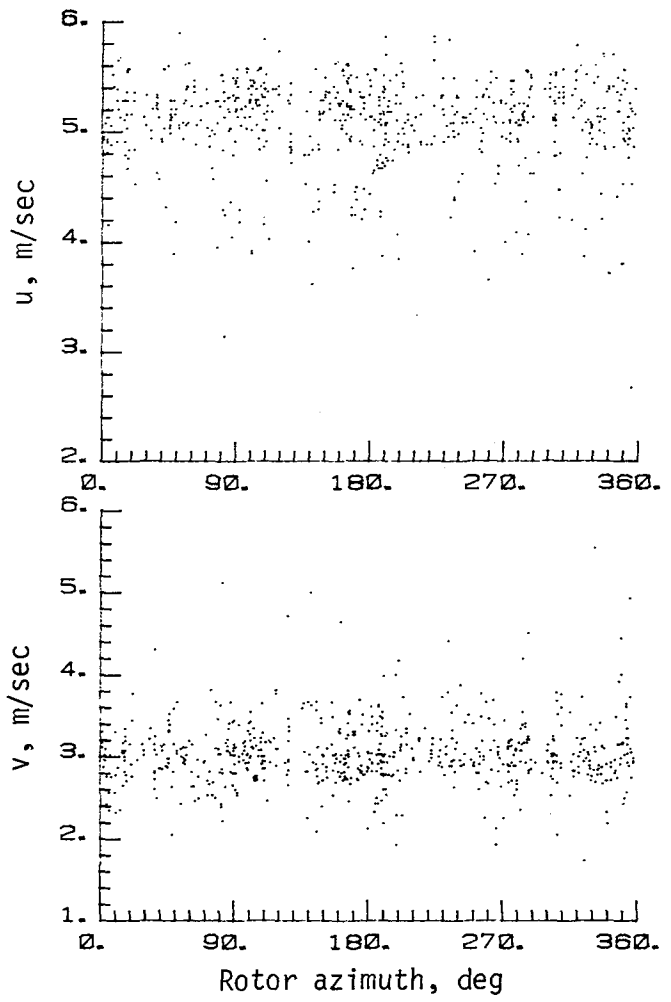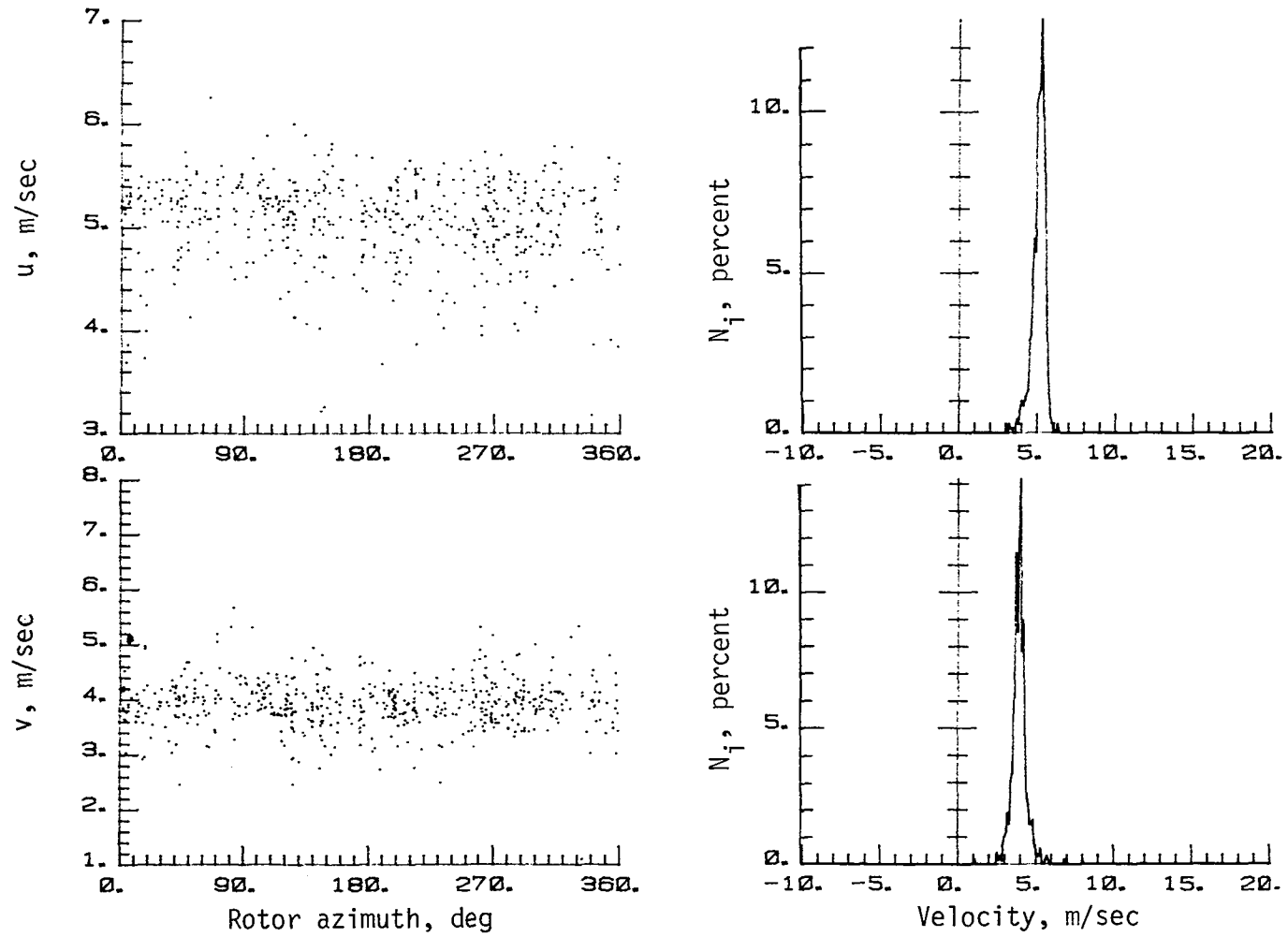(m)   S/R = 0.324;   x/R = 0.2;   y/R = -0.1;   z/R = 0.

Figure A4.- Continued.

(n) S/R = 0.324;   x/R = 0.2;   y/R = 0;   z/R = 0.

Figure A4.- Concluded.

REFERENCES

1. Mayo, William Taylor, Jr.: Laser Doppler Flowmeters - A Spectral Analysis.
   Ph. D. Thesis, Georgia Inst. of Technol., May 1969.

2. Biggers, James C.; and Orloff, Kenneth L.: Laser Velocimeter Measurements of the
   Helicopter Rotor-Induced Flow Field. J. American Helicopter Soc., vol. 20,
   no. 1, Jan. 1975, pp. 2-10.

3. Biggers, James C.; Lee, Albert; Orloff, Kenneth L.; and Lemmer, Opal J.: Mea-
   surements of Helicopter Rotor Tip Vortices. Preprint No. 77.33-06, 33rd Annual
   National Forum, American Helicopter Soc., May 1977.

4. Ballard, John D.; Orloff, Kenneth L.; and Luebs, Alan B.: Effect of Tip Planform
   on Blade Loading Characteristics for a Two-Bladed Rotor in Hover. NASA
   TM-78615, 1979.

5. Landgrebe, Anton J.; and Johnson, Bruce V.: Measurement of Model Helicopter
   Rotor Flow Velocities With a Laser Doppler Velocimeter. J. American Helicopter
   Soc., vol. 19, no. 3, July 1974, pp. 39-43.

6. Landgrebe, Anton J.; Taylor, Robert B.; Egolf, T. Alan; and Bennett, John C.:
   Helicopter Airflow and Wake Characteristics for Low Speed and Hovering Flight
   From Rocket Interference Investigations. Proceedings 37th Annual Forum,
   American Helicopter Soc., May 1981, pp. 51-65.

7. Standard for Metric Practice. E 380-79, American Soc. Testing & Mater., c.1980.

8. Rhodes, David B.: Projection Optics for a Laser Velocimeter. NASA Tech Brief
   LAR-12328, Spring 1979.

9. Young, Warren H., Jr.; Meyers, James F.; and Hoad, Danny R.: A Laser Velocimeter
   Flow Survey Above a Stalled Wing. NASA TP-1266, AVRADCOM TR 78-50, 1978.

10. Hoad, Danny R.; Meyers, James F.; Young, Warren H., Jr.; and Hepner, Timothy E.
    (appendix A by James I. Clemmons, Jr.): Laser Velocimeter Survey About a
    NACA 0012 Wing at Low Angles of Attack. NASA TM-74040, 1978.

11. Meyers, James F.: Applications of Laser Velocimetry to Large Scale and
    Specialized Aerodynamic Tests. TSI Q., vol. V, no. 4, Nov./Dec. 1979,
    pp. 5-12.

12. Landgrebe, Anton J.; and Egolf, T. Alan: Prediction of Helicopter Induced Flow
    Velocities Using the Rotorcraft Wake Analysis. Preprint No. 1002, 32nd Annual
    National V/STOL Forum, American Helicopter Soc., May 1976.

13. Mayo, W. T., Jr.; Shay, M. T.; and Riter, S.: The Development of New Digital
    Data Processing Techniques for Turbulence Measurements With a Laser
    Velocimeter. AEDC-TR-74-53, U.S. Air Force, Aug. 1974. (Available from DTIC
    as AD 784 891.)

1. Report No. NASA TM-83246 AVRADCOM TR 82-B-7	2. Government Accession No.	3. Recipient's Catalog No.
4. Title and Subtitle PRELIMINARY ROTOR WAKE MEASUREMENTS WITH A LASER VELOCIMETER		5. Report Date March 1983
		6. Performing Organization Code 505-42-23-01
7. Author(s) Danny R. Hoad, David B. Rhodes, and James F. Meyers		8. Performing Organization Report No. L-15080
		10. Work Unit No.
9. Performing Organization Name and Address NASA Langley Research Center and Structures Laboratory AVRADCOM Research and Technology Laboratories Hampton, VA 23665		11. Contract or Grant No.
		13. Type of Report and Period Covered Technical Memorandum
12. Sponsoring Agency Name and Address National Aeronautics and Space Administration Washington, DC 20546 and U.S. Army Aviation Research and Development Command St. Louis, MO 63166		14. Army Project No. 1L262209AH76

15. Supplementary Notes
Danny R. Hoad: Structures Laboratory, AVRADCOM Research and Technology Laboratories.
David B. Rhodes and James F. Meyers: NASA Langley Research Center.

16. Abstract

An experimental investigation using a laser velocimeter (LV) was conducted in the Langley 4- by 7-Meter Tunnel to determine rotor wake characteristics. The purpose of the project was to define the effect of various fuselage widths and rotor-fuselage spacings on time-averaged and detailed time-dependent rotor wake velocity characteristics. Definition of time-dependent velocity characteristics was attempted with the LV by associating a rotor azimuth position with each velocity measurement. The results were discouraging in that no apparent time-dependent velocity characteristics could be discerned from the LV measurements. Since the LV is a relatively new instrument in the rotor wake measurement field, the cause of this lack of periodicity is as important a result as the basic research objectives. An attempt was made to identify the problem by simulated acquisition of LV-type data for a predicted rotor wake velocity time history. Power spectral density and autocorrelation function estimation techniques were used to further substantiate the conclusion that the primary cause of the lack of time-dependent velocity characteristics was the nonstationary flow condition generated by the periodic turbulence level that currently exists in the open-throat configuration of the wind tunnel.

17. Key Words (Suggested by Author(s)) Laser velocimeter Helicopter wake Fluid dynamics	18. Distribution Statement Unclassified - Unlimited Subject Category 34

19. Security Classif. (of this report) Unclassified	20. Security Classif. (of this page) Unclassified	21. No. of Pages 90	22. Price* A05

National Aeronautics and
Space Administration

Washington, D.C.
20546

THIRD-CLASS BULK RATE

Postage and Fees Paid
National Aeronautics and
Space Administration
NASA-451

U.S.MAIL

NASA